AMERICAN MUSEUM
Novitates

PUBLISHED BY THE AMERICAN MUSEUM OF NATURAL HISTORY
CENTRAL PARK WEST AT 79TH STREET, NEW YORK, NY 10024
Number 3352, 54 pp., 36 figures, 5 tables December 31, 2001

Cranial Anatomy in Tenrecid Insectivorans: Character Evolution Across Competing Phylogenies

ROBERT J. ASHER[1]

ABSTRACT

Soft-tissue characters from the cranial vasculature and anterior nasal fossa are described and figured for several tenrecs and other insectivoran-grade mammals. A number of variations in blood supply and anterior nasal anatomy exist among observed specimens, including the involution of certain branches of the stapedial artery, blood supply to the jaw, relation of the external carotid to pharyngeal musculature, connections of the vomeronasal duct and paraseptal cartilage, presence of a papillary cartilage, and others. When the observed anatomy is distilled into 20 discrete anatomical characters and optimized onto recent insectivoran phylogenetic trees, these soft-tissue characters are more consistent with a reconstruction based on osteological and dental characters than with one based on molecular characters. Nevertheless, all recently proposed phylogenies require homoplasy from this dataset, and potential synapomorphies for both a monophyletic Lipotyphla and endemic African clade can be optimized onto recent phylogenetic proposals.

INTRODUCTION

Living tenrecs consist of three subfamilies restricted to Madagascar: the Tenrecinae (*Tenrec, Setifer, Hemicentetes, Echinops*), Oryzorictinae (*Microgale, Oryzorictes, Limnogale*), and Geogalinae (*Geogale*; see Eisenberg and Gould, 1970). Two African genera (*Potamogale* and *Micropotamogale*) comprise the Potamogalinae and are usually listed as part of the Tenrecidae as well (Stephan et al., 1991; Nowak, 1999). Tenrecines (particularly *Echinops* and *Setifer*) resemble hedgehogs such as *Erinaceus* and *Atelerix* in their cover of dense spines. *Microgale* and *Geogale* resemble some shrews in their pel-

[1] Division of Paleontology, American Museum of Natural History. E-mail: asher@amnh.org

 ISSN 0003-0082

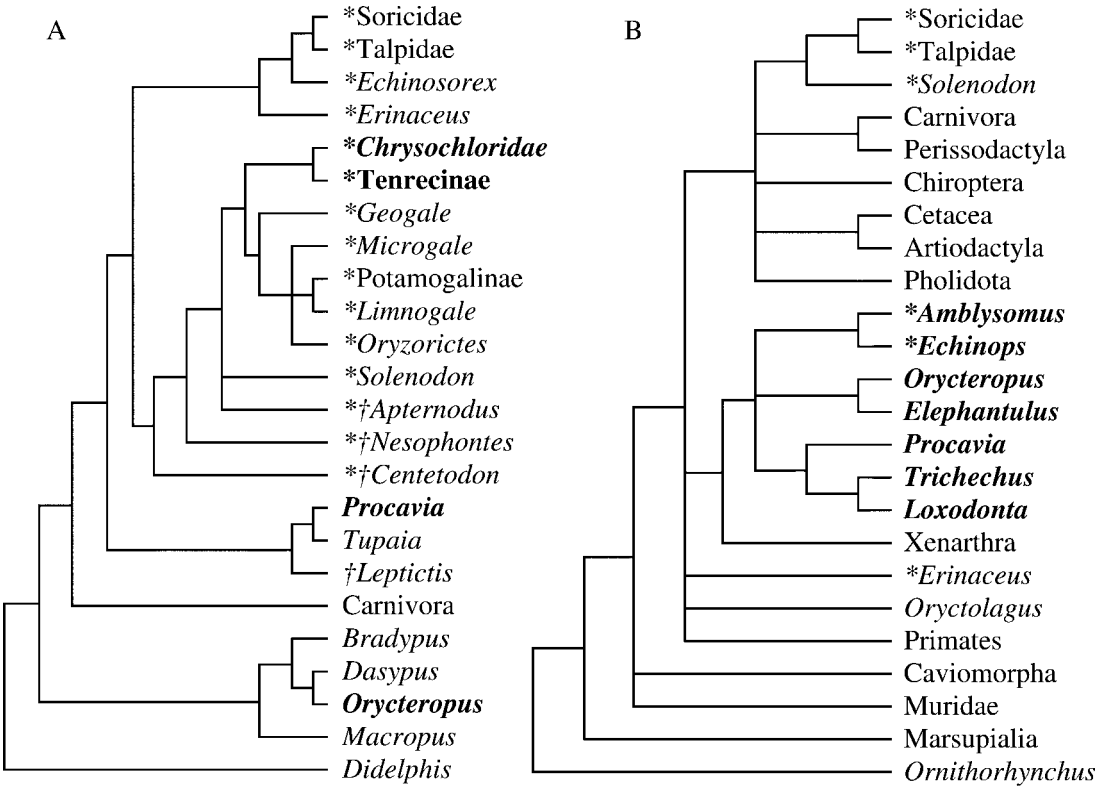

Fig. 1. Competing phylogenetic hypotheses for African insectivorans. A. As part of the Lipotyphla (after set no. 1 of Asher, 1999). B. As part of the Afrotheria (after fig. 1 of Stanhope et al., 1998). Endemic African taxa are listed in bold; insectivorans are marked with an asterisk, fossils with a cross.

age and size; *Oryzorictes* has molelike fossorial habits; and potamogalines and *Limnogale* are semiaquatic, resembling desmans (e.g., *Galemys*) in their riverine habitat.

Throughout the 20th century, this diverse group of small placental mammals has been considered to be part of the ''Lipotyphla'', a taxon coined by Haeckel (1866) to include living moles, hedgehogs, shrews, golden moles, and the Caribbean *Solenodon* (fig. 1A). Recently, a growing body of molecular evidence (Stanhope et al., 1998; Mouchaty et al., 2000; van Dijk et al., 2001; Madsen et al., 2001; Murphy et al., 2001) has been interpreted in favor of the hypothesis that the endemic African elements of the Lipotyphla (i.e., tenrecs and golden moles) are in fact more closely related to a larger endemic African clade consisting of elephants, sea cows, hyraxes, aardvarks, and elephant shrews (fig. 1B). However, this conclusion is not unambiguously supported by these molecular data. For example, the parsimony trees published as ''supplementary data'' (available with free registration at www.nature.com) by Murphy et al. (2001) do not support the inclusion of the single sampled tenrec, *Echinops telfairi,* within the Afrotheria. In fact, a mammalian ''supertree'' (Liu et al., 2001), summarizing results from slightly over 400 phylogenetic analyses published through early 1999, favors the inclusion of both tenrecs and golden moles in the traditionally recognized order Lipotyphla.

The core of the ''Afrotheria'' (Stanhope et al., 1998), consisting of elephants, sea cows, and hyraxes (collectively known as paenungulates), has had a long history among vertebrate biologists (Simpson, 1945; McKenna and Bell, 1997). Even the association of

aardvarks and elephant shrews with paenungulates is a hypothesis that many zoologists find palatable, if only because the ordinal-level affinities of elephant shrews and aardvarks have been unclear for some time (Thewissen, 1985; MacPhee, 1994; Woodall, 1995). However, the association of African tenrecs and golden moles with a paenungulate-aardvark-elephant shrew clade, to the exclusion of such insectivoran-grade taxa as hedgehogs and shrews, would not have been made without molecular data produced during the last few years (e.g., Madsen et al., 2001); this hypothesis may rightly be considered a controversial ''molecular alternative'' to the view that insectivoran-grade taxa form a natural assemblage (e.g., Butler, 1988). At the same time, more recent morphologically based phylogenetic evaluations of insectivoran monophyly (e.g., MacPhee and Novacek, 1993; Asher, 1999) are at best lukewarm regarding the integrity of this taxon. If tenrecs and golden moles are not part of the ''Afrotheria'', then it is far from clear where their true phylogenetic affinities lie.

Purpose of the Present Study

A reason for this lack of confidence in insectivoran relationships may be that basic information about the anatomy of several insectivoran-grade groups remains unknown. Even with the notable contributions of Roux (1947), Bugge (1974), and MacPhee (1981), details on cranial vasculature in the Tenrecidae has to date been adequately described in less than half of its constituent genera. Published information on the tenrecid nasal fossa is even more scarce, even though Broom (1915b) and Hofer (1982a) have made a good start. This lack of anatomical knowledge for tenrecs is surprising, given the fact that both regions have historically served as important sources of phylogenetic information in other mammalian groups (e.g., Kuhn, 1971; Maier, 1980; Wible, 1987; Sánchez-Villagra, 2001).

The present study makes a contribution to this shortfall by describing cranial arterial supply in *Potamogale*, *Micropotamogale*, *Geogale*, *Microgale*, *Echinops*, *Tenrec*, the nontenrecid *Erinaceus*; and the anterior nasal region for these taxa plus the tenrec *Setifer*. All of these animals are insectivoran grade and have traditionally been classified in the Lipotyphla sensu Haeckel (1866). After describing the cranial anatomy of these taxa, I distill this information into a limited number of discrete characters and code them for the preceding taxa plus 16 other mammals, including the marsupial *Didelphis*. I then map these characters onto phylogenetic trees representing alternative hypotheses of insectivoran relationships, and note which hypothesis best explains their distribution.

A definitive solution to the phylogeny of insectivoran-grade mammals must await a simultaneous analysis of morphological and sequence data and sample relevant living and fossil taxa. The scope of this paper is much more limited, providing basic anatomical data that may be relevant for larger biological issues. In the short term, I use these data to evaluate previously existing phylogenetic hypotheses of African insectivoran phylogeny.

Taxonomic Terminology

The following taxonomic conventions will be used throughout this text: ''Placental'' mammals include crown group members of the Eutheria. ''Eutheria'' is more inclusive and encompasses members of the stem lineage leading to placental mammals (Novacek et al., 1997). The ''Lipotyphla'' denotes extant chrysochlorids, erinaceids, *Solenodon*, soricids, talpids, tenrecids, the subfossil *Nesophontes*, and several extinct Tertiary groups including (for example) apternodontids, dimylids, erinaceomorphs, and geolabidids (Carroll, 1988; Gould, 1995; McKenna and Bell, 1997; Asher, 1999). In the 19th and early 20th centuries, ''Insectivora'' commonly included lipotyphlans plus menotyphlans (i.e., scandentians and macroscelideans). During the last 50 years, ''Insectivora'' has most often been used interchangeably with ''Lipotyphla'', and is so regarded here. However, I use ''Insectivora'' in an explicitly gradistic sense. ''Insectivora'' and ''insectivoran'' are taxonomic terms and do not imply any particular dietary strategy, although ''insectivore'' does (cf. ''carnivoran'' vs. ''carnivore''). The ''Afrotheria'' refers to the group designated by Stanhope et al. (1998),

TABLE 1
Variations in Anatomical Terminology
(Term used in this paper were chosen based on precedence and/or common usage. Variations observed in the literature are listed on the right.)

This paper	Variations
Nasopalatine duct cartilage	Palatine and nasopalatine duct cartilage (Maier, 1980)
Definition: Laterally and medially situated cartilaginous support for the nasopalatine duct. Following Maier (1980), the palatine cartilage is found lateral to the nasopalatine duct and the nasopalatine duct cartilage medial to the duct.	
Inferior stapedial ramus	"Distal part of the stapedial artery system" (Bugge, 1974)
Definition: Stapedial artery distal to origin of the superior stapedial ramus and proximal to the origin of mandibular and infraorbital arterial rami, which it supplies. May involute in some taxa (e.g., *Tenrec ecaudatus*).	
Internal carotid artery	Promontorial artery (MacPhee, 1981), arteria promontorii (McDowell, 1958)
Definition: "Promontory artery" refers to segment of internal carotid in transpromontorial position (Wible, 1986) as it courses on ventrum of pars cochlearis, distal to origin of proximal stapedial artery.	
Ramus infraorbitalis	Infraorbital artery (Cartmill and MacPhee, 1980)
Definition: One of two terminal branches of the inferior stapedial arterial ramus, beginning at the origin of the ramus mandibularis. Supplies the upper dentition and oral cavity, posterior palate, and face en route to the rostrum via the infraorbital foramen/canal. Target structures are annexed by a maxillary branch of the external carotid artery in some taxa (e.g., *Tenrec ecaudatus*). "Infraorbital artery" may be recognized as distinct from "ramus infraorbitalis" when it is a branch of the maxillary artery and travels adjacent to the infraorbital nerve.	
Ramus mandibularis	Inferior alveolar artery (Agur and Lee, 1991)
Definition: One of two terminal branches of the inferior stapedial arterial ramus, beginning at the origin of the ramus infraorbitalis. Supplies the mylohyoid muscle and jaw. May be annexed by the external carotid artery in some taxa (e.g., *Tenrec ecaudatus)*.	
Sinus canal foramen	Cranioorbital foramen (MacPhee, 1994), anterior opening of orbitotemporal canal (Wible and Rougier, 2000)
Definition: Anterior exit point in (typically) the alisphenoid for the sinus canal through which the superior stapedial arterial ramus supplies the supraorbital artery as the latter enters the orbitotemporal fossa.	
Sphenorbital fissure	Foramen lacerum anterioris (McDowell, 1958)
Definition: Opening in sphenoid into orbitotemporal fossa for exit of ophthalmic and maxillary divisions of trigeminal nerve.	

that is, proboscideans, sirenians, hyracoids, tubulidentates, macroscelideans, tenrecids, and chrysochlorids. Proboscideans and sirenians are collectively referred to as the Tethytheria (Fischer, 1996), and these two plus hyracoids are referred to as the Paenungulata (Shoshani, 1993). Stanhope et al. (1998) proposed the name "Afrosoricida" to denote a clade containing extant chrysochlorids and tenrecids. However, 40 years earlier McDowell (1958) proposed the name "Tenrecoidea" as a superfamily with the same content. Other workers have used "Tenrecoidea" in a broader sense both formally (e.g., Gill, 1884) and informally (Asher, 1999) so as to include *Solenodon* and/or extinct apternodontids, in addition to tenrecs and golden moles. Here, I follow McDowell in using "Tenrecoidea" to indicate a tenrec-chrysochlorid clade (cf. Mouchaty, 1999).

Anatomical Terminology

I follow McDowell (1958), Novacek (1986), and MacPhee (1994) for osteological terminology; Bugge (1974), MacPhee (1981), and Wible (1984) for arterial terminology; and Sturm (1936), Kuhn (1971), and Maier (1980) for nasal terminology. Variations on anatomical terms used by these and other investigators are listed in table 1.

ABBREVIATIONS

Institutional

AIG	Universität Göttingen, Anatomisches Institut (Germany)
AIM	Universität München, Anatomisches Institut (Germany)
AMNH-B	American Museum of Natural History, Bluntschli Collection (USA)
IZEA	Institut de Zoologie et d'Ecologie Animale, Lausanne (Switzerland)
MCZ	Museum of Comparative Zoology, Cambridge (USA)
MNHN	Museum Nationale d'Histoire Naturelle, Paris (France)
MPIH	Max Planck Institut für Hirnforschung, Frankfurt (Germany)
HID	Universität Düsseldorf, Vogt Institut für Hirnforschung (Germany)
ZIUT	Universität Tübingen, Zoologisches Institut (Germany)

Anatomical

acc	alicupular commissure
acf	anterior carotid foramen
ap	ascending pharyngeal artery
atl	anterior transverse lamina
ba	basilar artery
bs	basisphenoid bone
bsm	arterial branch to submandibular gland
bu	buccal artery
cc	common carotid artery
ce	external carotid artery
ci	internal carotid artery
co	cochlea of inner ear
cp	cupular process
cs	cupular spur
d	dentary bone
dc	anastomotic branch for deep cervical artery
ea	ethmoidal artery
ect	ectotympanic bone
es	esophagus
fa	facial artery
fo	foramen ovale
gp	greater palatine artery
hf	hypoglossal foramen
icn	internal carotid nerve
ijv	internal jugular vein
in	incus
jf	jugular foramen
lc	longus capitis muscle
li	lingual artery
lnd	lateral nasal duct
ma	malleus
mk	Meckel's cartilage
mx	maxilla
nf	nasal fossa
nld	nasolacrimal duct
npd	nasopalatine duct
npdc	nasopalatine duct cartilage
ns	nasal septum
ob	outer bar of paraseptal cartilage
oc	occipital artery
op	ophthalmic artery
pa	posterior auricular artery
pac	papillary cartilage
pb	petrosal bone
pc	paraseptal cartilage
pd	posterior belly of digastric muscle
pf	piriform fenestra
pme	posterior meningeal artery
pmx	premaxilla
pnf	posterior nasal fossa
pp	palatine papilla
ps	proximal stapedial artery
ptv	pterygoid venous plexus
rc	rectus capitis muscle
rca	Reichert's cartilage
rg	artery to retropharyngeal glands
ri	inferior stapedial arterial ramus
rio	ramus infraorbitalis (artery)
rlt	retropharyngeal lymphatic tissue
rm	ramus mandibularis (artery)
rp	posterior stapedial arterial ramus
rs	superior stapedial arterial ramus
rt	temporal arterial rami
rtp	rostal tympanic process of petrosal
sa	superior alveolar artery
sap	superior alar cartilage
scg	superior cervical ganglion
sm	stapedius muscle
so	supraorbital artery
spa	sphenopalatine artery
st	stapes bone
sth	superior thyroid artery
stp	stylopharyngeus muscle
sut	superficial temporal artery
t(x,y)	arterial trunk (for arteries x and y given in parentheses)
tf	transverse facial artery
thp	thyropharyngeus muscle
tt	tensor tympani muscle
V	cranial nerve 5, trigeminal

ve	vertebral arteries
VII	cranial nerve 7, facial
VIII	cranial nerve 8, vestibulocochlear
vnd	vomeronasal duct
vno	vomeronasal organ
X	cranial nerve 10, vagus
XII	cranial nerve 12, hypoglossal
za	zona annularis

MATERIALS AND METHODS

Soft-tissue characters were obtained by examining the histologically processed specimens listed in table 2. Analysis of soft-tissue anatomy was accomplished by inspecting histological slides using a transmitted light microscope at low (1–4×) magnification. In addition, photographs of these sections were taken using a Pixera digital camera and a Macintosh Powerbook. In most cases, photographs were taken at regular intervals (e.g., every 0.05–0.1 mm) and could subsequently be ''stacked'' using the public domain NIH Image program (developed at the U.S. National Institutes of Health and available on the internet at http://rsb.info.nih.gov/nih-image). These stacks usually consist of 50–100 slices and can be used to flip through consecutive images in regions of anatomical interest.

Representations of cranial arteries were based on these histological images using a multistep process. First, images in a stack were aligned with the ''register'' option in NIH Image, using the inferior nasal septum, basisphenoid, mandibular condyle, and epitympanic recess as landmarks. Second, structures of interest in each slice of a stack (e.g., ossified parts of the basicranium and arterial branches) were manually selected; other parts of the image were deleted. Third, from this modified stack a rotatable three-dimensional image was created using the ''project'' option of NIH Image; from this projection an image of this stack at an optimum viewing angle was produced on an ink-jet printer. Fourth, the image was manually traced with pencil and paper; finally, this tracing was scanned into Adobe Photoshop, appropriately colored, and labeled using Adobe Illustrator.

Representations of nasal cartilages were also based on histological sections, but used the wax-plate method introduced by Born (1883) and later modified by W. Maier (Zoologisches Institut, Universität Tübingen). In this procedure, the relevant anatomical structures were first traced onto 2-mm styrofoam plates using a transmitted light microscope equipped with a camera lucida. Styrofoam tracings were then cut out and glued together to create a three-dimensional model of this region. Photographic slides were taken of the three-dimensional reconstruction, and from these a preliminary pencil and paper tracing was made. The Uni-Tübingen departmental graphic artist, Gabriela Schmid, then re-drew the tracing into the final figure with an airbrush under the supervision of the author and W. Maier.

The figures produced using these methods accurately represent the anatomical relations of cranial arteries and nasal cartilages. The existence of major cranial arteries is not difficult to verify in most histologically prepared specimens; however, the preservation of smaller, more distal branches may depend on numerous technical vagaries. The specimen of *Echinops telfairi* (table 2), for example, preserved arteries in unusually good detail and allowed for the reconstruction of such small, terminal branches as the posterior meningeal branch of the occipital artery (fig. 2). In other specimens this vessel was either absent or did not preserve well enough to be traced. It is also important to consider that histologically processed material has undergone invasive processing (e.g., decalcification and dehydration) that may distort the proportions of some anatomical structures. Therefore, absolute measurements of such specimens must be taken with great caution.

Morphological Character Coding

From the anatomical descriptions made possible by these methods, a number of discrete anatomical characters were constructed. No single method of transforming morphological observations into characters appropriate for phylogeny algorithms is without drawbacks (Strong and Lipscomb, 1999). Variable morphology coded into binary ''presence/absence'' characters maximally subjects primary hypotheses of homology

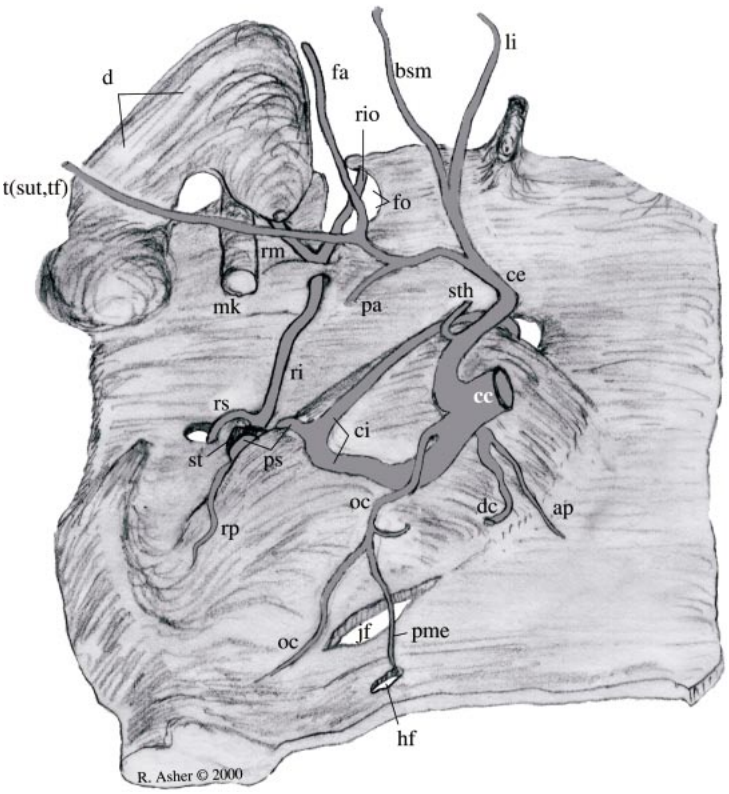

Fig. 2. Reconstructed cranial vasculature of *Echinops telfairi* (ZIUT HL 18). Specimen is figured in ventral aspect; lateral is at left, anterior at top.

(sensu De Pinna, 1991) to falsification (Pleijel, 1995; Lee and Bryant, 1999). With this coding method, a researcher's assumptions about evolutionary process (i.e., transformations between multiple character states) are not concealed within a single character. However, this method may spuriously overweight as ''absent'' characters that are in fact inapplicable (Strong and Lipscomb, 1999; Lee and Bryant, 1999). To continue an example used by Maddison (1993), organisms that lack a tail would be coded as ''absent'' for other characters regarding tail pigmentation. Depending on how many colors are observed in tailed taxa, those that are tailless would show multiple ''homologies'' of absent blue, absent yellow, and so on. This strict binary coding falsely treats certain states as biologically real, when in fact their existence is semantic; the character state ''blue: absent'' has not actually been observed in any organism and should not provide evidence with which to define a clade (Hawkins et al., 1997; Strong and Lipscomb, 1999).

Alternatively, variable morphology may be coded into multistate characters, with ''missing'' entries used for taxa that are inapplicable for a given character. This technique avoids the overweighting and reificationist pitfalls of binary coding described above, but of course requires assumptions about evolutionary process that binary coding lacks. In addition, the treatment of inapplicable characters as ''missing'' may yield odd state assignments to ancestral nodes, as when the common ancestor of tailless taxa is optimized as having possessed a tail (Platnick et al., 1991; Strong and Lipscomb, 1999).

Given these considerations, I have attempted in this study to maximally subject primary hypotheses of homology to falsification by favoring the use of binary charac-

TABLE 2
Specimens Examined in Histological Collections[a]

Taxon	ID	CRL	SVL	HL	ST(μm)	S	EM	Age[b]
Blarina brevicauda	Asher's collection			≈25.0	15	HE	P	neo/postnatal
Canis lupus Frankfurt Zoo specimen	ZIUT		57	20.0	12	AD	P	embryo
Chrysochloris asiatica	ZIUT	95.0		25.0	30	AH	C	neo/postnatal
Crocidura russula (every second slice mounted)	ZIUT	65.0		≈24.0	15	A	P	neo/postnatal
Didelphis azarae	ZIUT		26	13.5	10	AD	P	embryo
Echinops telfairi	ZIUT		33	18.0	10	AH	P	fetus
Echinops telfairi (specimen from AIM)	Asher's collection			≈35.0	20	HE	P	neo/postnatal
Erinaceus europaeus	ZIUT		37	19.0	10	A	P	embryo
Erinaceus europaeus	ZIUT		31	19.0	10/20	A	P	embryo
Erinaceus "romanicus" (= *E. concolor*)	ZIUT			≈35.0	40	A	C	neo/postnatal
Geogale aurita	MCZ 45499			≈14.0	15	AD	P	neo/postnatal
Geogale aurita	MCZ 45504			26.0	30	AH	C	neo/postnatal
Geogale aurita	ZIUT	50.0	43	21.0	15(1–38) 20(39–80)	AH	P	neo/postnatal
Hemicentetes semispinosus	HID 0581 (=MPIH 1964/86)	42.5		25.0	10	KB,G	P	fetus
Microgale dobsoni	HID 0601 (=MPIH 1964/103)	31.0		15.0	10	KB,G	P	fetus
Microgale pusilla	MNHN 1912-68 (in ZIUT collection)		50	22.0	20	AD	P	neo/postnatal
Micropotamogale lamottei	IZEA 939 (in ZIUT collection)			≈50.0	40	AH	C	neo/postnatal
Micropotamogale lamottei	AIG C2273 I			≈7.3	10	WA	P	embryo
Micropotamogale lamottei	AIG C2273 III			≈9.1	10	A/et al.	P	embryo
Micropotamogale lamottei	AIG B1227 (boxes 0176-0177)			≈37.9	40–50	A	C	neo/postnatal
Nandinia binotata	AIG E2211			≈11.0	10	A	P	embryo
Orycteropus afer (only middle ear sections available)	ZIUT	105.0		65.0	40	AH	C	neo/postnatal
Potamogale velox (Coll. Utrecht, M545)	ZIUT		30	17.0	10	AD	P	embryo
Setifer setosus (1975, Poduschka collection)	ZIUT				30, 40	A	C	neo/postnatal
Setifer setosus (=MPIH 1964/93)	HID 0579	52.0		24.0	10	K-B	P	fetus
Solenodon paradoxus (nose only)	ZIUT				15	A	P	neo/postnatal

TABLE 2
(Continued)

Taxon	ID	CRL	SVL	HL	ST(μm)	S	EM	Age[b]
Solenodon sp. (currently at AMNH) (middle ear only)	MPIH 6863	123		87	15	A, PAS-AB	P?	neo/postnatal
Sorex araneus	HID 0715 (= MPIH 1964/102a)		≈12.5		10	A	P	embryo
Sorex araneus	ZIUT	40			15	AD	P	neo/postnatal
Tenrec ecaudatus	ZIUT		32.0	20	10	AD	P	fetus
Tenrec ecaudatus	AMNH-B InSer20			14	10	A, HE	P	embryo
Tenrec ecaudatus	AMNH-B InSer49			35	10	A, HE	P	neo/postnatal

[a]Abbreviations: **A**, Azan stain; **AD**, Azan-Domagk stain; **AH**, Azan-Heidenhain stain; **C**, celloidin embedding medium; **CRL**, crown rump length, tip of head to rump in fetal position; **EM**, embedding medium; **G**, Gabe stain; **HE**, hematoxylin and eosin stain; **HL**, head length; **ID**, institutional provenance/other identification of specimen; **K-B**, Klübe-Barerra stain; **P**, paraffin embedding medium; **PAS-AB**, periodic acid Schiff-alcian blue stain; **S**, stain; **SVL**, snout-vent length, from apex to coccyx (= SSL, Scheitel-Steiß Länge); **ST**, slice thickness; **WA**, Weigert-Azophloxin stain.

All units are in millimeters, except where noted.

All series are cut in frontal (= coronal) sections, except where noted.

[b]Age is divided into three categories based on development of deciduous teeth: embryo (teeth not fully developed), fetus (teeth not fully erupted), and neo/postnatal (teeth erupted). The postnatal category includes adults.

ters, but have employed multistate characters in cases where binary coding would have resulted in overly redundant, morphologically unobserved, or (following Simmons and Geisler, 1998) uninformative characters.

DESCRIPTION OF MORPHOLOGICAL CHARACTERS

Many important reviews with information on mammalian cranial anatomy have been written during the past 150 years (e.g., Dobson, 1882; Parker, 1885; Tandler, 1899; Fischer, 1901; Broom, 1896, 1897, 1916; Leche, 1902, 1907; Sicher, 1913; De Beer, 1929, 1937; Roux, 1947; Lindahl, 1948; Maier, 1980; MacPhee, 1981, Wible, 1984; Novacek, 1993). Several of these authors have focused on one or both of two anatomical regions: (1) arterial pattern to cranial organs and (2) anterior nasal capsule anatomy. Discussion in this paper is organized around these two areas. From these descriptions, several characters are presented. For some taxa, multiple sectioned individuals of different ontogenetic stages are available (table 2), allowing for description of polymorphisms and differences during ontogeny. The approximate age of all specimens is listed in table 2.

Anatomical descriptions are accompanied by frequent references to original histological sections (table 2). In the Zoologisches Institut, Universität Tübingen (ZIUT) and American Museum of Natural History Bluntschli (AMNH-B) collections, references to original sections are made by indicating the slide, column, and row numbers. For example, slide 11 of the ZIUT 20-mm head length (HL) *Tenrec ecaudatus* specimen (table 2) has 25 slices on it, distributed across 5 columns and 5 rows. The second anteriormost slice on this slide is the second slice of the first column, and would be indicated in the following text by "11.1.2". More posterior slices are indicated by higher column and row numbers. Histological specimens processed by Heinz Stephan during his time at the Max Planck Institut für Hirnforschung (MPIH) in Frankfurt (e.g., *Microgale dobsoni*) are labeled according to the distance in 0.01 mm units from the starting point of sectioning; thus, slice 200 is 2 mm posterior to

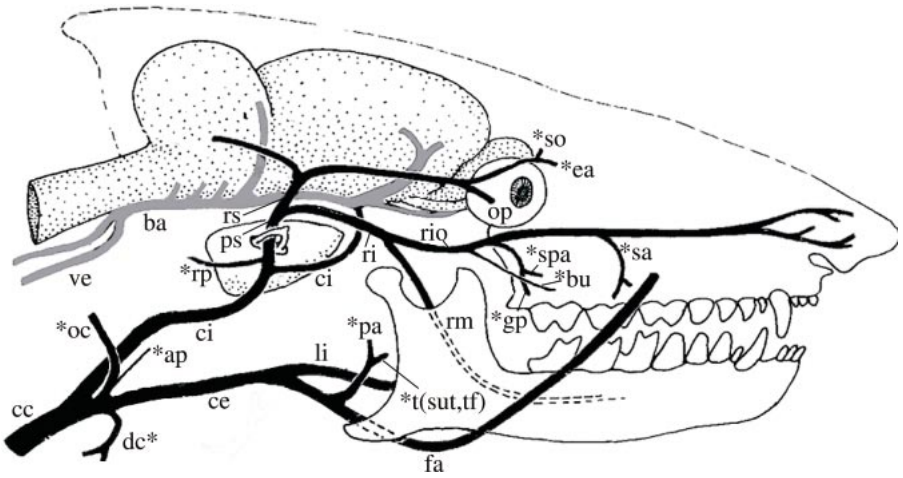

Fig. 3. Hypothesized pattern of cranial arterial supply in a primitive placental mammal (after Cartmill and MacPhee, 1980 and Wible, 1984). Asterisks indicate an artery commonly found among tenrecids, but not necessarily inferred as part of primitive pattern by authors cited above.

the tip of the rostrum and lies 2 mm anterior to slice 400.

Cranial Arterial Supply

Several authors have described what is hypothesized to be the primitive arterial pattern upon which modern placentals have acquired modifications to varying degrees (e.g., Bugge, 1974; Presley, 1979; Cartmill and MacPhee, 1980; Wible, 1984, 1987; Wible et al., 2001). The possibility that this pattern actually describes primitive states for tenrecid or other insectivoran groups remains to be demonstrated. Nevertheless, it is useful for descriptive purposes and is shown in figure 3. In addition to the proximal stapedial, internal, and external carotid branches discussed by the above authors as primitive for placental mammals, figure 3 depicts several terminal branches of the stapedial and external carotid arteries that are frequently observed among tenrecids.

In this primitive cranial arterial pattern, the common carotid artery ascends in the neck and divides into the internal and external carotid arteries. Along the ventrum of the pars cochlearis, the internal carotid gives off the proximal stapedial artery and continues anteriorly in a transpromontorial position (sensu Wible, 1986). After passing through the stapes, and still within the middle ear, the stapedial artery bifurcates into superior and inferior rami. The superior ramus leaves the tympanic cavity, running dorsad and forward into the sinus canal. The inferior stapedial ramus continues anteriorly along the ventrum of the tympanic roof. After leaving the middle ear, it bifurcates into the ramus infraorbitalis and ramus mandibularis ventral to foramen ovale (Wible, 1984: 40, 186; 1987: 121). The ramus infraorbitalis runs forward toward the infraorbital canal and face, and the ramus mandibularis supplies the jaw.

Through these carotid branches, most of the head receives blood supply: the brain and eye via the internal carotid artery (supplemented by the vertebral arteries); the mandible and infraorbital region via the inferior stapedial ramus; the meninges, supraorbital, and part of the nose via the superior stapedial ramus; and the occiput, tongue, face, palatine, buccal, and temporal regions via the external carotid. Wible (1987) has noted that certain placentals (e.g., armadillos), and possibly the basal eutherian *Prokennalestes* (Wible et al., 2001), have a connection between the superior stapedial and occipital vasculature via the arteria diploëtica magna. Hence, this condition may also characterize the placental common ancestor; however, the relations of the arteria diploëtica magna were not recorded in this study.

Among the mammals described below, *Echinops* and *Micropotamogale* best approx-

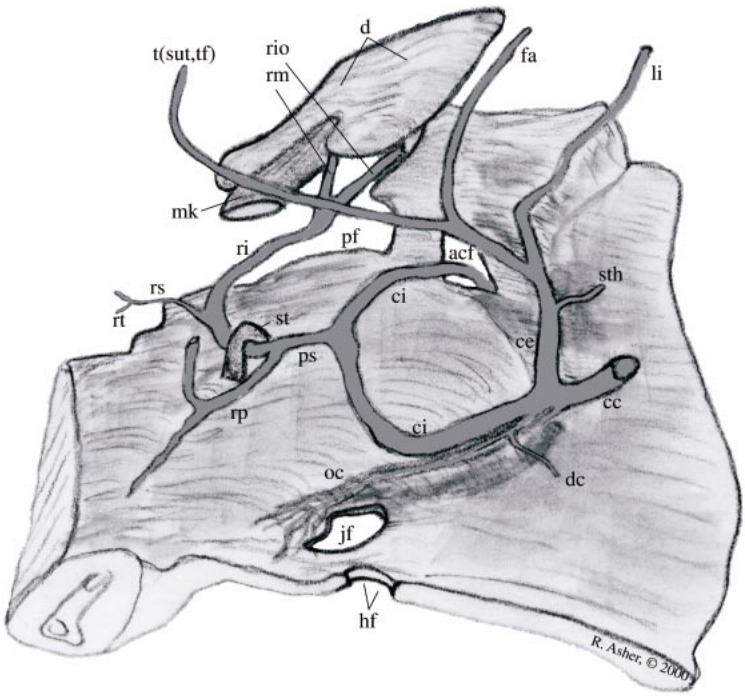

Fig. 4. Reconstruction of cranial arteries in *Potamogale velox* (ZIUT HL 17 mm). Orientation as in figure 2.

imate the pattern shown in figure 3, exhibiting variations only in supply to the eye. Otherwise, there are several deviations from this arterial pattern exhibited by living insectivorans in general and by tenrecids in particular. These are described below in six tenrecs (*Potamogale, Micropotamogale, Geogale, Microgale, Echinops,* and *Tenrec*) and the hedgehog *Erinaceus.* The descriptions proceed from proximal to distal, starting at the carotid bifurcation, then following the internal carotid, stapedial, and external carotid branches. In general, a common set of structures is described for each specimen. However, because the available histological specimens vary in quality, some specimens (e.g., the *Echinops* and 31-mm snout-vent length *Erinaceus* specimens) are described in slightly more detail than others. Descriptions are based on specimens listed after the taxonomic heading of each section. Using the technique described above, a graphic reconstruction of arteries present between the carotid bifurcation and the posterior jaw is presented for the tenrecs in figures 4–8.

Potamogale velox (ZIUT, HL 17 mm; fig. 4)

Common and internal carotid branches

The bifurcation of the common carotid in *Potamogale* lies ventrolateral to the jugular ganglion, ventral to the superior cervical ganglion, and medial to the internal jugular vein (e.g., slice 44.1.5).

The internal carotid enters the middle ear posteromedially, medial to the posterior digastric and lateral to the rectus capitis muscles (slice 43.3.4; fig. 9). In adult *Potamogale,* the internal carotid entrance (via the posterior carotid foramen) is defined by the tympanic process of the basisphenoid and the rostral tympanic process of the petrosal anteromedially, and by the caudal tympanic process of the petrosal posterolaterally. In this 17-mm HL specimen, these elements are not fully ossified and no such foramen is evident. After its entrance into the tympanic cavity, the internal carotid then travels anterolaterally along the ventrum of the pars cochlearis, eventually giving off a stapedial

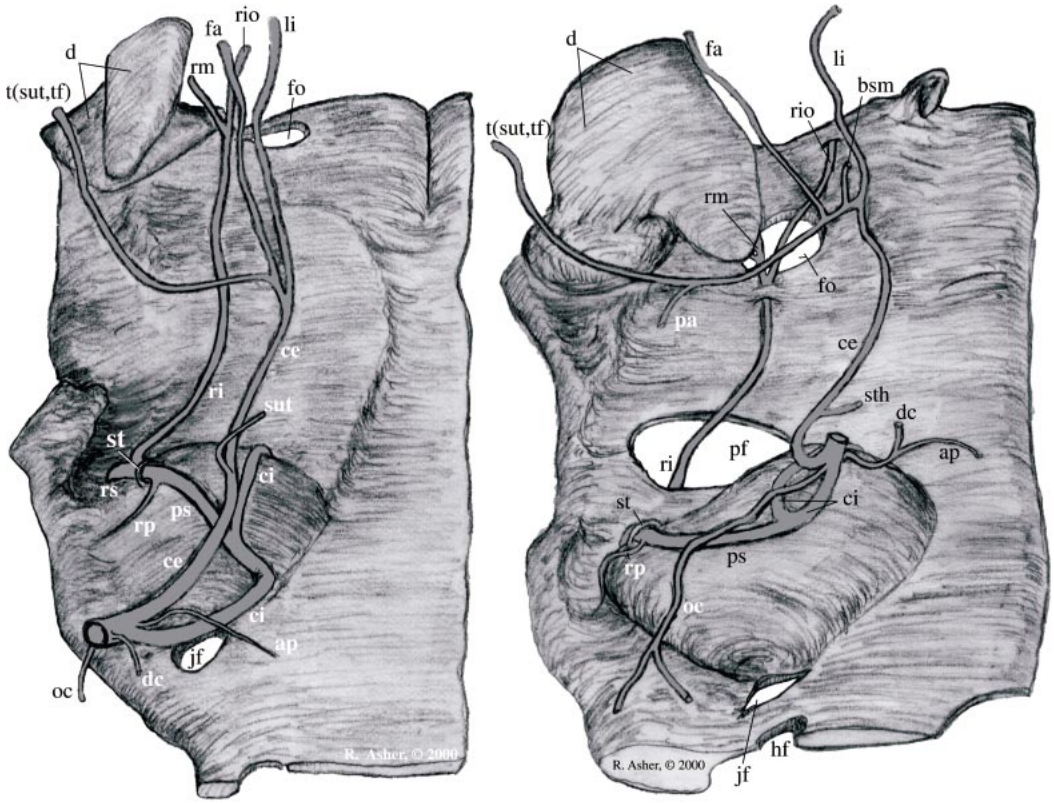

Figs. 5, 6. Reconstructions of cranial arteries; orientation as in figure 2. **5.** (Left) *Micropotamogale lamottei* (IZEA 939); **6.** (Right) *Geogale aurita* (MCZ 45499).

branch (slice 40.3.3). Distal to this point, the internal carotid artery continues anteromedially still on the ventrum of the pars cochlearis, accompanied by the internal carotid nerve (36.5.5). At the anteromedial margin of the pars cochlearis, dorsal to the auditory tube, the internal carotid artery enters the braincase via a foramen between the cartilaginous basisphenoid and petrosal (36.1.1). As the internal carotid artery courses dorsomedially, the cavernous venous sinus lies lateral to the artery and medial to the large trigeminal ganglion. At this point the internal carotid pierces the dura mater and joins the circulus arteriosus (33.3.4).

Farther anteriorly, as the optic nerve is evident passing through the cartilaginous orbitosphenoid, a branch of the circulus arteriosus apparent above the optic nerve gives off a small ophthalmic artery that follows the nerve through the optic canal (27.5.6) and farther distally to the eye itself.

Dorsal to the cavum epiptericum, a large branch from the circulus arteriosus runs laterally along the internal margin of the braincase (29.5.6). This is the middle cerebral artery. In the 17-mm HL *Potamogale* specimen branches from this vessel are thin-walled and difficult to trace, but they appear to annex most of the supply to the cranial meninges. This is accomplished in most other animals discussed here by the stapedial-supplied middle meningeal artery.

Stapedial branches

Before its passage through the obturator foramen of the stapes, the stapedial artery gives off a posterior stapedial branch. This artery leaves the tympanic cavity and enters the stapedius fossa, where it supplies the stapedius muscle. It then courses laterally, posterior to the facial nerve, and ramifies as it passes into the occipital region.

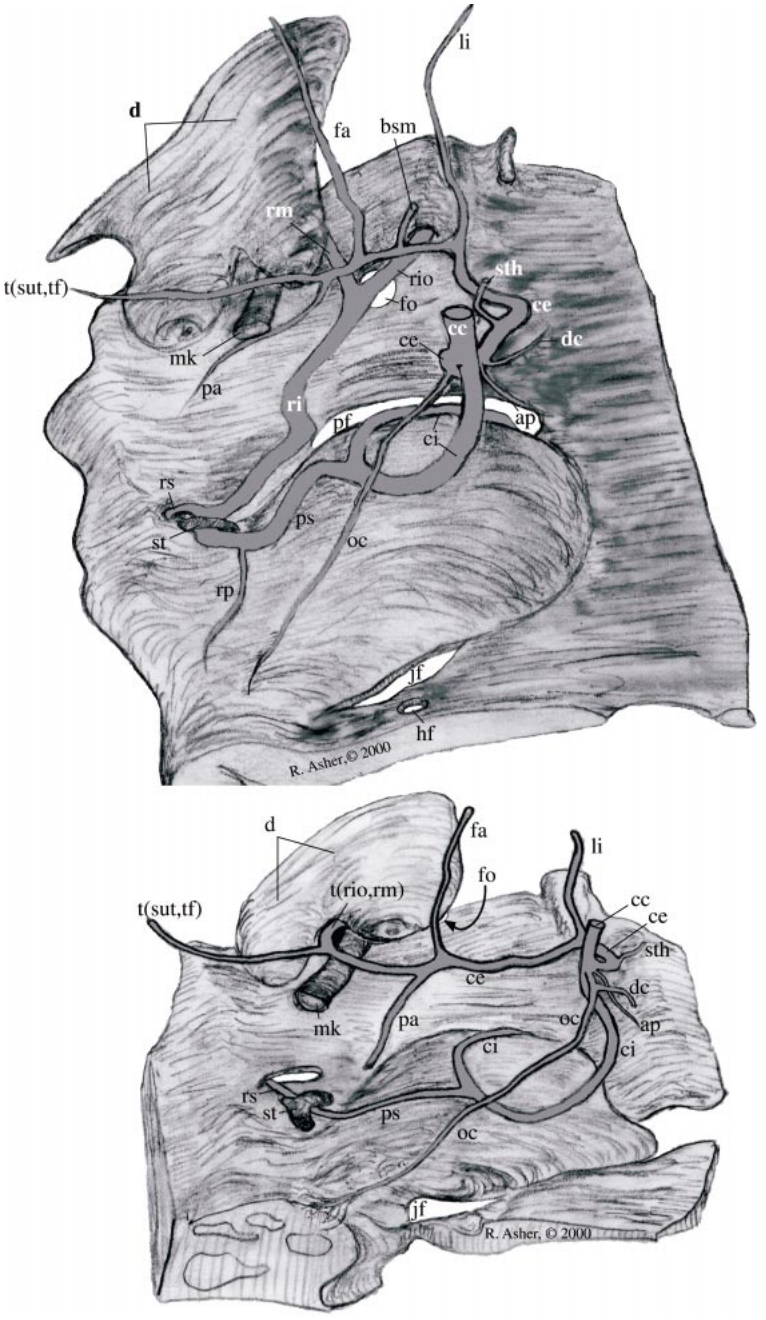

Figs. 7, 8. Reconstructions of cranial arteries; orientation as in figure 2. **7.** (top) *Microgale dobsoni* (MPIH 1964/103); **8.** (bottom) *Tenrec ecaudatus* (ZIUT HL 20 mm).

Distal to the stapes, the stapedial artery courses ventral to the facial canal. Still within the tympanic cavity, and at the anterior margin of the cartilaginous facial canal, it gives off a small superior ramus (slice 38.3.5); this branch travels laterally on the roof of the middle ear, medial to the incus, and exits the tympanic cavity medial to the


9
sm
rp
rc
pd
ci
lc
es

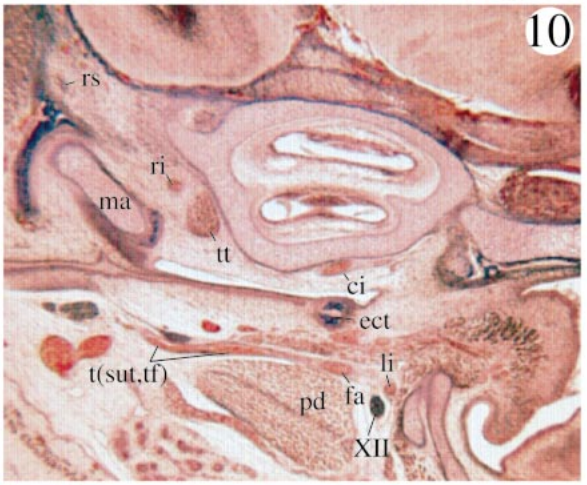
10
rs
ri
ma
tt
ci
ect
t(sut.tf)
li
pd
fa
XII

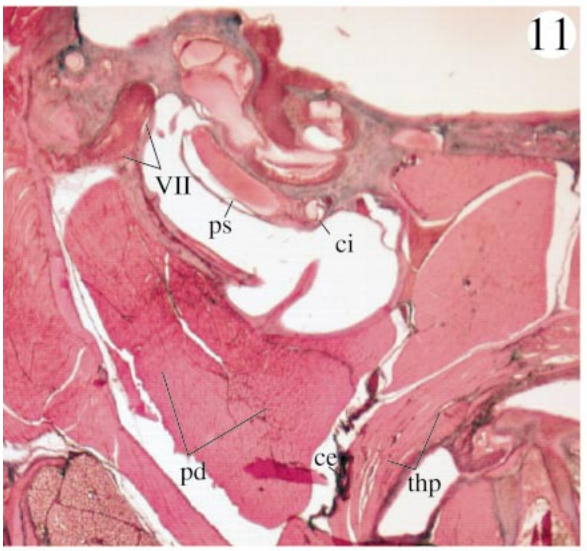
11
VII
ps
ci
pd
ce
thp

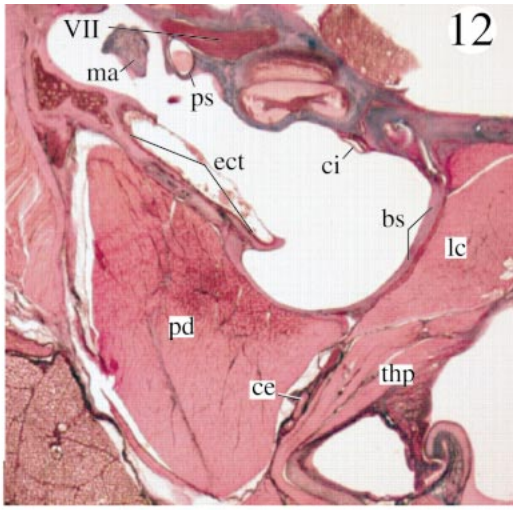
12
VII
ma
ps
ect
ci
bs
lc
pd
ce
thp

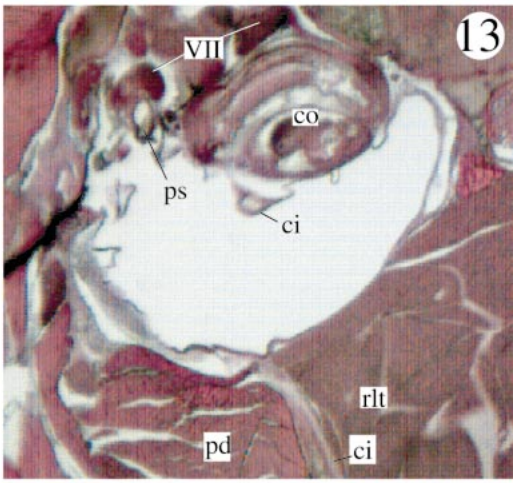
13
VII
co
ps
ci
rlt
pd
ci

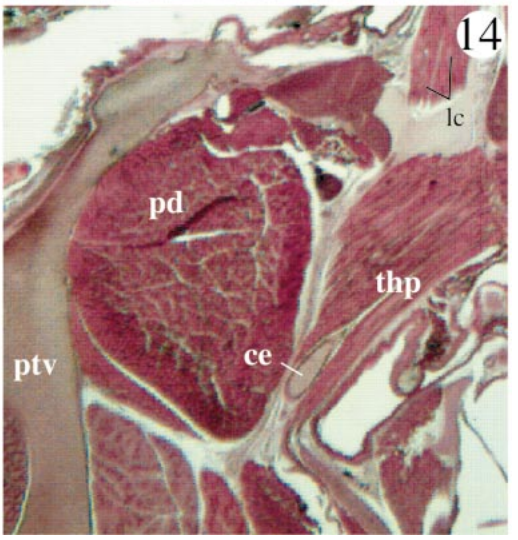
14
lc
pd
thp
ptv
ce

epitympanic recess before entering the braincase. Superior stapedial branches at this point are very small and hard to trace, but they appear to supply some temporal musculature via small foramina in the squamosal dorsal to the epitympanic recess, as well as a minor part of the cranial dura. In contrast to other tenrecids, and to insectivorans generally, the superior stapedial ramus of *Potamogale* is not a major cranial artery. This is consistent with the observation that the sinus canal (the anteroposteriorly directed conduit on the internal aspect of the squamosal that carries the superior stapedial ramus in most insectivorans) is absent in adult *Potamogale* skulls (Asher, 1999; contra McDowell, 1958).

After bifurcation of the superior and inferior rami, the inferior stapedial ramus courses anteromedially along the roof of the middle ear, medial to the malleus and lateral to the tensor tympani muscle (slice 37.2.3; see fig. 10). It leaves the middle ear anteriorly, just anterolateral to the origin of the tensor tympani muscle, without passing through a foramen in the alisphenoid. Immediately posterior to foramen ovale, and within the fibers of the lateral pterygoid muscle, the inferior stapedial ramus bifurcates into the mandibular and infraorbital rami (slice 34.5.3). Distal to this bifurcation, the mandibular division of the trigeminal nerve exits the foramen ovale, traveling with the ramus mandibularis toward Meckel's cartilage. Farther anteriorly, the ramus infraorbitalis passes dorsomedially through a foramen in the cartilaginous anlage of the alisphenoid, or the alisphenoid canal (e.g., slice 32.5.1). Thereafter, it runs within the secondary braincase, immediately ventral to the large trigeminal ganglion.

Soon after exiting the sphenorbital fissure and entering the orbitotemporal fossa, still ventral to the first two trigeminal divisions, the ramus infraorbitalis gives off a buccal branch laterally (27.5.5). Farther distally, the ramus infraorbitalis gives off a dorsal palatine branch medially (27.2.2), which courses ventromedially toward a sulcus leading to the palate, and gives off no major sphenopalatine branch, but supplies only the greater palatine artery. However, a vein is apparent traversing the dorsal palatine canal and draining the posterior nasal fossa ventrolaterally, via a foramen superior to the greater palatine canal.

Distal to the origin of the dorsal palatine artery, the ramus infraorbitalis continues in its path ventral to the maxillary division of the trigeminal nerve. As the maxillary division of the trigeminal approaches the infraorbital canal, the artery divides into several sub-branches. One of these runs dorsolaterally toward the eye (23.2.6); this may be a homologue of the ''lacrimal'' branch, even though this specimen of *Potamogale* does not have a lacrimal gland. Another branch runs ventrolaterally, and within the short infraorbital canal, it enters a foramen in the maxilla as a superior alveolar artery (21.5.4). The remaining infraorbital arteries travel along with the branches of the maxillary division of trigeminal, through the short infraorbital canal, and supply the face.

External carotid branches

At a point very close to the carotid bifurcation, two occipital branches leave the external carotid, coursing posterolaterally (44.1.5). Both of these contribute to the arterial component of a vascular plexus (e.g., 47.3.1) situated in a fascial plane between the sternomastoid (lateral) and posterior body of the digastric (dorsomedial). Rostral to this occipital plexus, the occipital artery sends a descending branch ventromedially that runs posterior to the common carotid, lateral to longus colli muscle fibers (47.3.1), and is accompanied by a vein. This is probably the

←

Figs. 9–14. Coronal sections through middle ear of tenrecid genera, as follows. **9.** *Potamogale velox* (ZIUT HL17 mm), anterior to jugular foramen, slice 43.3.4. **10.** *Potamogale velox* (ZIUT HL 17 mm), posterior to anterior carotid foramen, slice 37.2.5. **11.** *Micropotamogale lamottei* (IZEA 939), anterior to jugular foramen, slice 181.2.2. **12.** *Micropotamogale lamottei* (IZEA 939), posterior to anterior carotid foramen, slice 177.2.1. **13.** *Geogale aurita* (MCZ 45504), anterior to jugular foramen, slice 105.3.1. **14.** *Geogale aurita* (MCZ 45504), anterior to anterior carotid foramen, slice 96.1.2.

carotid anastomotic channel for the deep cervical artery; however, it is impossible to be sure because the subclavian origin of the deep cervical artery takes place below the plane of sectioning in this specimen.

Between the digastric muscle (laterally) and longus capitis (medially), and ventral to the hypoglossal nerve, the external carotid gives off two small branches ventromedially to the region of the larynx and thyroid gland (40.2.1).

At a point lateral to the thyroid cartilage and medial to the hypoglossal nerve, the lingual artery leaves the external carotid trunk (37.2.3; fig. 10). It reaches the posterior margin of the tongue via a path medial to fibers of the hyoglossus muscle and lateral to posterior hyoid cartilage. Dorsal to the body of the hyoid bone, it enters the tongue.

Distal to the lingual artery, the external carotid courses laterally in a plane dorsal to the digastric muscle and ventral to the anterior margin of the ectotympanic bone (37.2.3; fig. 10). Here the external carotid divides into the facial artery, which initially travels dorsal to the digastric muscle, and a trunk for the posterior auricular, superficial temporal, and transverse facial arteries. No obvious posterior auricular artery is evident leaving the external carotid. However, in the region where it is expected to originate from the external carotid (close to the facial and lingual arteries), vessels are small and difficult to trace; hence, its perceived absence may be an artifact of preservation in this specimen.

Micropotamogale lamottei (IZEA 939; fig. 5)

Common and internal carotid branches

The common carotid artery bifurcates ventral and posterior to the auditory bulla (204.2.2), lateral to longus capitis and ventromedial to sternomastoid muscles. Compared to the younger specimen of *Potamogale* described above, the carotid in this *Micropotamogale* specimen bifurcates at a more inferior point in the neck. The internal carotid enters the middle ear via a foramen defined by the basisphenoid anteromedially and caudal tympanic process of the petrosal posterolaterally (186.1.2), and gives off the stapedial artery on the ventrum of the pars cochlearis (181.2.2; fig. 11). Both arteries are of very large caliber relative to the inner ear. The internal carotid artery travels for a short distance dorsomedially, in a transpromontorial position, before entering the braincase via the anterior carotid foramen in the tympanic roof, anteromedial to the pars cochlearis and lateral to the root of the basisphenoid bullar wall (173.1.2; fig. 12).

Stapedial branches

Before passing through the stapes, the proximal stapedial artery gives off a posterior stapedial artery (183.2.1), which courses into the stapedius fossa and supplies the stapedius muscle. After passing through the stapes, the stapedial artery divides into superior and inferior rami medial to the epitympanic recess and within the middle ear (173.1.2). The superior ramus then enters the braincase via a foramen in the tympanic roof medial to the epitympanic recess, travels dorsolaterally toward the cranial sidewall, and enters the sinus canal. No temporal branches are evident near the stapedial bifurcation, but they may originate farther distally from the superior stapedial ramus.

The inferior stapedial ramus courses anteromedially along the roof of the middle ear, passing medial to the ectotympanic anterior crus (165.2.1). At the posterior margin of the mandibular condyle and anterior margin of the ectotympanic, the inferior stapedial ramus leaves the middle ear medial to the auditory tube (163.2.1). Prior to the origin of the ramus mandibularis, the inferior ramus is separated from the trigeminal ganglion by the alisphenoid. It then passes ventral to the foramen ovale and bifurcates into the ramus mandibularis (coursing ventrolaterally with the mandibular trigeminal branch) and ramus infraorbitalis (154.2.2). Adjacent to this bifurcation, anterior to the foramen ovale and posterior to the alisphenoid canal, is the opening of the transverse canal (156.2.1), which drains a sinus within the basisphenoid bone (McDowell, 1958: 147). Anterior to the foramen ovale, the ramus infraorbitalis courses medially, giving off muscular branches laterally, before entering the cavum epiptericum via the alisphenoid canal

(152.1.2) dorsal to the origin of the lateral pterygoid muscle (149.2.2).

Slightly anterior to the lateral wall of the sphenorbital fissure, the ramus infraorbitalis gives off a buccal branch (114.1.2) that travels anterolaterally, amidst temporalis muscle fibers, dorsal to the toothbearing posterior maxilla, toward the lateral wall of the oral cavity. Medial to the origin of the buccal artery, the dorsal palatine artery branches off from the ramus infraorbitalis (114.1.2). The dorsal palatine artery travels ventromedially toward the posterior palate, and sends off a sphenopalatine branch medially into the choanae of the nasal fossa, accompanied by a nerve, before continuing anteriorly as the greater palatine artery.

The ramus infraorbitalis continues anteriorly, ventral to the infraorbital nerve, and sends off a small arterial branch dorsally through the fibers of the nerve (103.1.1). This artery continues anteriorly with other infraorbital arterial and nervous branches, and passes through the short infraorbital canal. Immediately distal to this small infraorbital sub-branch, a superior alveolar artery is given off from the main ramus infraorbitalis (e.g., slice 99.2.1) and courses ventromedially relative to the infraorbital nerve. In slice 90.2.1, the main ramus infraorbitalis, traveling ventrolateral to the infraorbital nerve, divides again into two arteries of similar caliber, both of which travel through the infraorbital canal along its ventrolateral margin (e.g., 85.2.1).

External carotid branches

At the carotid bifurcation, a small ascending pharyngeal branch is evident running dorsomedially (199.2.2). Posterior to the bifurcation, a slightly larger artery is visible branching from the carotid and coursing medially (206.2.1). For the same reasons enumerated above for *Potamogale*, this is most likely the carotid anastomotic channel for the deep cervical artery. The occipital artery is apparent lateral to the separate external carotid in slice 203.2.2. The next visible external carotid branch anterior to the carotid bifurcation is a superior thyroid artery, running ventromedially (194.1.2).

The external carotid then continues anteriorly, lateral to the thyropharyngeus (or inferior constrictor) muscle and medial to the digastric muscle (e.g., 173.1.2; fig. 12). Ventral to the anterior margin of the ectotympanic and tubal canal, the external carotid divides into a lingual artery, a small branch that enters the body of the digastric muscle, and an arterial trunk for the facial and temporal external carotid branches (169.1.2). As in *Potamogale* described above, no posterior auricular artery is evident in this specimen.

Geogale aurita (MCZ 45504, 45499; fig. 6)

Common and internal carotid branches

Unless specified otherwise, observations below are based on MCZ 45504. The carotid bifurcation is apparent between the sternomastoid (laterally) and longus capitis (medially) muscles (107.1.2). Near the origin of the external carotid, an occipital artery is evident beginning a posterolateral course from the common carotid (slice 106.2.1 of MCZ 45504). This artery runs through lymphatic tissue continuous with the retropharyngeal region, and subsequently passes between the digastric (dorsally) and sternomastoid (ventrolaterally) muscles, supplying nearby structures en route, and eventually those in the occiput.

The internal carotid runs dorsally, lateral to retropharyngeal lymphatic tissue (106.3.2; fig. 13). Very close to its entrance into the ventral apex of the tympanic cavity, defined posteriorly by the tympanic processes of the petrosal, the internal carotid gives off the proximal stapedial artery (106.3.2; fig. 13). The internal carotid artery then comes into contact with the pars cochlearis, running anteromedially from the ventral apex of the pars cochlearis to the anterior carotid foramen. This foramen is located lateral to the body of the sphenoid and medial to the anterior pole of the petrosal, and provides passage for the internal carotid into the braincase, where it supplies the circulus arteriosus.

Stapedial branches

The proximal stapedial artery is evident passing through the stapes ventral to the facial nerve (106.2.1; fig. 13). Just proximal to

the stapes, a posterior stapedial ramus is evident coursing posterolaterally (107.3.1). Distal to the stapes, the proximal stapedial courses dorsolaterally, adjacent to the facial canal. Unfortunately, none of the available sectioned *Geogale* specimens (table 2) preserves ossifications in the middle ear perfectly. Nevertheless, it is evident that prior to its bifurcation, the stapedial artery passes dorsal to the facial nerve and origin of the tensor tympani muscle via a foramen in the petrosal, close to the piriform fenestra. It bifurcates into inferior and superior rami within the braincase (103.3.2; see also MCZ 45499 slice 44.4.2).

The superior stapedial ramus gives off a temporal branch via a foramen in the squamosal dorsal to the epitympanic recess. Distally, it supplies the cranial meninges during its anterior course within the sinus canal. Anteriorly, branches from the superior stapedial ramus are evident leaving the sinus canal foramen close to the dorsal margin of the sphenorbital fissure (e.g., in slice 27.4.4 of MCZ 45499). One of these arteries reenters the braincase via the ethmoid foramen and courses anteriorly on the dorsolateral margin of the nasal fossa, along the floor of the anterior cranial fossa. Another courses anterolaterally ventral to the cranial sidewall, just medial to the origin of temporal musculature and dorsal to the optic nerve (e.g., slice 26.1.1 of MCZ 45499). This supraorbital artery, accompanied by a nerve, passes dorsal to the eyeball and supplies lacrimal gland tissue along the way. A stapedial-supplied ophthalmic artery is evident coursing ventrally to a position adjacent to the optic nerve, at which point it moves laterally with the nerve toward the eyeball.

The inferior stapedial ramus first becomes distinct at the lateral end of the geniculate ganglion of the facial nerve (MCZ 45504, slice 102.3.2). It travels anteromedially lateral to the nerve and leaves the braincase via the piriform fenestra. The ramus inferior travels within the tympanic cavity until a point close to the anterior margin of the ectotympanic (MCZ 45504, slice 92.3.2), where it passes through a distinct foramen in the alisphenoid bone and leaves the middle ear (e.g., MCZ 45499, slice 37.3.4).

Ventral to foramen ovale and amidst fibers of the mandibular division of the trigeminal nerve, the inferior stapedial ramus bifurcates into mandibular and infraorbital arterial rami (MCZ 45504, slice 88.1.1). Immediately after its origin, the ramus mandibularis gives off a branch laterally that travels dorsal to the lateral pterygoid muscle toward the temporomandibular joint (86.2.1) and is accompanied by a nerve from the mandibular division of the trigeminal. The artery and nerve pass just anterior to the synovial capsule of the temporomandibular joint and enter the body of the temporalis muscle as the muscle inserts along the posterior margin of the coronoid process (e.g., slice 31.3.4 of MCZ 45499).

The ramus infraorbitalis travels anteriorly, past foramen ovale and mandibular nerve fibers, before entering the cavum epiptericum via an alisphenoid canal and running ventral to branches of the trigeminal nerve (MCZ 45499, slice 33.1.3). At the sphenorbital fissure, the ramus infraorbitalis gives off a buccal artery laterally, followed thereafter by a dorsal palatine artery that courses ventromedially into a common recess leading to the sphenopalatine and greater palatine foramina (slice MCZ 45499, slice 26.4.2). Just posterior to the maxillary toothrow, a superior alveolar artery is evident leaving the ramus infraorbitalis (MCZ 45499, slice 23.4.5). Distal to the superior alveolar artery, the ramus infraorbitalis divides into two smaller arteries that remain in proximity to the infraorbital nerve as it passes through the infraorbital canal.

External carotid branches

The first visible branch from the external carotid is a common trunk for the ascending pharyngeal and a branch that anastomoses with the deep cervical branch of the subclavian artery (slice 104.2.2). The latter artery runs medially from the external carotid and starts a posteroinferior course just lateral to the longus capitis muscle. The ascending pharyngeal artery travels dorsally lateral to the longus capitis muscle, sends off branches into nearby lymphatic tissue, and courses dorsomedially toward the skull base. Distal to the ascending pharyngeal trunk, the external carotid gives off a superior thyroid artery

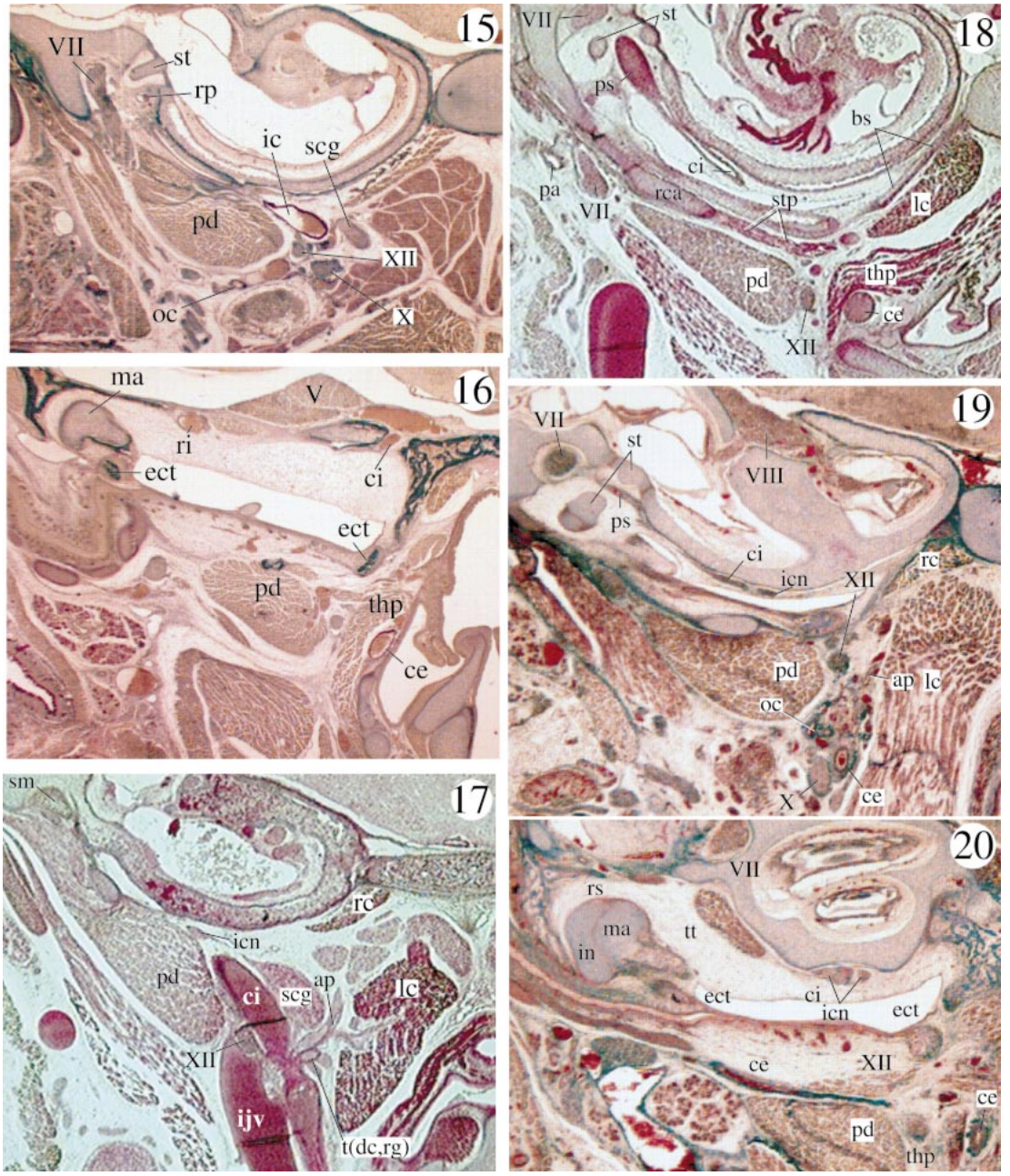

Figs. 15–20. Coronal sections through middle ear of tenrecid genera, as follows. **15.** *Microgale dobsoni* (MPIH 1964/103), anterior to jugular foramen, slice 1190. **16.** *Microgale dobsoni* (MPIH 1964/103), through anterior carotid foramen, slice 1080. **17.** *Echinops telfairi* (ZIUT HL 18 mm), anterior to jugular foramen, slice 68.1.1. **18.** *Echinops telfairi* (ZIUT HL 18 mm), posterior to anterior carotid foramen, slice 63.4.2. **19.** *Tenrec ecaudatus* (ZIUT HL 20 mm), anterior to jugular foramen, slice 67.1.4. **20.** *Tenrec ecaudatus* (ZIUT 20 mm), posterior to anterior carotid foramen, slice 61.2.4.

(slice 101.2.2). No other major branches leave the external carotid until after it passes medial to a slip of thyropharyngeus muscle (e.g., slice 96.1.2; fig. 14). Distal to this point, the external carotid divides into a laterally coursing trunk for the facial, posterior auricular, superficial temporal, and transverse facial arteries, and an anteriorly coursing trunk for the lingual artery (e.g., slice 39.1.4 in MCZ 45499). Close to this division, it also gives off a small branch that travels toward the submandibular gland. After giving off the facial artery, the lateral trunk courses posterior and slightly ventral to the angular process of the jaw (e.g., slices 40.1.3 to 40.3.3 in MCZ 45499); it does not travel in the space between the condyle and angular process as is the case in some other specimens (e.g., *Echinops*) described here.

Microgale dobsoni (MPIH 1964/103; fig. 7)

Common and internal carotid branches

The internal and external carotid arteries bifurcate lateral to the longus capitis muscle and posteroventral to the superior cervical ganglion (1130). The ascending pharyngeal (running dorsomedially) and a branch to the thyroid region (ventromedially) are evident at the bifurcation (1140). The occipital artery also takes its origin from this region, evident proximally in its lateral course sandwiched between the internal jugular vein and common carotid (1150).

The internal carotid artery enters the middle ear lateral and anterior to the superior cervical ganglion (slice 1190; fig. 15). In most adult *Microgale* skulls, the rostral and caudal tympanic processes of the petrosal form a low ridge that weakly defines a sulcus, dorsal to which the internal carotid enters the middle ear (MacPhee, 1981: 209). However, no discrete posterior carotid foramen is present, and the internal carotid enters the middle ear via an unossified membrane medial to the posterior digastric muscle and posterior to Reichert's cartilage (slice 1190; fig. 15). Within the middle ear, the internal carotid artery courses anteromedially along the ventrum of the pars cochlearis, eventually entering the braincase via an anterior carotid foramen medial to the anterior petrosal, within the epitympanic wing of the sphenoid (slice 1080; fig. 16). An older *M. pusilla* individual (table 2) also shows the foramen within the sphenoid tympanic roof, but farther anterior to the pars cochlearis (e.g., slice 51.3.1). This variability (due either to ontogeny or interspecific difference) corresponds with the uncertainty expressed by MacPhee (1981: 209) as to the position of the anterior carotid foramen in *Microgale*. He figured (p. 209) the anterior carotid foramen as occurring within the piriform fenestra close to the sphenoid-petrosal suture, or more anteriorly within the sphenoid epitympanic wing.

Anterior to the entrance of the internal carotid artery into the braincase, as the optic nerve leaves the braincase via the optic canal, an ophthalmic artery originates from the circulus arteriosus and runs with the nerve inside the canal (e.g., slice 830).

Stapedial branches

A posterior stapedial arterial ramus of large-caliber branches off from the proximal stapedial ventral to the stapes (slice 1190; fig. 15). The posterior ramus courses laterally through the stapedius fossa and continues posterolaterally to enter the occipital region at a point ventral to the petromastoid and dorsolateral to the posterior body of the digastric muscle (slice 1280).

Distal to its passage through the stapes, the stapedial artery travels along the medial roof of the epitympanic recess, lateral to the facial canal. At this point, still within the tympanic cavity, the stapedial bifurcates into superior and inferior rami, both of large caliber (slice 1130). The superior ramus passes through a foramen in the roof of the epitympanic recess to supply the cranial meninges and enter the sinus canal. The inferior ramus courses anteriorly along the roof of the middle ear, passing lateral to the origin of the tensor tympani muscle. As the inferior ramus passes ventral to foramen ovale, it bifurcates into mandibular and infraorbital arterial rami (slice 960). The ramus mandibularis follows the mandibular branch of the trigeminal nerve toward the mandibular foramen of the jaw. The ramus infraorbitalis runs anteriorly, passing through the alisphenoid canal and coursing ventral to the trigeminal ganglion.

The ramus infraorbitalis emerges from the inferior margin of the sphenorbital fissure ventral to the infraorbital nerve and medial to a large vein (slice 800). As the sphenorbital fissure opens into the orbitotemporal fossa, the ramus infraorbitalis gives off two branches (slice 770): one dorsolaterally to supply a buccal artery and the lacrimal and orbital regions, and another ventromedially to supply the dorsal palatine and sphenopalatine arteries. Above the posterior margin of the maxillary toothrow, the ramus infraorbitalis gives off a superior alveolar artery, which passes through a foramen in the maxilla at the posterior margin of the infraorbital canal to supply the upper cheek teeth. As the ramus infraorbitalis enters the infraorbital canal, it ramifies with the branches of trigeminal maxillary nerve; by the anterior margin of the canal, both artery and nerve show distinct branches for supply of the face (slice 570).

External carotid branches

Very close to the carotid bifurcation, the occipital artery originates ventral to the hypoglossal nerve and medial to the internal jugular vein (slice 1150). As the occipital artery passes ventral to the jugular vein, the vein gives off an accompanying vessel (slice 1200). The occipital artery then enters a fascial plane between the digastric and sternomastoid muscles and continues to course posterolaterally.

Just anterior to the origin of the occipital artery, the external carotid gives off dorsomedially running ascending pharyngeal and ventromedially running anastomotic deep cervical branches (slice 1140). Larger than both of these is the superior thyroid artery, originating slightly more distally from the external carotid and coursing ventrally adjacent to the thyroid cartilage. Immediately after giving off the superior thyroid artery, the external carotid passes medial to a slip of thyropharyngeus muscle (slice 1100: fig. 16). Distal to this slip of muscle, the external carotid divides into the lingual artery, a branch to the submandibular gland, and a common trunk for the facial, posterior auricular, and distal branches to the temporal and facial regions (slice 1020).

Echinops telfairi (ZIUT, HL 18 mm; fig. 2)

Common and internal carotid branches

The common carotid bifurcates immediately ventral to the superior cervical ganglion and medial to the internal jugular vein (68.1.1; fig. 17).

After its separation from the external carotid (e.g., slice 67.4.1), the internal carotid travels anterolaterally toward the middle ear promontory. As in other adult tenrecines, the posterior ventrum of the auditory bulla is not ossified, and the internal carotid passes through no foramen as it enters the tympanic cavity. The internal carotid reaches the promontorium and gives off the proximal stapedial artery (63.4.2; fig. 18). The superior cervical ganglion lies medial and posterior to the artery as it reaches the pars cochlearis (68.1.1; fig. 17), and sends off the internal carotid nerve to accompany the internal carotid artery as it travels on the ventrum of the pars cochlearis. After the internal carotid artery gives off the stapedial branch (63.4.2; fig. 18), the internal carotid artery and nerve course to the anteromedial margin of the pars cochlearis, where they enter the braincase via a foramen in the sphenoid, posterior and dorsal to the auditory tube (e.g., slice 54.3.2). Shortly thereafter, the internal carotid artery pierces the dura mater and joins the circulus arteriosus, medial to the trigeminal nerve (50.4.2).

Stapedial branches

Prior to passing through the obturator foramen of the stapes, the proximal stapedial artery gives off a small posterior stapedial ramus (65.2.2) which exits the tympanic cavity posterolaterally, adjacent to the facial nerve. Lateral to the stapes, the stapedial artery runs ventral to the facial canal, at which point (still within the middle ear) it divides into large superior and inferior rami (60.3.2). The superior ramus enters the braincase via a foramen in the roof of the epitympanic recess, where it supplies branches to the meninges and temporal musculature (slice 58.4.4) before entering the sinus canal.

As the superior stapedial ramus leaves the sinus canal anteriorly through a foramen in the partially ossified alisphenoid bone (e.g., 37.5.3), located in the dorsal margin of the sphenorbital fissure, it supplies the ophthalmic artery. The latter vessel courses adjacent to the optic nerve and follows it toward the eyeball. Anterior to the ophthalmic artery, the superior stapedial ramus gives off two arteries that enter the anterior cranial fossa via ethmoid foramina: one medially, supplying the posterior ethmoidal region via olfactory foramina of the cribriform plate, and another laterally, supplying the meninges of the anterior cranial fossa (33.5.4). The distalmost portion of the superior stapedial ramus, the supraorbital artery, remains extracranial after leaving the dorsal margin of the sphenorbital fissure, and runs anteriorly along a path ventral to a venous sinus, medial to the eye, and lateral to the nasal capsule (slice 34.3.3).

The inferior stapedial ramus continues on the roof of the middle ear, just lateral to the tensor tympani muscle. Anterior to the cochlea, medial to the posterior margin of the jaw joint, the inferior ramus exits the tympanic cavity via a foramen within the body of the alisphenoid (53.1.2), immediately posterior to the foramen ovale. As the inferior ramus passes ventral to the foramen ovale, it bifurcates into a large ramus mandibularis, accompanied in its ventrolateral course by the mandibular division of the trigeminal nerve (50.4.2), and a ramus infraorbitalis that continues anteriorly. Immediately after its origin, the ramus mandibularis gives off a branch to the temporomandibular joint that courses laterally along the posterior margin of the glenoid fossa, dorsal to the body of the lateral pterygoid muscle (50.4.2).

Unlike most other tenrecs examined here, the ramus infraorbitalis does not reenter the braincase via a distinct alisphenoid canal, but instead via the anterior part of the foramen ovale. Once in the cavum epiptericum, the infraorbital runs ventrally to the trigeminal ganglion and gives off small branches to surrounding structures (e.g., ventrally to the medial pterygoid muscle via the anterior portion of foramen ovale in slice 48.4.4). Anterior to the cavum epiptericum, as the sphenorbital fissure opens laterally into the orbitotemporal fossa, the infraorbital gives off a large buccal branch laterally (slices 37.5.2 and 41.2.2). This artery travels anterolaterally, passing posterior to the upper toothrow to supply the buccal wall of the oral cavity. The ramus infraorbitalis then gives off a dorsal palatine branch medially (37.5.2). Accompanied by the dorsal palatine nerve, this artery enters a common recess for the sphenopalatine and greater palatine vessels and nerves. Distally within the descending palatine canal, the dorsal palatine artery divides into a greater palatine (e.g., slice 33.5.4) and smaller sphenopalatine branch. The former courses ventromedially toward the dorsal margin of the hard palate, accompanied by the greater palatine nerve. The sphenopalatine branch continues medially and passes into the respiratory channel of the nasal fossa.

Distal to its palatine branches, the ramus infraorbitalis continues its anterior course ventral to the infraorbital nerve. At a point dorsal to the posterior margin of the upper toothrow, the ramus infraorbitalis sends laterally a common trunk for the lacrimal and superior alveolar arteries (slice 30.2.4). Within the short infraorbital canal, the ramus infraorbitalis divides into several distinct branches, most of which travel with branches of the maxillary division of the trigeminal to structures of the face (slice 17.5.5).

External carotid branches

Very close to the carotid bifurcation, the external carotid gives off a single arterial trunk that in turn divides into two branches: the occipital artery laterally, and a common trunk leading to ascending pharyngeal, lymphatic, and deep cervical branches medially. This trunk leaves the external carotid directly ventral to the superior cervical ganglion (68.1.1; fig. 17) and supplies a slender, dorsomedially running ascending pharyngeal branch that courses along the medial margin of the longus capitis muscle (slice 66.3.1; fig. 17), supplying it en route to a space between the basisphenoid and medial

promontory. No major extension of the ascending pharyngeal artery enters the braincase. Ventral to the origin of the ascending pharyngeal artery from the medial trunk is another artery that courses posteromedially (slices 70.2.1, 68.1.1; fig. 17). Lateral to the sympathetic cervical chain, this artery breaks up into smaller vessels supplying the lymphatic tissue between the basisphenoid and posterior pharyngeal region (70.2.1). One branch from this artery travels posteroventrally, lateral to longus capitis, longus colli, and transverse processes of superior cervical vertebrae.

The occipital trunk runs laterally adjacent to the hypoglossal nerve (70.2.1). Farther distally, it connects to a large, ventromedially coursing recurrent branch that communicates with retropharyngeal lymphatic tissue (slice 71.2.2). Distal to this point it gives off a small posterior meningeal branch that follows the hypoglossal nerve toward the hypoglossal foramen (slice 72.3.2) and into the posterior cranial fossa. The occipital artery then courses posterolaterally toward the occiput in a plane between the posterior digastric and sternomastoid muscles.

Anterior to the occipital-ascending pharyngeal trunk and lateral to the thyroid cartilage, the external carotid gives off a large ventromedially running superior thyroid artery (slice 66.2.1). Anterior to the origin of the superior thyroid, the external carotid passes medial to a slip of thyropharyngeus muscle (e.g., slice 63.4.2; fig. 18), emerging from this brief lateral cover as the stylopharyngeus muscle passes dorsally over it (slice 61.4.2). Dorsolateral to the thyroid cartilage the external carotid divides into a laterally coursing common trunk for the facial, temporal, and posterior auricular branches (58.3.1) and a medially coursing trunk for the mylohyoid, submandibular, and lingual arteries. Anteriorly, the lateral trunk gives off a superficial temporal/transverse facial trunk that runs anterolaterally toward the posterior margin of the jaw, ventral to the mandibular condyle and dorsal to the angular process of the mandible. The facial artery is situated at the inferior margin of the mandible during much of its anterior course (e.g., slice 53.1.2).

Tenrec ecaudatus (ZIUT, HL 20 mm; fig. 8)

Common and internal carotid branches

The common carotid bifurcates lateral to the longus capitis muscle and medial to the ventrally running vagus nerve (e.g., slices 64.4.4 and 65.4.4).

The internal carotid enters the posteriorly unossified middle ear lateral to the superior cervical ganglion, medial to the digastric muscle (70.2.4), and is accompanied by the internal carotid nerve. It then turns anteriorly onto the ventrum of the cochlea, giving off the stapedial branch (slice 67.1.4; fig. 19). The internal carotid artery then continues anteriorly, entering the braincase medial to the pars cochlearis via a foramen in the basisphenoid close to its articulation with the petrosal. Well anterior to the entrance of the internal carotid artery into the braincase, a branch from the circulus arteriosus is apparent within the optic canal, traveling with the optic nerve (46.1.2). This ophthalmic artery continues anteriorly with the nerve to supply the eyeball.

Stapedial branches

The proximal stapedial passes through the obturator foramen of the stapes (67.1.4; fig. 19) without giving off a posterior stapedial branch. It then continues dorsolaterally, ventral to the facial nerve, dorsal to the malleus within the epitympanic recess, entering the cranial cavity via a space just medial to the squamosal tympanic roof (slice 61.3.4). Within the braincase, it travels lateral to a venous sinus and medial to the cranial diploë, supplying the middle meningeal artery. No inferior stapedial ramus is evident throughout the course of the stapedial artery through the tympanic region.

External carotid branches

Close to the carotid bifurcation, a very small ascending pharyngeal artery is apparent coursing dorsomedially, lateral to fibers of the longus capitis muscle and medial to the hypoglossal nerve (e.g., slice 67.1.4; fig. 19). The occipital artery also leaves the carotid stem close to its bifurcation and courses posteriorly along the ventromedial margin of

the digastric muscle, following the muscle to its origin. As in *Potamogale*, the occipital artery forms a vascular plexus associated with several venous channels ventral to the origin of the digastric muscle (e.g., slice 78.3.4).

Sharing a common trunk with the occipital artery is a small branch that travels posteriorly, immediately lateral to longus capitis and colli muscles (e.g., slice 66.4.4), toward the atlantoaxial joint, at which point is becomes small and difficult to trace.

Anterior to the carotid bifurcation, the external carotid courses anteromedially and gives off a superior thyroid branch that courses ventromedially toward the thyroid gland and cartilage (62.4.4). Distal to this branch, a slip of muscle attaching to the thyroid lamina and a ligamentous raphe connected dorsally to the basicranium (thyropharyngeus or inferior pharyngeal constrictor) passes lateral to the external carotid (61.2.4; fig. 20).

Lacking an inferior stapedial ramus, the jaw and infraorbital region of *Tenrec ecaudatus* are supplied via branches of the external carotid. At a point defined by the tympanic membrane dorsally, hypoglossal nerve medially, and digastric muscle ventrally, the external carotid bifurcates into a large, laterally running trunk and an anteriorly running lingual artery, which supplies the tongue. The laterally running trunk first gives off facial and posterior auricular arteries (e.g., slice 62.3.1). At a point between the angular process and condyle of the mandible, it bifurcates into a trunk for the superficial temporal and transverse facial arteries, and a larger trunk for the mandibular and infraorbital arterial rami (57.2.2). As it reaches the superior margin of Meckel's cartilage, this trunk divides into the ramus infraorbitalis and ramus mandibularis (53.4.1). The former runs ventral and posterior to the mandibular division of the trigeminal nerve and continues medially to enter the alisphenoid canal slightly anterior to the foramen ovale (51.1.2). Thereafter, the ramus infraorbitalis runs ventral to the trigeminal nerve within the cavum epiptericum. The ramus mandibularis continues anteriorly dorsolateral to Meckel's cartilage and medial to the jaw.

Erinaceus europaeus (ZIUT, SVL 31 and 37 mm), *E. concolor* (ZIUT, HL 33 mm)

Common and internal carotid branches

The common carotid in *Erinaceus europaeus* (ZIUT 31-mm SVL) bifurcates as it is sandwiched lateral to the superior cervical ganglion and medial to the vagus nerve, close to the jugular ganglion (e.g., slide 55 of the 31-mm SVL individual). Just as the internal carotid branch is about to enter the middle ear, the ascending pharyngeal leaves the internal carotid and moves dorsomedially (56.2.2), giving off branches medially en route (slice 54.3.2). A large artery, presumably occipital, is evident lateral to the sternomastoid muscle in all three available *Erinaceus* specimens (e.g., slices 54.1.1 to 50.2.4 in the 31-mm SVL individual). In more anterior slices, this large artery runs ventrally, following the common carotid into the neck and presumably joining with it. The origin of this artery from the common carotid well proximal to the internal-external bifurcation seems likely based on their proximity on the inferior margin of the sections. However, this cannot be verified, as both arteries run below the plane of sections in all available *Erinaceus* specimens.

After the internal carotid gives off the proximal stapedial artery within the tympanic cavity, the internal carotid artery continues anteromedially along the ventrum of the pars cochlearis accompanied by the internal carotid nerve, and enters the braincase via the anterior carotid foramen, located between the basisphenoid and cochlea (e.g., 57.1.3 of the 37-mm SVL *E. europaeus*). The greater petrosal nerve leaves the facial geniculate ganglion and joins the internal carotid nerve shortly before the anterior carotid foramen (e.g., slice 50.1.2 in the 31-mm SVL *E. europaeus,* slice 57.1.3 in the 37-mm SVL *E. europaeus,* and slice 141.1.2 in the adult *E. concolor*). This nerve enters the pterygoid ''canal'' (which is actually very short in the younger specimens) at the anteromedial margin of the ventral cochlea, just anterior to the anterior carotid foramen (e.g., slice 47.3.3 in the 31-mm SVL *E. europaeus*). In the *E. concolor* specimen, a very small vidian artery runs anteromedially from its internal carotid origin and is situated medial to the

nerve of the pterygoid canal throughout most of its course (e.g., slice 129.2.1).

In the younger specimens (31-mm SVL and 37-mm SVL *E. europaeus*), the ophthalmic artery arises from the internal carotid (via the circulus arteriosus) and accompanies the optic nerve through the optic canal. However, the *E. concolor* specimen shows a series of arteries arising from the infraorbital that supply optic structures; no artery accompanies the optic nerve through the optic canal. Bugge (1974: fig. 4B), based presumably on adult specimens, also figured optic supply as arising from the inferior stapedial ramus (which is posteriorly continuous with the infraorbital) in *Erinaceus europaeus.* Interestingly, he figures optic blood supply in another erinaceine, *Hemiechinus auritus,* as arising from the superior stapedial ramus (1974: fig. 4A).

Posterior stapedial branches of *Erinaceus*

Just prior to passing through the stapes, the proximal stapedial artery of the 31-mm SVL *Erinaceus* individual gives off a posteriorly running posterior stapedial ramus (56.2.2). This artery enters the stapedius fossa, then runs ventral to the digastric muscle just prior to passing into the occiput (slice 61.3.1), appearing relatively large in caliber.

MacPhee (1981: 202–203) noted that the posterior stapedial artery was not universally present in the *Erinaceus* samples available to him. He suggested that in older specimens, this ramus involutes. In the different sample available for this study there is also variation; only the specimen described above (the smallest and presumably youngest individual) shows a posterior ramus originating immediately medial to the stapes, proximal to the passage of the stapedial artery through the obturator foramen. Neither the 37-mm SVL *Erinaceus europaeus* nor the postnatal *E. concolor* show a branch leaving the proximal stapedial prior to passing through the stapes within the tympanic cavity. However, both of these specimens show a posterolaterally directed branch with a more proximate carotid origin, close to the bifurcation and ventromedial to the middle ear. In the *E. concolor* specimen, this branch leaves the internal carotid dorsal to a mass of thyroid glandular tissue and the hypoglossal nerve and ventrolateral to longus capitis muscles (190.1.2). It then runs laterally toward the posterior origin of the digastric muscle, at which point it curves dorsolaterally around the petromastoid bone and gives off branches en route (210.1.2). In the 37-mm SVL *Erinaceus* specimen, an arterial branch leaves the carotid very close to its bifurcation, sharing a common trunk with the ascending pharyngeal artery (68.3.2). It then runs laterally, passing dorsal to the hypoglossal nerve, posterolateral to the jugular (vagus) ganglion, anterior to the internal jugular vein, and between the digastric (dorsally) and sternomastoid (ventrally) muscles (slice 74.1.4). As it runs behind the skull, it curves around the ventral margin of the petromastoid.

In its relationship to the petromastoid and posterior digastric, this branch resembles the posterior stapedial artery of the younger *Erinaceus* individual. However, in its relationship to the hypoglossal nerve, sternomastoid muscle, ascending pharyngeal (of the 37 mm SVL specimen), and jugular vein, it resembles the occipital artery of most other animals described here. If this branch is an occipital artery, the identity of the large, laterally coursing vessel present in all three *Erinaceus* specimens would be in question.

Bugge (1974: plate 1B) figured a large artery supplying the occiput with an origin close to the carotid bifurcation; however, the figure is cropped distal to the bifurcation, so it is unclear if the origin of this ''occipital'' artery is proximal to this point. Less ambiguous is Tandler (1899:746), who documented in at least one *Erinaceus europaeus* individual an occipital artery that originates from the internal carotid close to its origin, distal to the carotid bifurcation.

Hence, three conclusions may be drawn based on these observations: (1) the posterior stapedial artery is unambiguously present in only the smallest (and presumably youngest) of the *Erinaceus* specimens described here, (2) all three *Erinaceus* specimens observed in this study (table 2) show a large artery supplying the occipital region that most likely originates from the common carotid, ventral to its bifurcation, and (3) given the results of Tandler (1899), some polymorphism

regarding the origin of the occipital artery is present in *Erinaceus.*

Other stapedial branches

Lateral to the stapes obturator foramen, the stapedial artery bifurcates into superior and inferior rami ventral to the facial canal, within the tympanic cavity (51.1.1 of 31-mm SVL *Erinaceus*). The superior stapedial ramus then enters the braincase via a foramen medial to the malleus in the epitympanic recess and enters the sinus canal, where it supplies cranial meninges and, via laterally running branches that pierce the squamosal, temporal musculature.

Anteriorly, as the superior stapedial leaves the sinus canal foramen in the *E. concolor* specimen, it gives off a supraorbital branch laterally and a trunk for two terminal branches: one entering the anterior braincase on the posterolateral nasal roof (ethmoidal artery), and the other turning dorsally and entering the diploë of the anterior cranial fossa (anterior meningeal artery; see *E. concolor* slice 103.1.1). In the younger two *Erinaceus* specimens, supraorbital and ethmoidal branches are also evident. However, the distal superior ramus branches of the younger two specimens differ from *E. concolor* in some respects. First, the anterior meningeal branch of the 37-mm SVL *E. europaeus* specimen is highly reduced. Second, the 31-mm SVL *E. europaeus* shows a small branch moving ventrally toward the lacrimal region proximal to its ethmoidal branches.

Distal to the bifurcation of the inferior and superior stapedial rami in the 31-mm SVL *E. europaeus* specimen (51.1.1), the inferior ramus travels along the roof of the middle ear, runs anterior to the origin of the tensor tympani muscle, and leaves the tympanic cavity without passing through any bony foramen. However, in the older *E. concolor* specimen, and in some dried adult skulls (e.g., ZIUT m140), a foramen in the alisphenoid for passage of the inferior ramus is evident. Ventral to foramen ovale, amidst fibers of the trigeminal mandibular division, the inferior ramus bifurcates into mandibular and infraorbital arterial rami (47.2.3). Distal to this bifurcation, the ramus infraorbitalis courses anteriorly along the margin of the alisphenoid bone. At no point in any of the available *Erinaceus* specimens does the ramus infraorbitalis reenter the braincase via an alisphenoid canal or travel within the cavum epiptericum. However, in the 31 mm SVL *E. europaeus* specimen, the ramus infraorbitalis passes through a short alisphenoid canal with an anterior terminus lateral to the sphenorbital fissure, osteologically similar to the condition in *Galerix* as figured by Butler (1988: 119).

Slightly anterior to the opening of the sphenorbital fissure in the 31-mm SVL *E. europaeus*, the ramus infraorbitalis gives off three branches: a small artery that runs laterally to the masseter, the dorsal palatine artery that runs medially toward the dorsal palatine foramen, and a small branch that moves dorsolaterally toward posterior ocular nerves and muscles (slice 41.3.2). Farther anteriorly, lateral to the infraorbital nerve and dorsal to a pterygoid vein, the ramus infraorbitalis gives off a buccal branch (slice 40.1.3) which runs anterolaterally, anterior to the base of the coronoid process.

Dorsal to the maxillary toothrow, the ramus infraorbitalis gives off an anterolaterally directed branch that runs ventral to the lacrimal gland and dorsal to the zygomatic process, giving off branches along the way and eventually reaching superficial tissues ventral to the eye (slice 31.2.2). The ramus infraorbitalis then, along with the accompanying nerve, enters the infraorbital canal, within which it gives off superior alveolar branches to the adjacent upper toothrow. Within the infraorbital canal, the ramus infraorbitalis divides into smaller sub-branches.

External carotid branches

The 37-mm SVL *Erinaceus* specimen shows a common trunk for the ascending pharyngeal and an occipital-like artery close to the carotid bifurcation (68.3.2). Farther distally, a superior thyroid branch runs ventromedially from the external carotid (slice 68.2.3). The external carotid continues anteriorly, medial to the hypoglossal nerve and ventral to the glossopharyngeal nerve (slice 65.3.3), and remains lateral to the thyropharyngeus muscle throughout its course (see also slice 190.1.2 in *E. concolor*).

As it approaches the origin of the thyropharyngeus muscle and cartilaginous anlage of the lateral hyoid, the external carotid divides into the lingual artery and a trunk for the posterior auricular, facial, and distal temporal branches. The latter vessels run laterally dorsal to the digastric muscle (slice 59.2.3).

List of Arterial Characters

From the preceding descriptions, a number of characters can be used to summarize observed morphological variation. Admittedly, these characters do not represent all of the observed variation. Additional characters regarding, for example, the anastomosis of the stapedial system with an arteria diploëtica magna (Wible, 1987) may be of use in future studies. Nevertheless, the characters defined below reflect consistent and easily identifiable differences in arterial supply across the observed taxa.

Among humans it is well known that differences exist in arterial supply across individuals; for example, the facial and lingual arteries in humans variably arise independently from the external carotid or share a common trunk (Agur and Lee, 1991: 562). With this in mind, differences observed above regarding, for example, the origins of the ascending pharyngeal, anastomotic channel for the deep cervical, and sphenopalatine arteries are not used here to form phylogenetic characters. On the other hand, some characters may vary during ontogeny but appear to be consistent among older stages (e.g., involution of an intratympanic posterior stapedial ramus in *Erinaceus*). The apparent absence of an external carotid-supplied posterior auricular artery in potamogalines is worth examination in future studies. However, the distribution of this small artery is not incorporated into phylogenetic analyses presented here because of the difficulty of consistently verifying its presence in the current histological sample.

Original histological sections were not available for several taxa. Data on *Bradypus* and *Dasypus* are taken from Wible (1984), on *Echinosorex* and *Tupaia* from Cartmill and MacPhee (1980), on *Procavia* from Lindahl and Lundberg (1946), and on *Talpa* from Tandler (1899), Sicher (1913), and Bugge (1974).

Characters summarized below (see also table 3) represent the intertaxon variability observed in taxa described above and others listed in table 2. As is the case for other characters defined here, polarity is not defined a priori, but rather a posteriori by the process of rooting undirected trees (Farris, 1982; Nixon and Carpenter, 1993). Hence, character state numbers listed below have no necessary bearing on polarity.

1. Posterior stapedial ramus: When present in adult taxa, this artery arises from the proximal stapedial medial to the stapes and runs posterolaterally into the stapes fossa (e.g., *Echinops,* state 0). In some taxa the proximal stapedial artery gives off no branches immediately medial to the stapes (e.g., *Tenrec,* state 1).

2. Superior stapedial ramus: In adult *Echinops,* the proximal stapedial bifurcates into superior and inferior rami after passing through the obturator foramen of the stapes. The superior ramus then courses in the sinus canal within the braincase along the surface of the lateral cranial wall (state 0). Several other taxa (e.g., *Potamogale*) show varying levels of involution of the superior stapedial ramus, all of which result in a small or absent superior ramus with supply of cranial structures such as eyes and meninges taken over by other arterial sources (state 1).

3. Inferior stapedial ramus: This inferior branch of the stapedial bifurcation, with target structures in the jaw, upper dentition, and/or face, is either present (e.g., *Echinops,* state 0) or absent (e.g., *Tenrec,* state 1).

4. Origin of ophthalmic artery: In *Setifer,* the ophthalmic artery arises from the internal carotid (state 0) and is apparent passing through the bony optic canal accompanied by the optic nerve. Several taxa show an ophthalmic artery originating from the superior stapedial ramus as it leaves the sinus canal (e.g., *Echinops,* state 1). Bugge (1974) described the ophthalmic artery in *Talpa* and *Erinaceus* as originating from the inferior stapedial-supplied ramus infraorbitalis (state 2). This pattern was also observed in the *Erinaceus concolor* specimen described above. Carnivorans such as *Nandinia* show an ophthalmic artery supplied by a branch of the

TABLE 3
Summary of Soft-Tissue Characters
(see text for full description)

No.	Name	States
1	posterior stapedial ramus	0 present; 1 reduced
2	superior stapedial ramus	0 present; 1 reduced
3	inferior stapedial ramus	0 present; 1 reduced
4	ophthalmic artery origin	0 internal carotid; 1 superior ramus; 2 infraorbital ramus; 3 external carotid
5	mandibular ramus origin	0 inferior stapedial; 1 external carotid
6	internal carotid entrance into braincase	0 medial to anterior pole of cochlea; 1 lateral to anterior pole of cochlea
7	bifurcation of stapedial artery	0 within tympanic cavity; 1 within braincase
8	course of proximal infraorbital ramus	0 within cavum epiptericum; 1 extracranial
9	course of proximal external carotid	0 medial to thyropharyngeus; 1 lateral to thyropharyngeus
10	anterior opening of vomeronasal duct	0 into nasopalatine duct; 1 into nasal fossa
11	outer bar	0 complete; 1 open
12	inferior nasopalatine duct	0 orally paired; 1 orally single
13	nasopalatine duct cartilage	0 reduced; 1 present
14	nasopalatine duct cartilage connections	0 isolated; 1 with paraseptal cartilage
15	nasolacrimal duct	0 present; 1 reduced
16	nasolacrimal duct cover	0 laterally open; 1 laterally shielded
17	papillary cartilage	0 present; 1 reduced
18	vomeronasal vessels	0 prominent; 1 scattered
19	shape of nasal septum	0 parallel; 1 oval
20	zona annularis	0 complete; 1 incomplete

external carotid (state 3). Polymorphisms are occasionally apparent in the origin of optic vasculature; hence, a given taxon may be coded as having arterial supply from multiple sources.

5. Origin of ramus mandibularis: In most taxa (e.g., *Echinops*), the arterial supply to the jaw is provided by the inferior stapedial ramus (state 0). Alternatively, the ramus mandibularis supplying the jaw may originate from the external carotid artery (e.g., *Tenrec,* state 1).

6. Internal carotid relation to anterior cochlea: As the internal carotid artery approaches the point at which it enters the braincase, it may be medial (e.g., *Microgale,* state 0; fig. 16) or lateral (*Chrysochloris,* state 1; fig. 21) to the anterior pole of the pars cochlearis of the petrosal.

7. Bifurcation of stapedial artery: Typically (e.g., *Echinops*), the proximal stapedial artery bifurcates into inferior and superior rami after passing through the obturator foramen of the stapes, within the tympanic cavity (state 0). *Geogale* and *Solenodon* (fig. 22) show a stapedial bifurcation above the roof of the middle ear, within the braincase (state 1).

8. Proximal course of ramus infraorbitalis: Posterior to the exit of the ophthalmic and maxillary divisions of the trigeminal nerve from the cranium, the ramus infraorbitalis may travel within the cavum epiptericum, ventral to trigeminal nerve bundles (e.g., *Echinops,* state 1), or it may be extracranial (e.g., *Blarina,* state 0).

9. External carotid relation to thyropharyngeus muscle: In *Echinops* (fig. 18) the external carotid passes medial to a slip of thyropharyngeus muscle, just proximal to its division into lingual, facial, and temporal trunks (state 0). Other taxa (e.g., *Micropotamogale*; fig. 12) show the external carotid artery consistently lateral to thyropharyngeal musculature (state 1).

Anterior Nasal Capsule

In a number of papers during the late 19th and early 20th centuries, Robert Broom emphasized the importance of the anterior mammalian nasal capsule for systematic purposes.

Based on nasal anatomy, Broom (1897) proposed two high-level groups of mammals: Archaeorhinata (including edentates and rodents) and Caenorhinata (including most other placental mammals). Further work (1898, 1902, 1909, 1915a, 1915b) led Broom to add aardvarks, lagomorphs, tree shrews, elephant shrews, and golden moles to his archaeorhinate grade. As this name implies, he regarded these taxa as representing a primitive grade of organization and argued that they shared several features of nasal anatomy with monotremes and marsupials. Most consistently, Broom's archaeorhinates lack cartilaginous support for the nasopalatine canal. Caenorhinates, in contrast, possess a nasopalatine canal well supported by cartilage (Broom, 1898: 712). Broom (1898) also implied that archaeorhinates often show a vomeronasal duct that opens directly into the nasal fossa. However, further study (e.g., Sánchez-Villagra, 1998, 2001) has shown that most marsupials possess a vomeronasal duct that opens directly into the nasopalatine canal, as in caenorhinates.

By focusing on the nasal region, Broom came up with taxonomic conclusions that, 100 years later, have received support from contemporary morphologists (e.g., MacPhee and Novacek, 1993) and/or molecular biologists (e.g., Mouchaty et al., 2000). These conclusions include the removal of macroscelidids, scandentians, and chrysochlorids from the ''Insectivora'' (Broom, 1915a, 1915b) and the basal position of rodents within Placentalia (Broom, 1897).

A number of other researchers have documented anatomical diversity in the nasal region across mammals (e.g., Sweet 1904; Ärnbäck Christie-Lindie, 1914; De Beer, 1929; Sturm, 1936; Reinbach, 1952a, 1952b; Kuhn, 1971; Hofer, 1977, 1982a, 1982b; Maier, 1980, 1991, 1997; Wöhrmann-Repenning, 1984, 1987, 1991; Wible and Bhatnagar, 1996; Frahnert, 1998; Asher, 1998; Mess, 1999; Göbbel, 2000; Sánchez-Villagra, 2001) and have to varying degrees noted phylogenetically informative differences. However, except for three unpublished academic dissertations (Schunke, 1996; Behrens, 1998; Asher, 2000), the anatomy of the anterior nasal capsule among tenrecs has been known only for tenrecine genera (Broom, 1915b; Roux, 1947; Hofer, 1982a); information on potamogalines, oryzorictines, and *Geogale* has until now been unavailable in the published literature. Here, I describe the anterior nasal capsule in *Potamogale*, *Micropotamogale*, *Geogale*, and *Microgale*, as well as *Echinops*, *Setifer*, *Tenrec*, *Solenodon*, and *Erinaceus.*

The following descriptions trace relevant anatomical structures as they occur from posterior to anterior. For readers who have access to some or all of the original histological material used here (table 2), section numbers are referred to throughout the descriptions in the format ''slide#.column#.row#'', as described above in the section on cranial arteries. Sections from the MPIH now located in Düsseldorf and New York are numbered by distance in 0.01 mm units from the anterior point of sectioning (typically the anterior rostrum). For some taxa, individuals representing multiple ontogenetic stages are represented (table 2). Morphological characters that vary ontogenetically will be detailed at the end of the descriptions. Each description focuses on a single individual identified after the taxon heading. Depending on availability, identifications use catalog numbers, specimen measurements, or simply institutional provenance. In all cases, details of the specimens listed in table 2 include unique aspects (e.g., section thickness, type of stain, embedding medium), which facilitate identification of the original specimen.

Maier (1993) has presented a model for the cranial anatomy of the common ancestor of placental and marsupial mammals, including information on nasal structures. Sánchez-Villagra (2001) has focused on the anatomy of the anterior nose among marsupials; and Giere et al. (1999) have discussed how one aspect of anterior nasal morphpology (the anterior opening of the vomeronasal organ) may have appeared in the therian common ancestor. In general, however, and unlike the case for cranial arteries, a widely accepted model for the anterior nasal anatomy of early placental mammals does not yet exist. Thus, the following descriptions focus on the major elements of nasal anatomy (fig. 23) as discussed by Broom (numerous papers cited above), Maier (1980), and Sánchez-Villagra (2001).

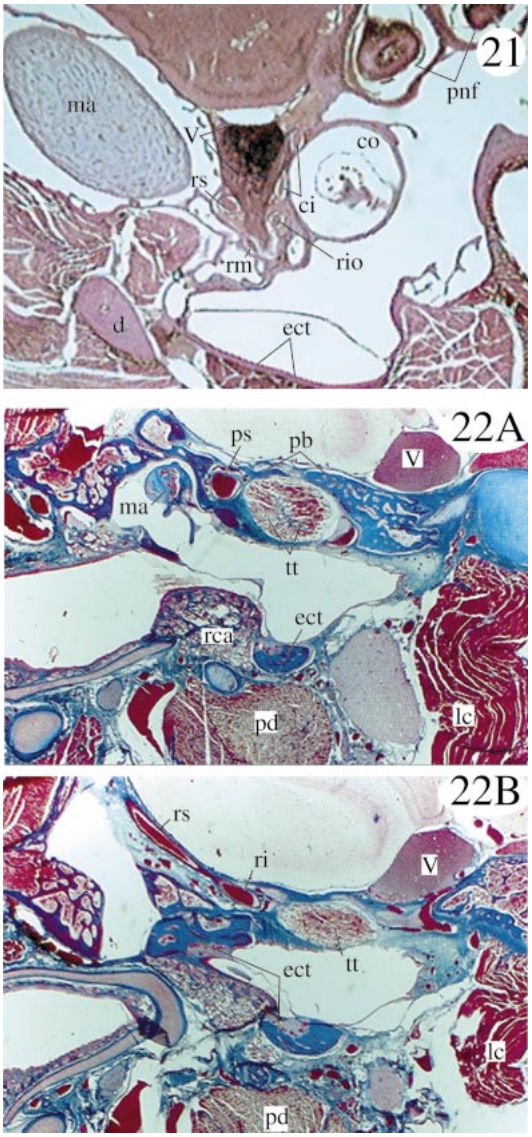

Figs. 21, 22. Coronal sections through middle ear of *Chrysochloris* and *Solenodon*; **21.** *Chrysochloris asiatica* (ZIUT HL 25 mm), slice 97.3.2. Note entrance of promontory artery into braincase lateral to anterior cochlea; contrast to fig. 16 of *Microgale*. **22A.** Epitympanic recess of *Solenodon* (MPIH 6863), slice 1270. Note undivided proximal stapedial artery passing through foramen in petrosal. **22B.** Section anterior to fig. 22A (slice 1221), showing bifurcation of stapedial artery into superior and inferior rami within braincase.

A general outline of nasal structures discussed in the following pages is as follows (see also fig. 23). The bilateral vomeronasal organ is situated anteriorly on the nasal floor, on either side of the nasal septum. A paraseptal cartilage supports the vomeronasal organ along its length. Anteriorly, the vomeronasal organ typically empties via the vomeronasal ducts into the nasopalatine ducts, which connect the nasal and oral cavities through the incisive foramina. A cartilaginous ''outer bar'' variably extends lateral to the vomeronasal duct, connecting medial and ventral components of the paraseptal cartilage. As the nasopalatine ducts empty into the oral cavity, they define a palatine papilla, situated ventral to the incisive foramina. Within this papilla, a spherical or tubelike papillary cartilage is sometimes present. The nasopalatine duct cartilage is usually evident along the lateral and posterior aspect of the nasopalatine ducts. Depending largely on the ontogenetic stage of the individual, the floor of the nasal capsule anterior to the premaxilla, or the ''anterior transverse lamina'', may be continuous with the medial aspect of the paraseptal cartilage (fig. 23B). A ''zona annularis'' is said to be present when the anterior transverse lamina is continuous with the sidewall and roof of the nasal capsule. The anteriormost nasal capsule consists of two nasal cupulae on either side of the nasal septum. Posterior and lateral to the cupulae are the cartilaginous superior alar processes. These provide attachments for small muscles of the rhinarium and variably show connections with the nasal sidewall, anterior transverse lamina, and cupular processes (fig. 23A). Variations on this general anatomical theme are described on a taxon-by-taxon basis below.

Potamogale velox (ZIUT, HL 17 mm; fig. 23)

As in other mammals, the bilateral vomeronasal organ of *Potamogale* lies on either side of the nasal septum on the nasal floor. In this specimen with a head length of 17 mm, it starts from a region below the anterior cribriform plate and stretches about 2.6 mm anteriorly to the incisive foramina. In the anteroposterior dimension, the vomeronasal or-

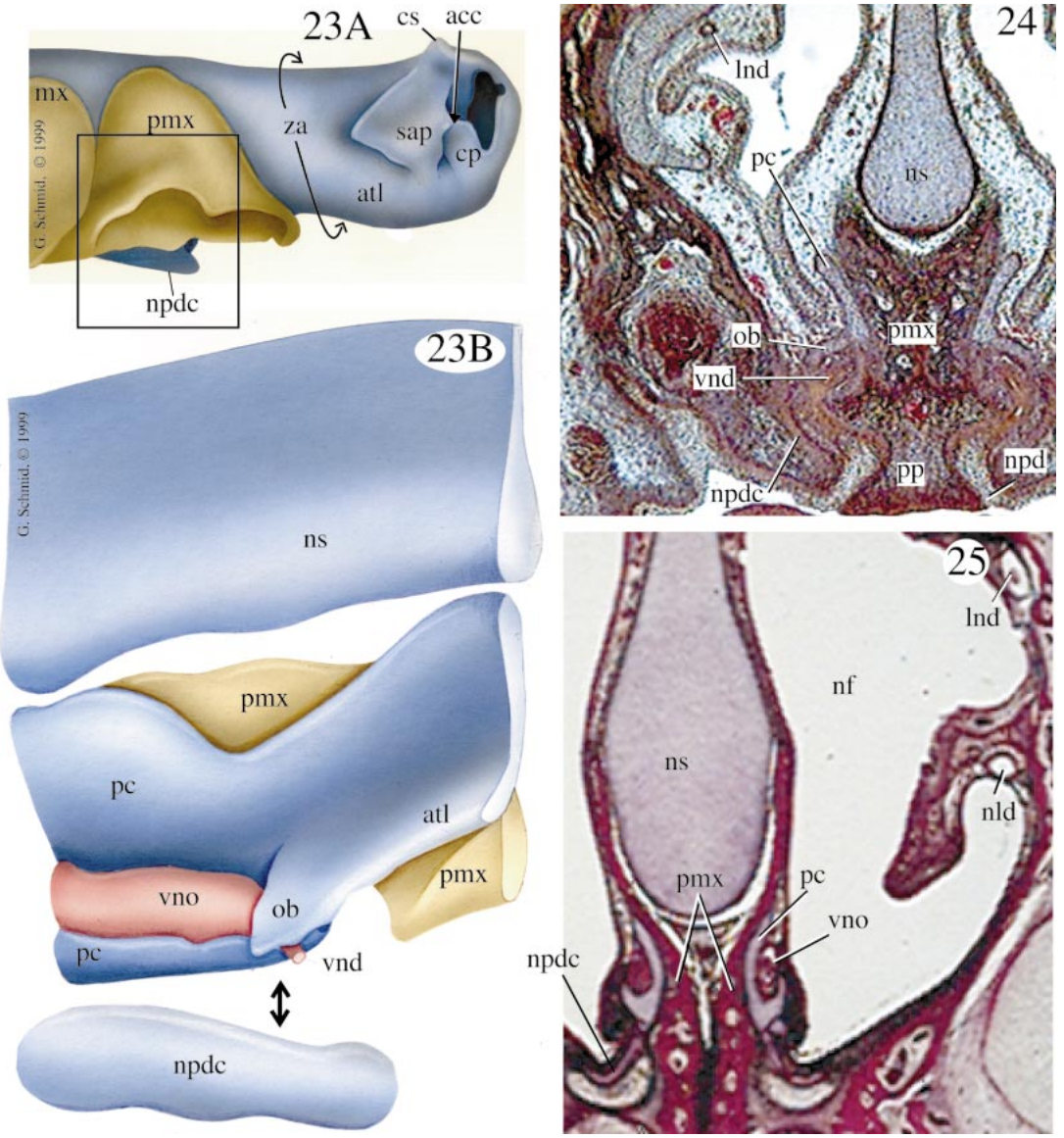

Figs. 23–25. Nasal models (23) and coronal sections (24, 25); **23A.** *Potamogale* (ZIUT HL 17 mm) cartilaginous nose, lateral view. Region in box is magnified in fig. 23B without external ossifications of maxilla and premaxilla. **23B.** *Potamogale* anterior nasal region, lateral view. Double-headed arrow represents approximate plane of coronal section shown in fig. 24. **24.** Palatine papilla of *Potamogale velox* (ZIUT HL 17 mm), slice 12.1.6. **25.** Anterior vomeronasal organ of *Solenodon paradoxus* (ZIUT), slice 102.1.2.

gan is 38% as long as the nasal fossa (6.9 mm) and 15% of the head length (17 mm). The vomeronasal organ in *Potamogale* extends farther posteriorly (i.e., ventral to the cribriform plate) than that of a specimen of *Cynocephalus,* described by Bhatnagar and Wible (1994: 47) as ''one of the relatively longest . . . reported thus far in mammals''. The large vomeronasal organ of *Potamogale* corresponds with its unusually large accessory olfactory bulb (Stephan et al., 1991). No single major blood vessel is apparent

traveling with the vomeronasal organ; however, numerous small vessels are evident along its length.

Along its entire medial and ventral aspects, the vomeronasal organ is supported by a J-shaped paraseptal cartilage (e.g., slice 16.2.4). At no point is the vomeronasal duct enclosed laterally by cartilage; however, immediately before it reaches the nasopalatine duct, an incomplete cartilaginous strut is present dorsal to the vomeronasal organ, extending laterally from the midpoint of the paraseptal cartilage (slice 12.1.6; fig. 24). Anteriorly, the organ grades into a narrow vomeronasal duct, which empties on each side directly into the nasopalatine ducts (e.g., slice 12.5.6), which in turn connect the nasal fossa and mouth via two openings on either side of the palatine papilla (slice 12.1.6; fig 24). The nasopalatine duct is laterally supported by a cartilage that runs ventromedially to the lateral rims of the incisive foramina; this nasopalatine duct cartilage is not connected to the paraseptal cartilage.

Broom's ''inferior septal ridge'' (1896: 593), consisting in most taxa of an anteroposteriorly running emargination of mucosa on the inferolateral aspect of the nasal septum and occasionally supported by anterior paraseptal cartilage or the adjacent anterior transverse lamina, is present in *Potamogale* far anterior to the vomeronasal organ. It lacks cartilaginous support.

There is a broad connection between the medial component of the paraseptal cartilage and the anterior transverse lamina (fig. 23B). DeBeer (1929: figs. 5–8) also noted continuity between these structures in *Sorex araneus*; in fact, he referred to both paraseptal cartilage (supporting the vomeronasal organ) and anterior transverse lamina (forming the nasal capsule floor anterior to the vomeronasal duct) by the single nomen ''anterior paraseptal cartilage''. Anterior to the premaxilla of *Potamogale*, the nasal cartilages form a complete, uninterrupted ring surrounding the nasal cavity, connecting the nasal septum, lamina transversalis anterior, and nasal sidewall and roof (fig. 23A). This cartilaginous ring is referred to here as a ''zona annularis'' (Gaupp, 1908). Kuhn (1971: 28) has recommended abandoning this term because of inconsistent usage; nevertheless, I retain ''zona annularis'' as defined above.

A remarkable aspect of *Potamogale* is the absence of the nasolacrimal duct—a common structure among mammals that usually lies in an anteroposteriorly running sulcus along the lateral nasal capsule (see figs. 25 and 26 for an illustration of this structure in *Solenodon* and *Erinaceus*). The nasolacrimal duct is also absent in the older *Potamogale* specimen described by Behrens (1998). This corresponds with the absent lacrimal gland in this individual, and is consistent with the observation that a lacrimal foramen is absent in adult *Potamogale* skulls (Asher, 1999).

The most conspicuous structures of the *Potamogale* anterior cartilaginous nose are the superior alar processes, located immediately posterior to the external nares (fig. 23A; slice 5.5.4). These provide a large surface area for attachment of facial muscles and connective tissue (slice 5.5.4). Dorsal to each of the anterior nasal cupulae lies a large, superiorly projecting ''spur'' (fig. 23A; slice 4.5.6; see Roux [1947: fig. 55] for a comparable structure in *Setifer*), dorsal to which runs a prominent alar-cupular muscle, which in turn originates from the dorsal aspect of the superior alar process (slice 6.3.2). The dorsal spur provides this muscle with a greater moment arm with which to act upon its insertion point in the superior rhinarium (slice 4.1.1). The superior alar processes are broadly connected to the floor of the anterior nose. In addition, a narrow alicupular commissure connects the superior alar process and cupular process (fig. 23a; slice 4.3.3). In contrast to the individual of *Setifer* figured by Roux (1947: fig. 55), the superior nasal fenestrae (located just posterior to the cupular spurs) in *Potamogale* are occluded by its large superior alar processes, and are not widely exposed dorsally.

Micropotamogale lamottei (IZEA 939)

The vomeronasal organ of *Micropotamogale* is approximately 3.5 mm in length and does not reach as far posteriorly as the first ethmoturbinal; in an adult specimen (IZEA 939) it extends only as far back as a frontal plane posterior to the canines and anterior to the anteriormost premolars (slice 48.3.2). In

this specimen (IZEA 939) the vomeronasal organ comprises about 13% of nasal fossa length (ca. 26 mm) and 7% of head length (ca. 50 mm). Fetal specimens (i.e., AIG 2273–1, 2273–3) show a more elongate vomeronasal organ, but still shorter than that seen in a *Potamogale* of comparable age (table 2). No major blood vessels are apparent coursing along the length of the vomeronasal organ; instead, numerous smaller vessels are visible.

Most of the support for the vomeronasal organ along its length is ossified, although some paraseptal cartilage remains ventral and lateral to the organ. In this regard, *Micropotamogale* resembles the specimens of *Geogale* described below. This is due to the advanced ontogenetic stage represented by the IZEA 939 *Micropotamogale* and all *Geogale* individuals (all showing fully erupted teeth).

Anteriorly, the cartilaginous outer bar does not cover the vomeronasal organ laterally. The vomeronasal ducts are apparent at the anterior extreme of the vomeronasal organ, consisting of tubes on either side of the nasal septum that empty into each nasopalatine duct, separated from the nasal fossa proper (e.g., slice 31.3.2). Elongate, thin cartilages support each nasopalatine duct laterally, and line the posterior margins of each incisive foramen (e.g., slice 32.1.2; fig. 27). These cartilages are not connected to other nasal floor or septal cartilages. The palatine papilla of *Micropotamogale* is dorsoventrally elongate, defined by each nasopalatine duct laterally (slice 32.1.2; fig. 27).

Anterior to the incisive foramina and dorsal to the premaxilla, the anterior transverse lamina is evident (slice 21.3.2) and shows no connection with paraseptal cartilages.

Immediately anterior to the premaxilla, the nasal cartilages form an uninterrupted ring, or zona annularis, connecting the nasal sidewall, floor, and roof (slice 17.3.1).

As in *Potamogale,* and in concordance with the observation that a lacrimal foramen is reduced in adult *Micropotamogale* skulls (Asher, 1999), *Micropotamogale* shows no nasolacrimal duct. Both potamogalines do, however, possess a duct for the lateral nasal gland that travels from the posterolateral nasal fossa anteriorly, ventral to the nasoturbinate (e.g., slice 35.3.2; see fig. 26 for the same structure in *Erinaceus*).

Well anterior to the nasopalatine ducts and the posterior margin of the anterior transverse lamina, the superior and inferior septal ridges are apparent (slice 10.3.1). Neither pair of ridges shows cartilaginous support.

The superior alar processes of *Micropotamogale* are smaller than those of *Potamogale* and do not extend far posterior or lateral to the nasal cupula. They originate posteriorly from the lateral margin of the anterior nasal floor (slice 7.1.2). No dorsal projections are evident on the anterior cartilaginous nose in the available adult specimens (IZEA 939), but they are evident in embryos (AIG 2273–1, 2273–3).

Geogale aurita (MCZ 45499; fig. 28)

The vomeronasal organ of *Geogale* is small compared to that of *Potamogale.* Its anteriormost point is directly over the posterior margin of the palatine papilla. Instead of traversing a large portion of the nasal floor as in *Potamogale,* the vomeronasal organ tapers to a posterior terminus at about the same transverse plane as the third upper incisor—roughly 1 mm posterior to its starting point. In the postnatal MCZ 45499, it comprises about 10% of nasal capsule length (about 10 mm) and 8% of head length (14 mm). Proportions are similar in the larger ZIUT individual (SVL 43 mm): the 1.2-mm vomeronasal organ comprises 9% of nasal capsule length (14.3 mm) and 6% of head length (21 mm).

The vomeronasal organ itself is kidney-shaped and laterally concave. Blood vessels are conspicuous dorsolateral and ventromedial to the vomeronasal organ. The paraseptal cartilages are most evident ventral to the vomeronasal organ along its length and are reduced medially. Relative to other animals examined here, there is very little space between the vomeronasal organ on each side of the septum. In other taxa, a dorsally extending flange of the paraseptal cartilage contributes to the space separating each half of the paired vomeronasal organ, whereas in *Geogale* bony elements of the nasal septum are evident medial to the vomeronasal organ

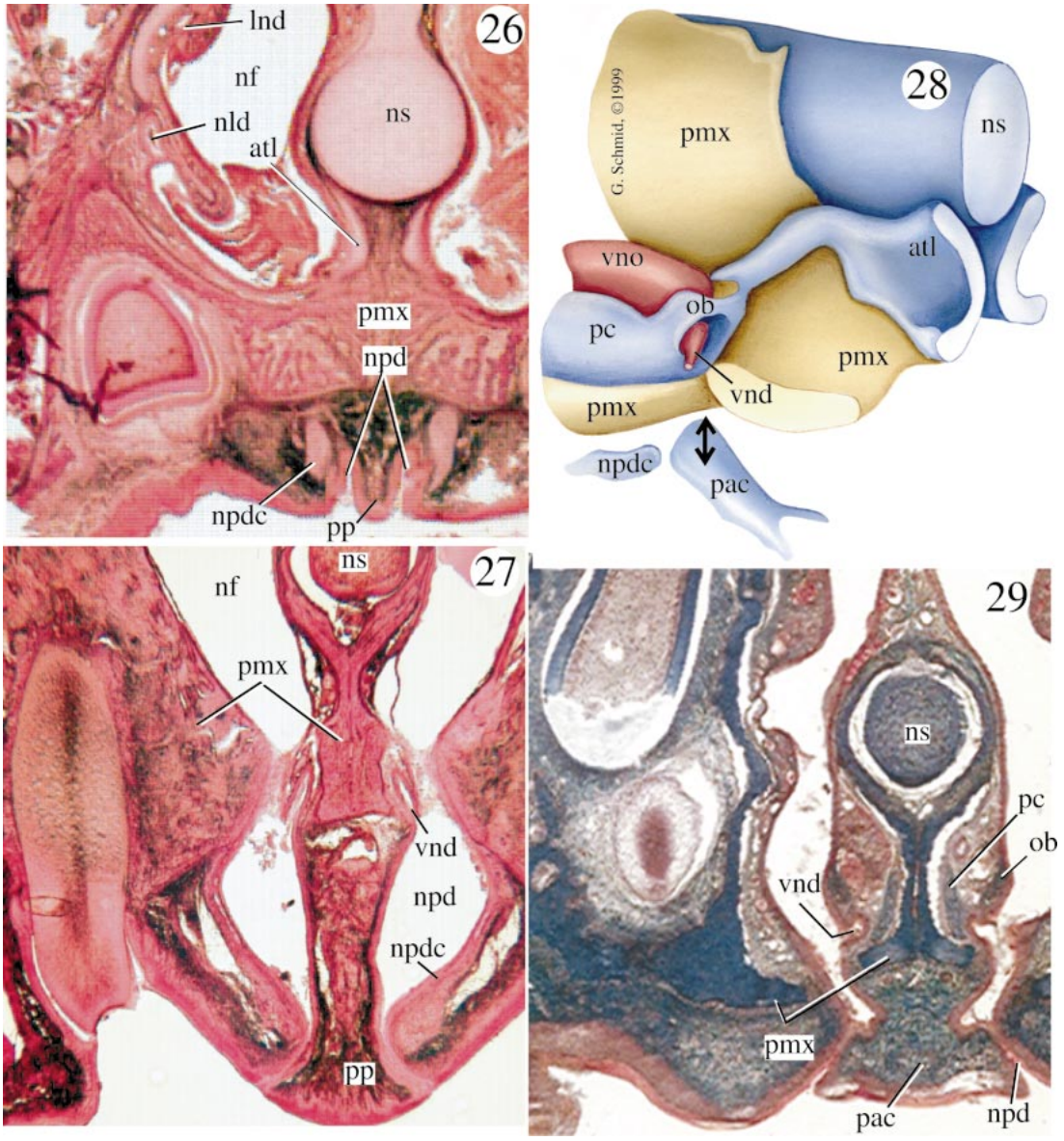

Figs. 26–29. Nasal model (28) and coronal sections through palatine papilla (26, 27, 29); **26.** *Erinaceus concolor* (ZIUT HL 35 mm), slice 32.1.1. **27.** *Micropotamogale lamottei* (IZEA 939), slice 32.1.2. **28.** *Geogale aurita* (MCZ 45499) anterior nasal region, lateral view. Double-headed arrow represents approximate plane of coronal section in fig. 29. **29.** *Geogale aurita* (MCZ45499), slice 8.1.4.

(compare figs. 24 and 29 or slices 14.2.4 of *Potamogale* and 8.5.5 of *Geogale*). This may be due to the advanced ontogenetic stage and consequent resorption of cartilage in the available *Geogale* specimens.

At the anterior margin of the vomeronasal organ of *Geogale*, just dorsal to the nasopalatine duct, a small outer bar connects the ventrolateral and ventromedial components of the paraseptal cartilage, lying dorsal to the vomeronasal duct (e.g., slice 8.1.5; figs. 28, 29).

Posterior to the anterior margin of the first upper incisors and continuing through the

length of the premaxilla, the cartilaginous nasal septum consists of a single anteroposteriorly running cylinder, surrounded by ossifications of the premaxilla (slice 11.2.3). In this region the septum lacks a connection to the nasal roof. This condition may simply be a result of resorption of cartilage in a relatively well-ossified postnatal individual, an interpretation supported by the observation that other adult specimens (e.g., IZEA 939 and AIG 1227 *Micropotamogale* and ZIUT *Sorex*) also lack a cartilaginous septum-roof connection in parts of the nasal fossa.

At its anterior margin, the vomeronasal organ gives off a well-defined vomeronasal duct (slice 8.2.3; fig. 29), which enters the nasopalatine canal dorsally as the latter opens into the nasal fossa proper. As in most other taxa described here, the nasopalatine canal is paired, opening on either side of a well-defined palatine papilla (slice 7.5.5). A very small nasopalatine duct cartilage is evident along the lateral margin of the incisive foramina (slice 8.5.1), which shows no connection to other nasal cartilages.

Within the palatine papilla is a cartilaginous body (slice 8.1.4; fig. 29), ending anteriorly in two points. Although ubiquitous among marsupials (Sánchez-Villagra, 2001), this papillary cartilage has been observed in relatively few placental taxa, such as *Elephantulus* and *Tupaia* (Wöhrmann-Repenning, 1984, 1987).

Just anterior to the rostral openings of the vomeronasal ducts is the inferior septal ridge, a laterally projecting flap of epithelial tissue, closely associated with the posterior margin of the anterior transverse lamina (slice 7.2.4). This structure extends ventrolaterally out from the posterior tip of the medial arm of the anterior transverse lamina, and supports both glandular and olfactory tissue.

The lack of prominent medial processes of the paraseptal cartilage contributes to the absence of a connection between it and the anterior transverse lamina. That is, the nasal cavity floor anterior to the vomeronasal duct is not broadly continuous with the paraseptal cartilage.

Geogale also displays a complete zona annularis, that is, continuity between the nasal septum, anterior transverse lamina, and nasal sidewall for a short distance immediately anterior to the first upper incisor (e.g., slice 4.4.3).

Geogale exhibits relatively large superior alar processes, located just posterior to the external nares, that serve as the site of origin of several facial muscles (e.g., slice 3.4.4). The alar processes are broadly connected to the nasal floor ventrally and show a narrow alicupular commissure anteriorly.

Microgale dobsoni (MPIH 1964/104)

The vomeronasal organ of *Microgale* is about 1.2 mm in length and extends posteriorly to a point close, but still anterior, to the first ethmoturbinal. It comprises roughly 14% of nasal fossa length (8.4 mm) and 8% of head length (15 mm). A large vein courses lateral to the vomeronasal organ on each side and forms the axis around which the organ has a kidney-shaped appearance (e.g., slice 280).

A J-shaped paraseptal cartilage supports the vomeronasal organ throughout its length, but at no point does the outer bar completely enclose the vomeronasal organ laterally. Anteriorly, the paired vomeronasal organ empties into the superior margin of each nasopalatine duct (slice 244; fig. 30). The nasopalatine canal is paired and connects the oral and nasal cavities on either side of the palatine papilla (slice 240). Lateral to the nasopalatine duct, an isolated nasopalatine duct cartilage is present (slice 244; fig. 30), showing no connection to other cartilages.

Immediately anterior to the nasopalatine duct, the inferior septal ridge is evident and is supported in part by the cartilage of the anterior transverse lamina (slice 220). The latter cartilage has a very narrow posterior connection to the paraseptal cartilage, dorsal to the frontal plane in which the nasopalatine ducts connect the oral and nasal cavities (slice 240).

Anterior to the premaxilla, a complete zona annularis is evident, connecting the nasal floor, sidewalls, and roof (slice 140). The superior alar cartilages of the external nose are evident in slice 80 and show a connection to the anterior nasal floor. Unlike the external nose of *Potamogale* (fig. 23A), no superiorly projecting cartilaginous spur is evident dorsally.

Echinops telfairi (ZIUT, HL 18 mm)

The posterior margin of the paraseptal cartilage in *Echinops* is coincident with the anterior margin of the first ethmoturbinal (slice 15.2.4); the vomeronasal organ itself appears a fraction of a millimeter farther anteriorly (slice 14.2.2). Rostrally, the vomeronasal organ terminates over the posterior incisive foramina. The vomeronasal organ (approximately 1.6 mm long) comprises 17% of nasal capsule length (9.5 mm) and 9% of head length (18 mm). Two venous channels are evident dorsolateral and ventromedial to the vomeronasal organ on each side (e.g., slice 11.3.4), each of which gives off several small branches toward the inferior part of the nasal septum.

The anterior paraseptal cartilage curves around the vomeronasal organ laterally (slice 10.5.4), but does not possess an outer bar passing dorsal to the vomeronasal organ or vomeronasal duct. The vomeronasal duct empties directly into the nasopalatine duct, well separated from the nasal cavity proper (slice 9.3.6). Farther anteriorly, the paired nasopalatine duct appears very atypical, as the conduits on each side coalesce with one another into a single channel that opens into the oral cavity (slice 8.3.6; fig. 31). As a result, the typical mammalian inverted mushroom-shaped palatine papilla is absent. This condition has been previously documented in *Echinops* and *Setifer* by Hofer (1982a). Cartilages supporting the nasopalatine duct are small; only a minor cartilaginous center is evident along the lateral margin of the incisive foramen. The paraseptal cartilage does not show a significant anterior continuity with the anterior transverse lamina (slice 9.5.5).

Just anterior to the incisive foramina and dorsal to part of the nasopalatine duct, anteroposteriorly running ridges on either side of the septum are evident (slice 9.2.5). The posterior margin of the anterior transverse lamina provides cartilaginous support for these inferior septal ridges. Farther anteriorly, bulges on each side of the nasal septum comprise the ''superior'' septal ridges, which have no cartilaginous support and contain glandular tissue (slice 5.1.5). Also in this region of the anterior nose, a complete zona annularis is evident.

Adjacent to the anterior termination of the nasolacrimal duct, the superior alar processes originate from the nasal sidewall and extend dorsolaterally (slice 3.6.4). No connection with the anterior nasal cupula is apparent.

Setifer setosus (ZIUT, celloidin-embedded individual)

The vomeronasal organ of this adult *Setifer* specimen extends approximately 5 mm posteriorly beyond the premaxilla, to the level of the first premolars (slice 75.2.1). Unfortunately, length estimates for the nasal fossa and head of this specimen are unavailable. One particularly large blood vessel lies lateral to the vomeronasal organ along most of its length; numerous other vessels of moderate caliber are also evident scattered throughout the organ (e.g., slice 64.1.1).

The paraseptal cartilage borders the vomeronasal organ ventrally and medially throughout its length. In some sections it extends lateral to the vomeronasal organ (e.g., slice 57.2.1), but the paraseptal cartilage does not give off an outer bar that passes dorsal to the vomeronasal organ or the vomeronasal duct.

At its anterior margin the vomeronasal organ grades into the vomeronasal duct, which enters the nasopalatine duct ventral to and separate from the nasal fossa (slice 48.1.1). The nasopalatine canal of *Setifer* leaves the nasal fossa paired; farther ventrally, however, *Setifer* resembles *Echinops* in that the canals on each side join with each other to form a single canal that opens into the oral cavity (slice 38.1.1; see also Hofer, 1982a). A very small nasopalatine duct cartilage is evident connected with the paraseptal cartilage (e.g., 48.3.1).

Anterior to the vomeronasal organ, the paraseptal cartilage ends, showing no continuity with the anterior transverse lamina. The posterior margin of the anterior transverse lamina supports the inferior septal ridge, extending out from the nasal septum, just dorsal and anterior to the nasal openings of the nasopalatine ducts (slice 47.2.1).

Anterior to the premaxilla, the nasal floor descends relative to the roof, greatly increas-

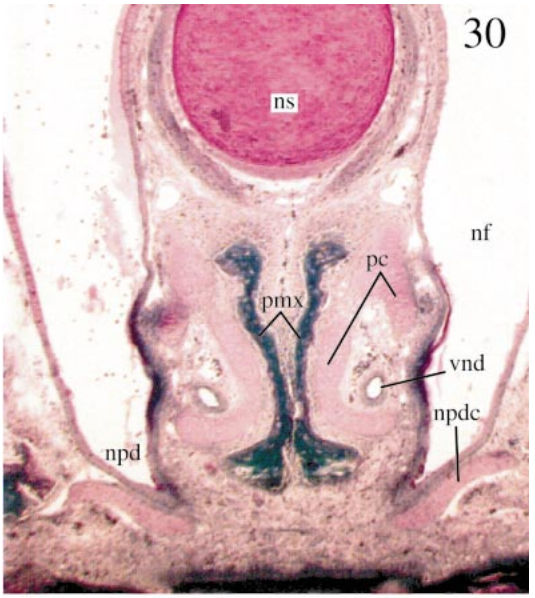

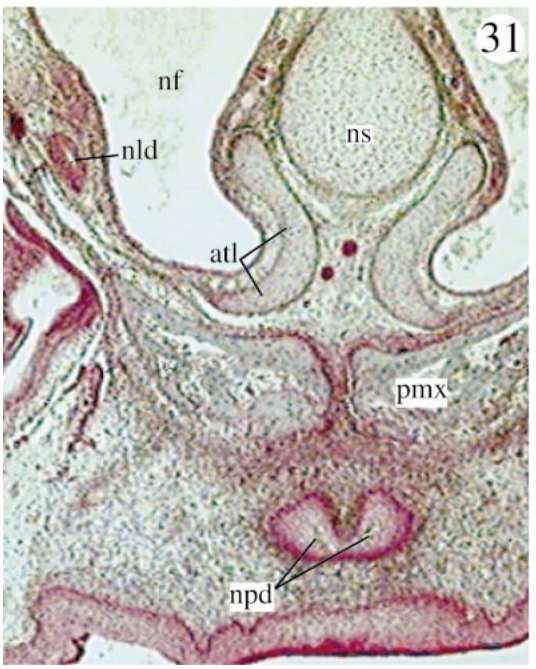

Figs. 30, 31. Anterior nasal coronal sections; **30.** *Microgale dobsoni* (MPIH 1964/103) just posterior to palatine papilla, slice 250. **31.** *Echinops telfairi* (ZIUT HL 18 mm) anterior to vomeronasal organ, slice 8.4.4.

ing the volume within the nasal cupula (compare slices 35.2.1 and 25.2.1). In this region, *Setifer* shows a broad continuity, or zona annularis, between the nasal septum, floor, and sidewall.

The superior alar processes are relatively narrow, showing only a short connection with the anterior nasal floor and no connection with the anterior nasal cupula. However, the alar processes do provide attachments for small muscles of the rhinarium (e.g., slice 13.2.1).

Tenrec ecaudatus (ZIUT, HL 20 mm; fig. 32)

Posteriorly, the vomeronasal organ and paraseptal cartilages extend to the upper canines. The vomeronasal organ itself measures approximately 1.5 mm in length. This makes up 14% of nasal fossa length (10.2 mm) and 7.5% of head length (20 mm). Several small blood vessels are apparent running parallel to the vomeronasal organ.

The paraseptal cartilage lies medial to the vomeronasal organ along its entire length and does not exhibit a complete outer bar laterally (fig. 32). The vomeronasal ducts are narrow, anterior continuations of each vomeronasal organ tube, emptying into the nasopalatine canal at a point well-separated from the nasal fossa (slice 7.5.1). A large palatine papilla is evident medial to the nasopalatine ducts as they open into the oral cavity.

A nasopalatine duct cartilage is present lateral to the nasopalatine ducts and is connected to both the paraseptal cartilage dorsomedially and the ''nasopalatine duct'' cartilage medially (slice 8.2.4; fig. 33). Kuhn (1971: 30) noted that confusion exists regarding the definitions of the ''palatine'' and ''nasopalatine duct'' cartilages; in some taxa (including *Tenrec*), the two are continuous anteriorly. As defined in previous studies (e.g., Maier, 1980), they are at least distinguishable posteriorly; the palatine cartilage exists lateral, and the nasopalatine duct cartilage medial, to the nasopalatine duct itself.

Anterior to the nasopalatine canal is the inferior septal ridge, supported medially by the superior arm of the anterior transverse lamina and containing olfactory epithelium

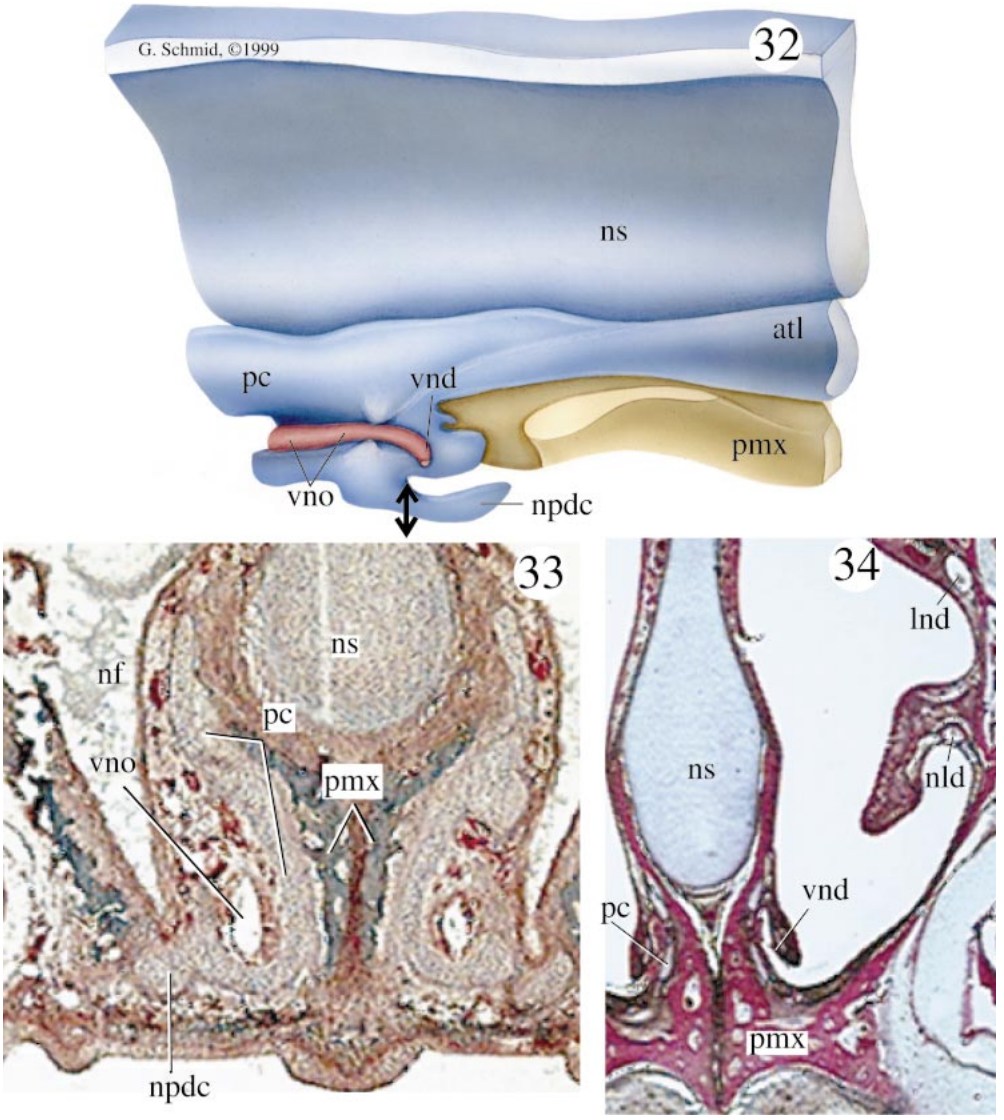

Figs. 32–34. Nasal model (32) and anterior nasal coronal sections (33–34); **32.** *Tenrec ecaudatus* (ZIUT HL 20 mm) anterior nasal region, lateral view. Double-headed arrow shows approximate plane of coronal section in fig. 33. **33.** *Tenrec ecaudatus* (ZIUT HL 20 mm), posterior to palatine papilla, slice 8.2.4. **34.** *Solenodon paradoxus* (ZIUT), anterior to palatine papilla, slice 100.3.1. Note vomeronasal duct opening into nasal fossa.

(slice 6.1.1). The medial arm of the anteriormost paraseptal cartilage has a narrow connection with the anterior transverse lamina. The connection between the nasal septum, floor, and sidewall in *Tenrec* is constricted, but present, at the point just anterior to the premaxilla and where the nasolacrimal duct enters the nasal fossa (slice 4.4.5).

A feature of the external nose that *Tenrec* shares with *Setifer* is the abrupt inferior extension of the anterior nasal floor, greatly enlarging the surface area available for olfactory epithelium in the anterior nose (slice 5.3.1). In *Tenrec*, the narrow superior alar processes originate from this ventrally extended nasal floor, and show no commissura

alicupularis connecting them to the anterior nasal cupulae.

Solenodon paradoxus (ZIUT)

Despite the enormous length of the *Solenodon* anterior nose, the vomeronasal organ is not elaborate. The vomeronasal organ is in fact quite small, failing to extend farther posteriorly than the row of upper incisors. Unfortunately, the available *Solenodon* specimen is only partially sectioned through the midrostrum, leaving no means of precisely inferring the nasal capsule or head length in this specimen. However, it is likely that the vomeronasal organ of *Solenodon* comprises a very small percentage of nasal capsule and head length, given the great size of the latter two structures in this genus. No major blood vessels are evident coursing adjacent to the vomeronasal organ.

The paraseptal cartilages are relatively small J-shaped structures that, as in most other mammals described here, course medially along most of the length of the vomeronasal organ (e.g., slice 110.3.1). At its anterior end, *Solenodon* shows a small outer bar which does not enclose the vomeronasal organ laterally, but ends in a free process. At the anterior margin of the vomeronasal organ, the vomeronasal duct opens ventrally, medial to the inferior septal ridge, and empties directly into the nasal fossa (slice 100.3.1; fig. 34) anterior to the superior margin of the nasopalatine duct (slice 106.3.2). Unlike other animals described here, and like some ''archaeorhinate'' taxa described by Broom (1897), the nasopalatine and vomeronasal ducts do not directly communicate (see also Menzel, 1979; Hofer, 1982b). However, *Solenodon* differs from Broom's ''archaeorhinates'' in possessing cartilaginous support for the nasopalatine duct. A connection is evident between the inferior arm of the paraseptal cartilage and the cartilage supporting the nasopalatine duct (slice 101.2.1; fig. 25). The latter cartilage is present at the superior margin of the nasopalatine duct, and extends lateral to the duct to the lateral rim of the bony incisive foramina. The nasopalatine ducts run posteroinferiorly to empty into the oral cavity adjacent to the palatine papilla (slice 108.2.2).

The relatively tiny medial arm of the paraseptal cartilage has no connection with the anterior transverse lamina, which lies far anterior to the vomeronasal organ and its cartilages. Although the nasal septum and floor are continuous throughout most of the elongate external nose of *Solenodon,* the connection between the nasal floor and sidewall is never complete, as *Solenodon* shows an anteroposteriorly running suture between nasal floor and roof adjacent to the nasolacrimal duct.

The superior alar processes of *Solenodon* are relatively small, consisting of an extended nasal sidewall that ends freely, with no connection to the anterior nasal cupula (e.g., slice 11.1.3).

Erinaceus europaeus (ZIUT, SVL 37 mm)

Posteriorly, the vomeronasal organ begins at a point slightly posterior to the anterior tip of the first ethmoturbinal (e.g., slice 21.3.2) and ends 1.6 mm anteriorly, over the incisive foramina. The vomeronasal organ comprises about 22% of nasal capsule length (7.3 mm) and 8% of head length (19 mm). No major blood vessels accompany the vomeronasal organ along its length.

The paraseptal cartilages are J-shaped (e.g., slice 17.2.3). Anteriorly, the vomeronasal duct is completely enclosed by the outer bar (slice 15.1.4), which begins posteriorly from the inferior arm of the paraseptal cartilage, runs dorsally over the vomeronasal duct, and joins the medial arm of the paraseptal cartilage as the duct empties into the nasopalatine canal. *Erinaceus* displays a paired vomeronasal duct, leaving the vomeronasal organ anteriorly and connecting directly into the nasopalatine duct (slice 14.5.1). The paired nasopalatine duct empties into the mouth on either side of a well-defined palatine papilla (e.g., slice 14.3.3; fig. 26). A small nasopalatine duct cartilage, continuous with the inferior portion of the paraseptal cartilage, is evident medially and anterolaterally to the nasopalatine canal (slice 14.2.4; fig. 26).

Anterior to the nasopalatine ducts, both inferior and superior septal ridges are apparent, without cartilaginous support (slice 12.5.2). As in *Potamogale,* the medial processes of

the paraseptal cartilages are continuous anteriorly with the anterior transverse lamina. This lamina is continuous with the nasal sidewall, roof, and septum throughout a large portion of the external nose anterior to the premaxilla (e.g., slice 9.2.3).

The superior alar processes show most continuity with the anterior floor of the nasal capsule (slice 9.1.4); anteriorly, they bifurcate around the external nares.

List of Nasal Characters

Several morphological differences are evident in specimens of different age. For example, like other cranial sense organs (e.g., eyes), the vomeronasal organ grows with negative allometry relative to body mass and is proportionately larger in younger specimens. Thus, a fetal *Micropotamogale* specimen (AIG 22733–3) with a head length of about 9 mm shows a posterior margin of the vomeronasal organ overlapping the anterior extent of the first ethmoturbinial. The vomeronasal organ in an adult *Micropotamogale* (IZEA 939) with a head length of about 50 mm, on the other hand, ends posteriorly near the upper canines, as described above. Even so, the vomeronasal organ in an embryo of *Potamogale* is considerably longer than that of similarly aged *Micropotamogale, Echinops, Tenrec,* and *Microgale* individuals examined in this study.

Adult specimens (e.g., ZIUT *Sorex,* AIG 1227 and IZEA 939 *Micropotamogale*) show resorption of certain regions of nasal cartilage not evident in fetal representatives of these taxa. This includes the medial wing of the paraseptal cartilage, the connection between the nasal septum and roof, and the connection between the paraseptal cartilage and anterior transverse lamina. The connection between the paraseptal and nasopalatine duct cartilages appears less ontogenetically variable, as both structures persist intact postnatally, and two relatively older specimens (*Setifer* and *Solenodon*) with erupted deciduous teeth show a connection between the two. Finally, as described above, tubercle-like ''spurs'' on the dorsum of the nasal cupulae are evident in the fetal *Potamogale* (fig. 23A) and two fetal *Micropotamogale* specimens. However, these are absent in the two available adult *Micropotamogale* specimens, and must therefore be presumed to disappear during the course of ontogeny.

There is of course nothing wrong with attempting to extract phylogenetic information from characters that are expressed only during a certain point in ontogeny. The problem arises when a given sample contains taxa representing different ontogenetic stages. Such is presently the case; therefore, I attempt to use characters that are consistently expressed in individuals of various ages. The remaining morphological differences described above are constant in those taxa represented in this study by adult and fetal specimens (table 2). This enables comparisons between taxa represented by only postnatal (*Geogale*) or fetal (*Potamogale*) specimens.

Some of the morphological variation described above (i.e., relations and cartilaginous support for the inferior septal ridge and connections of the superior alar cartilage and nasal cupulae) may provide valuable character information for phylogenetic purposes. However, based on the present sample, it is difficult to unambiguously refine the observed morphology into discrete character states. Hence, these characters are for present purposes not considered in the following pages.

Table 4 includes character data for several taxa that are not described above. This information is based on observations of specimens listed in table 2, as well as the work of authors cited below. Specifically, data on nasal structure in *Bradypus* is taken from Schneider (1955); in *Dasypus* from Broom (1897) and Reinbach (1952a, 1952b); in *Echinosorex* from Broom (1915a) and Wöhrmann-Repenning (1984); in *Orycteropus* from Broom (1909) and W. Maier (personal commun.); in *Procavia* from Broom (1898), Lindahl (1948), and Weisser (1992); in *Talpa* from Fischer (1901) and Broom (1915b); and in *Tupaia* from Broom (1915a), Maier (1980), and Wöhrmann-Repenning (1984). Not all characters relevant to this study are described by these authors; hence, where information on a given character is lacking, I code it as ''missing''.

The following characters are numbered after the nine arterial characters described above, so as to correspond with the matrix

TABLE 4

Soft-Tissue Character Matrix

(Characters correspond in number to those listed in the text and in table 3. Taxa representing endemic African orders are in bold; insectivorans are marked with an asterisk. See text for sources of character information for taxa not represented by histological sections listed in table 2. **A** indicates a polymorphism between states 0 and 1, **B** between states 0 and 2, and **C** between states 0 and 3. **9** indicates an inapplicable character, which is treated by parsimony algorithms as missing data.)

Taxon	Character	
	1234567891	1111111112
	0	1234567890
**Blarina*	0001010010	0011011010
Bradypus	1110109???	??090?1?0?
Canis	111C109010	1011001110
****Chrysochloris***	100901001A	0009011110
**Crocidura*	0001010010	0010011111
Dasypus	1110109??1	0009001010
Didelphis	1110109010	000900A000
****Echinops***	0001000100	0109001010
**Echinosorex*	?00???01?0	1011011?10
**Erinaceus*	100B000010	A011011010
****Geogale***	0001001100	1010000010
****Hemicentetes***	0011109110	1011001010
****Microgale***	000A000100	1010001010
****Micropotamogale***	0001000110	1010191110
Nandinia	1113119010	1010001011
Orycteropus	1010119??0	0011001?00
****Potamogale***	0100000110	1010191110
Procavia	1110109170	00110?1110
****Setifer***	0000000100	1111001110
**Solenodon*	000?001101	1011001111
**Sorex*	100?0?0??0	0011011010
**Talpa*	?002A????0	10110?1?10
****Tenrec***	101C109100	1011001010
Tupaia	10111?11?0	001?0?000?

presented in table 4 (see also table 3). As detailed previously, a ''0'' character state assignment does not necessarily imply primitiveness.

10. Anterior relation of vomeronasal duct: *Solenodon* and *Dasypus* differ from other animals examined here in possessing a vomeronasal duct that empties directly into the nasal fossa (state 1) rather than into the nasopalatine duct (e.g., *Tenrec,* state 0).

11. Paraseptal cartilage and anterior vomeronasal organ (''outer bar''): Among marsupials, a strut of paraseptal cartilage consistently encloses the vomeronasal organ anterolaterally (e.g., *Didelphis,* state 0; Sánchez-Villagra, 2001). This is variably present among placental mammals; in many taxa the paraseptal cartilage is laterally open along its anterior half (e.g., *Micropotamogale,* state 1).

12. Oral opening of nasopalatine duct: The nasopalatine duct opens into the oral region via a single, unpaired channel in *Echinops* and *Setifer* (state 1; Hofer, 1982a). In other taxa, the nasopalatine duct is paired and opens into the mouth on either side of the palatine papilla (e.g., *Tenrec,* state 0).

13. Presence of nasopalatine duct cartilage: Broom (e.g., 1898) noted that marsupials consistently lack cartilaginous support for the nasopalatine duct as it passes ventrally from the nasal fossa into the oral cavity (e.g., *Didelphis,* state 0). Some placentals, on the other hand, often show a cartilage medial and/or lateral to the nasopalatine duct (e.g., *Tenrec,* state 1). Many authors assign the medial (nasopalatine) and lateral (palatine) components different names (e.g., Maier, 1980); however, as mentioned above, Kuhn (1971) noted that these cartilages may be continuous and difficult to distinguish from one another. Due to this ambiguity, all cartilaginous support for the nasopalatine duct is here labeled ''nasopalatine duct cartilage''.

14. Connection of nasopalatine duct and paraseptal cartilages: When present, the nasopalatine duct cartilage may show a connection to the paraseptal cartilage posterior to the nasopalatine duct (e.g., *Tenrec,* state 1). Alternatively, it may appear adjacent to the duct with no connection to the paraseptal cartilage (e.g., *Microgale,* state 0).

15. Presence of nasolacrimal duct: Most taxa show a glandular duct running from the anteromedial margin of the eye, along the sidewall of the cartilaginous nose ventral to the maxilloturbinal, and opening anteriorly within the nasal cupula adjacent to the external nares (e.g., *Tenrec,* state 0). Potamogalines, on the other hand, show no trace of any such duct (state 1).

16. Lateral cover of nasolacrimal duct: The extent to which the nasolacrimal duct is shielded laterally by cartilage varies (W. Maier, personal commun.). In *Echinops,* there is no cartilaginous barrier lateral to the duct at any point except for its anterior extreme, when it opens into the nasal cupula

(state 0). *Erinaceus,* on the other hand, shows a lateral extension of the anterior transverse lamina dorsal to the anterior margin of the premaxilla that shields the nasolacrimal duct laterally, well before it empties anteriorly into the nasal cupula (state 1).

17. Papillary cartilage: Some taxa exhibit a cartilaginous structure within the palatine papilla (e.g., *Geogale,* state 0). Broom (1896) and Sánchez-Villagra (2001) noted the presence of a papillary cartilage in most marsupials; however, such a structure is lacking in a *Didelphis* individual examined in this study (table 2) and in those examined by Wöhrmann-Repenning (1984), although it is present in others (Sánchez-Villagra, personal commun.). Most placentals lack a papillary cartilage (e.g., *Tenrec,* state 1).

18. Vomeronasal organ blood vessels: In several taxa, a prominent blood vessel travels anteroposteriorly along with the vomeronasal organ tucked into its lateral side, giving the vomeronasal organ a kidney-shaped appearance when viewed coronally (e.g., *Didelphis,* state 0). Other animals show blood vessels scattered throughout the vomeronasal epithelium that do not travel in any single, well-defined fossa in the vomeronasal organ (e.g., *Potamogale,* state 1).

19. Shape of nasal septum: Sánchez-Villagra (2001) noted that a parallel-sided nasal septum (when viewed coronally) is ubiquitous among marsupials (e.g., *Didelphis,* state 0), and contrasts with the ventrally ovoid septum present in many placental mammals (e.g., *Echinops,* state 1).

20. Zona annularis: Anterior to the premaxilla, the nasal cartilages may form a complete, uninterrupted ring of cartilage around the nasal fossa, joining the anterior transverse lamina with the nasal sidewall and roof (e.g., *Echinops,* state 0). Alternatively, these structures may not be fully continuous at any point anterior to the premaxilla (e.g., *Solenodon,* state 1).

CHARACTER OPTIMIZATION

By themselves, the 20 previously defined characters of the cranial arterial supply and anterior nose (table 3) do not decisively favor any single hypothesis of insectivoran relationships, such as those outlined by Stanhope et al. (1998) and Asher (1999). Asher (2000) undertook a phylogenetic analysis of these and other morphological data for the taxa described above, plus a variety of other mammals. This analysis yielded resolution within the Tenrecidae (the most densely sampled group), but was less resolved for larger questions regarding insectivoran relationships. Since that study was completed, several additional molecular-based phylogenies have been published (Mouchaty et al., 2000; van Dijk et al., 2001; Madsen et al., 2001; Murphy et al., 2001). Eventually, these data will be incorporated into a simultaneous analysis (sensu Nixon and Carpenter, 1996); however, for the present, this paper is concerned only with mapping the characters described above onto competing phylogenetic hypotheses of insectivoran-grade mammals and noting which hypothesis best explains their distribution.

A difficulty in comparing the optimization of these characters on trees depicted in figure 1 is the nonoverlapping taxon sample. The most insectivoran taxa that have been sampled in any molecular study published to date is eight (Emerson et al., 1999), and the best sample of insectivorans in a molecular study that supports the Afrotheria is the six genera of Stanhope et al. (1998). Phylogenetic trees constructed by the most recent studies (van Dijk et al., 2001; Murphy et al., 2001; Madsen et al., 2001) sample at most five, without the Caribbean taxon *Solenodon.* This contrasts with two dozen insectivoran genera, each based on observations on several individuals, included in a recent morphological study (Asher, 1999). On the other hand, these molecular analyses have a much better sample across Mammalia as a whole than that of Asher (1999), and include putatively homologous phylogenetic data across disparate ecological and functional niches (e.g., elephants and bats).

Hence, in order to compare the fit of the previously described characters on competing phylogenies, it is necessary to use trees that contain a smaller number of taxa held in common by recent molecular and morpho-

logical studies for which the anatomical data discussed above are available. Such a sample consists of 12 taxa and is depicted in figure 35. Nine of these 12 taxa are genera used in both Asher (1999) and Stanhope et al. (1998); two are families (Chrysochloridae and Talpidae), and one is an order (Carnivora). Chrsochlorids and talpids were sampled at the familial level due to the availability of histological data for certain genera in these families (*Chrysochloris* and *Talpa*), that are closely related to the genera used by Stanhope et al. (*Amblysomus* and *Scalopus*), for which histological samples were lacking. Similarly, carnivorans were sampled at the ordinal level because available histological samples (*Canis* and *Nandinia*) do not overlap with the genera used by Stanhope et al (1998: fig. 1; *Felis* and two phocids).

Asher (1999) presented results from eight different phylogenetic analyses of an osteological and dental dataset, with each varying assumptions about character weighting, ordering, and missing data. The length and consistency index of these trees based on the new character set defined above is presented in table 5. Of these eight analyses, set no. 1 is the most defensible philosophically (Farris, 1983; Kluge, 1989), as it includes all sampled characters and taxa and does not impose weighting or ordering schemes on the dataset based on secondary considerations. For this reason, set no. 1 of Asher (1999) is figured in this paper and used for comparative purposes.

Stanhope et al. (1998) used a number of tree-reconstruction techniques for their molecular dataset, and figured three trees based on these analyses. Their figure 1 (1998: 9969, reproduced here as fig. 1B) is a ''majority rules neighbor joining bootstrap tree'' based on mitochondrial rRNA, and their figures 2 and 3 (1998: 9971) are reduced-taxon trees based on both nuclear and mitochondrial DNA. As of 6 March 2001, of all the phylogenetic trees published in support of the Afrotheria, figure 1 of Stanhope et al. (1998) shows the best sample of insectivorans and has maximal overlap with the sample discussed here. Therefore, this tree is used here to represent the molecular hypothesis of insectivoran relationships.

Differences Between Trees Based on Soft-Tissue Dataset

Figure 35 shows the soft-tissue characters described in the previous section optimized on these trees. The phylogeny of Asher (1999: set no. 1) requires 43 steps (CI = 0.55) and that of Stanhope et al. (1998: fig. 1) 50 steps (CI = 0.45). A parametric significance test of this difference (Kishino and Hasegawa, 1989; calculated using PAUP* version 4.0b8, Swofford, 2001) yields a two-tailed P-value of 0.0692. Similarly, a nonparametric Wilcoxon Rank Sum test (Templeton, 1983; also calculated using PAUP* version 4.0b8) yields a T-value of 2; given n = 6 degrees of freedom this value indicates two-tailed significance between alpha levels 0.05 and 0.10 (Rohlf and Sokal, 1995: 136). Two-tailed statistical tests are appropriate since both of these trees were selected a priori, with no necessary expectation that one would better explain the soft-tissue dataset than the other (Swofford et al., 1996: 505). Hence, the phylogeny of Asher (1999) better explains the soft-tissue data discussed above than that of Stanhope et al. (1998), but without a decisive level of significance.

Possible Evolution of Cranial Characters Among Insectivoran-Grade Mammals

In order to better explore the possible evolution of the soft-tissue characters described above, I have mapped them (fig. 36) onto a more taxonomically complete tree produced by the osteological and dental dataset of Asher (1999: set no. 1). If this topology is correct regarding, for example, the placement of *Solenodon* and monophyly of the Lipotyphla, then a number of previously underemphasized morphological synapomorphies are worth discussing.

Affinities of *Solenodon*

First, contrary to the view outlined by McDowell (1958) that evidence for a tenrec-*Solenodon* clade was restricted to the dentition, one of the most unique soft-tissue character transformations recorded during the course of this study was observed only among most tenrecs and *Solenodon.* In these taxa, the ex-

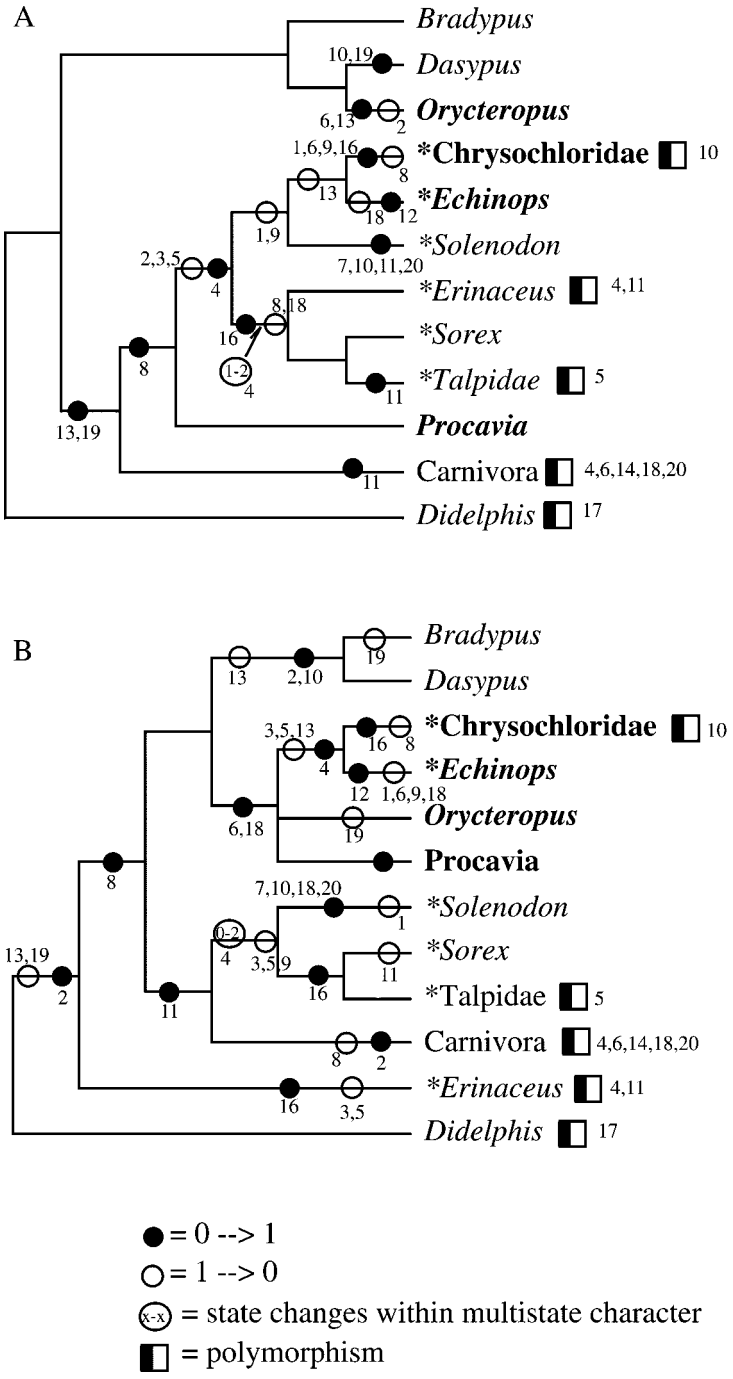

Fig. 35. Soft-tissue characters mapped onto competing phylogenies, assuming accelerated transformation (i.e., favoring reversals). Endemic African taxa are in bold; insectivorans are indicated with an asterisk. **A.** Analysis from set no. 1 of Asher (1999), requiring 43 steps with a CI of 0.55. **B.** Analysis from Stanhope et al. (1998: fig. 1) requiring 50 steps with a CI of 0.45. Consistency Indices (CI) are calculated excluding uninformative characters.

TABLE 5

Length of Trees from Asher (1999)

(Based on soft-tissue dataset presented in this paper. See Asher (1999) for explanation of assumptions behind each analysis.)

Analysis number from Asher (1999)	Assumptions from Asher (1999)	Tree length based on present dataset	CI (excluding uninformative characters)
1	equally weighted all characters included multistate unordered	43	0.55
2	weighted post hoc all characters included multistate unordered	43	0.55
3	equally weighted some characters excluded multistate unordered	50	0.45
4	equally weighted all characters included multistate ordered	44	0.53
5	weighted post hoc some characters excluded multistate unordered	44	0.53
6	equally weighted some characters excluded multistate ordered	53	0.42
7	weighted post hoc all characters included multistate ordered	44	0.53
8	weighted post hoc some characters excluded multistate ordered	46	0.50

ternal carotid artery runs medial to a slip of the thyropharyngeus muscle, immediately prior to the origin of the artery's facial and lingual branches (character 9, state 0; figs. 14, 16, 18, and 20). In most other mammals, including potamogalines and *Hemicentetes*, the external carotid remains lateral to the thyropharyngeus muscle throughout its course (fig. 12).

As reconstructed assuming accelerated transformations (Swofford and Begle, 1993: 20) on set no. 1 of Asher (1999), the node containing *Solenodon* plus tenrecs and *Chrysochloris* shows the medial course of the external carotid relative to thyropharyngeus to be a synapomorphy. It is equally parsimonious to reconstruct this character state as evolving in parallel in *Solenodon* and certain tenrecs, depending on the nature of the unresolved *Geogale-Microgale*-potamogaline node. In any event, this character varies within tenrecs; as noted, *Hemicentetes* and potamogalines show the putatively primitive state with the external carotid consistently lateral to the constrictor musculature throughout the artery's course (fig. 12). *Chrysochloris* shows this more general condition as well.

Another notable character shared by *Solenodon* and at least one tenrec (*Geogale*) is the supratympanic bifurcation of the stapedial artery (character 7, state 1). Figure 22A shows the undivided proximal stapedial artery of *Solenodon* passing through the tympanic roof via a foramen in the petrosal, an-

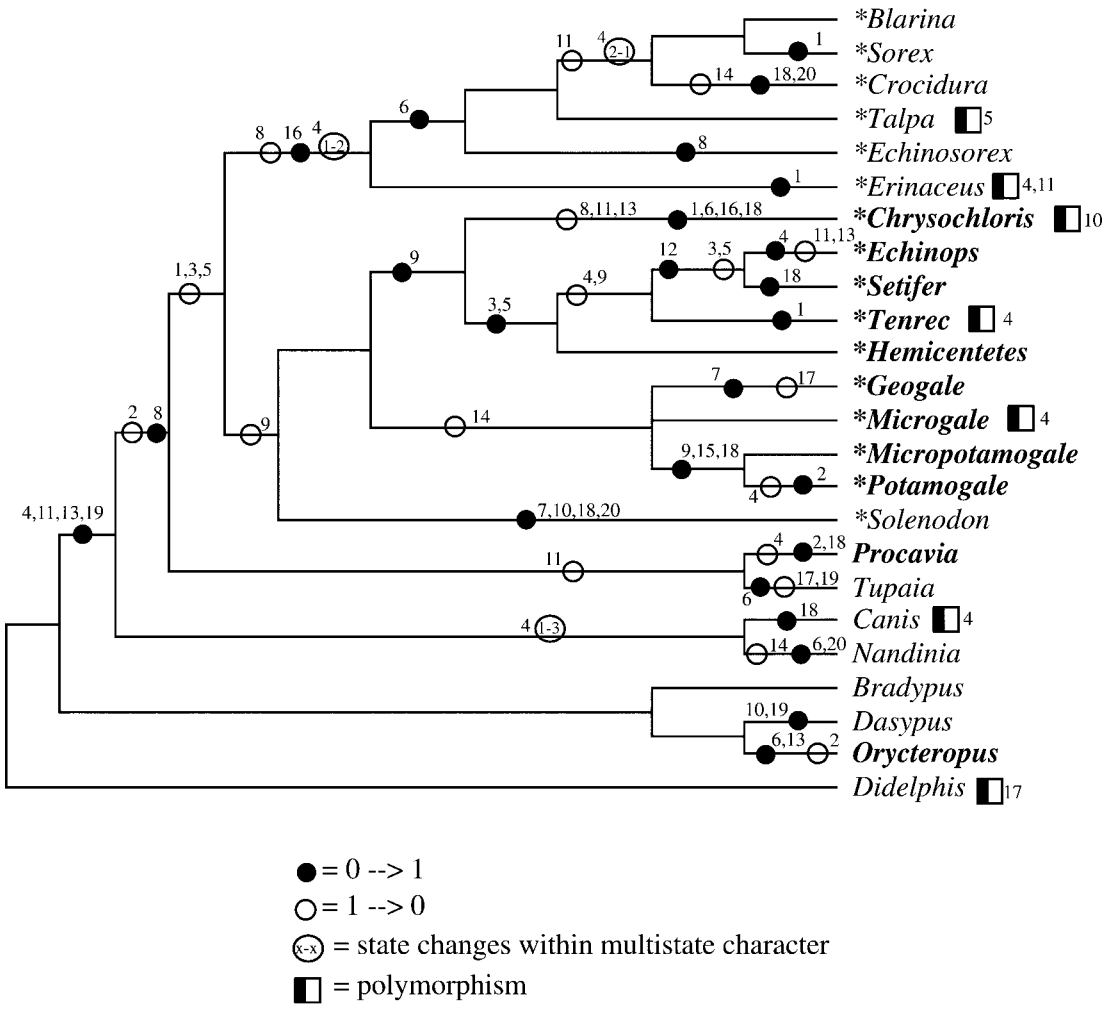

Fig. 36. Soft-tissue characters mapped onto topology produced by set no. 1 of Asher (1999), assuming accelerated transformation (i.e., favoring reversals), retaining taxa not shared with Stanhope et al. (1998). This tree requires 78 steps and has a CI of 0.38 (excluding uninformative characters). Endemic African taxa are in bold; insectivorans are indicated with an asterisk.

terior to the promontory, medial to the epitympanic recess, and lateral to the origin of the tensor tympani muscle. Figure 22B shows a slightly more anterior slice in which the intracranial proximal stapedial divides into superior and inferior rami, above the tegmen tympani's anterior margin. After its origin superior to the petrosal, the inferior stapedial leaves the cranial cavity anteroventrally through the piriform fenestra. The path and bifurcation of the stapedial artery in *Solenodon* closely resemble those discussed above for *Geogale,* but have not been observed in any other mammal, including tenrecs, examined during the course of this study. All topologies recovered by Asher (1999) optimize this character state as evolving homoplastically in the two taxa.

Intra-tenrecid phylogeny

The nested position of *Chrysochloris* within the Tenrecidae, adjacent to tenrecines, is a very unusual feature of set no. 1 from Asher (1999). Soft-tissue data discussed here do not unambiguously support this association. As

shown in figure 36, only a reversal of character 9 from medial to thyropharyngeus to the more common lateral state supports this node. However, as previously discussed, this optimization is dependent on the assumption of accelerated transformations, and in fact all tenrecines except *Hemicentetes* show the specialized, medial state of character 9. Further data are required to better test this novel association.

Potamogalines, *Geogale,* and *Microgale* show a nasopalatine duct cartilage isolated from the paraseptal cartilage (character 14, state 0; see figs. 23, 24, 28, 30). This contrasts with the more common condition in which the two cartilages share a connection (e.g., *Tenrec*; see figs. 32, 33). Thus, this character is consistent with a oryzorictine-potamogaline clade and the consequent paraphyly of Malagasy tenrecs (Asher, 1999). Outside of oryzorictines and potamogalines, an isolated nasopalatine duct cartilage has also been observed in specimens of the carnivoran *Nandinia* and shrew *Crocidura* (table 2).

Lipotyphlan Monophyly

Several arterial characters traditionally regarded as primitive for placental mammals (fig. 3), and thus of allegedly no value for recognizing monophyletic taxa within placentals, are in fact optimized as synapomorphies for lipotyphlans in figures 35A and 36. Of the taxa included in figure 35, only *Erinaceus, Sorex, Talpa, Solenodon,* most tenrecs, and *Chrysochloris* possess patent posterior, superior, and inferior rami of the stapedial artery (characters nos. 1–3, state 0), in addition to a ramus mandibularis that arises from the inferior stapedial ramus (character 5, state 0). However, the relatively high consistency of these characters is somewhat artefactual, as it is known that other mammals not discussed here (e.g., tree shrews, some rodents, rabbits, bats, and elephant shrews), and one that is (*Orycteropus*), possess one or both stapedial rami with their potential tributaries (Bugge, 1974; MacPhee, 1981; Wible, 1987). Similarly, the dense taxon sample of tenrecs depicted in figure 36 indicates considerable homoplasy, as *Potamogale* shows a reduced superior stapedial ramus, both *Tenrec* and *Hemicentetes* lack an inferior ramus, and adult specimens of *Tenrec, Sorex, Erinaceus,* and *Chrysochloris* lack patent posterior stapedial rami.

Nevertheless, support for the Lipotyphla from these allegedly primitive characters does not disappear completely with the recognition that they occur in other parts of the mammalian tree. ''Primitive'' and ''derived'' are relative terms, and the appearance of a certain character state at a basal node in any phylogeny does not rule out the possibility that subsequent recurrences of that state are derived for a different group. Hence, patent inferior, superior, and posterior stapedial rami (for example) would fail to comprise synapomorphies for a monophyletic Lipotyphla only if its immediate sister group(s) also possessed these characters, and this has yet to be demonstrated.

Morphological Support for Afrotheria

Osteological or dental support for an Afrotheria including tenrecs and golden moles is lacking (Asher, 1999). However, two soft-tissue characters present interesting distributions that could be consistent with monophyly of the Afrotheria. First, golden moles and *Orycteropus* both have an internal carotid artery that enters into the braincase lateral to the anterior pole of the cochlea (character 6, state 1; fig. 21). Although data from elephant shrews have not been incorporated into this study, this character state has also been observed in serial sections of *Elephantulus* at the Zoologisches Institut, Tübingen. In contrast, tenrecs and *Procavia* show the more widely distributed condition of an internal carotid artery entering the braincase medial to the anterior pole of the cochlea (fig. 16; see also Lindahl and Lundberg, 1946), indicating that if this character is a synapomorphy, it either does not define Afrotheria as a whole or that some homoplasy has occurred during its evolution. When considering a larger mammalian sample, the latter seems to be the case, as some shrews (*Blarina* and *Crocidura*) and the carnivoran *Nandinia* have been observed to possess an internal carotid artery lateral to the anterior cochlea as it enters the braincase (Asher, 2000).

A second potential Afrotherian morpho-

logical synapomorphy concerns vomeronasal organ vasculature. *Procavia, Chrysochloris*, potamogalines, and *Setifer* show small vomeronasal blood vessels dispersed throughout the organ (character 18, state 1); this contrasts with the more typical condition of a single, large vessel running lateral to the organ and forming an axis around which the organ takes a kidney-shape. Most other taxa observed during this study show the latter character state. However, like certain African taxa, and again indicative of homoplasy, *Solenodon, Canis*, and *Crocidura* show the former state.

SUMMARY AND CONCLUSIONS

Insectivoran-grade mammals, represented in this study primarily by tenrecs, show a remarkable variety of vascular and nasal specializations, indicating that previous estimations of their homogeneity (e.g., McDowell, 1958: 168) are incorrect. Of particular note among the arterial specializations are the reduced superior stapedial ramus in *Potamogale* (character 2, state 1; figs. 4, 10); the absent inferior ramus in *Hemicentetes* and *Tenrec* (character 3, state 1; fig. 8); the intracranial stapedial bifurcation in *Geogale* (fig. 6) and *Solenodon* (character 7, state 1; fig. 22); the external carotid artery medial to thyropharyngeus muscle in most tenrecs and *Solenodon* (character 9, state 1; figs. 14, 16, 18, and 20); and the internal carotid artery lateral to the cochlea in *Chrysochloris* (character 6, state 1; fig. 21), similar to the condition in certain endemic African mammals (e.g., *Orycteropus*). In the anterior nose, *Echinops* and *Setifer* share an unpaired oral opening of the nasopalatine canal (character 12, state 1; fig. 31; see also Hofer, 1982a); *Geogale* possesses a papillary cartilage (character 17, state 0; fig. 29); *Erinaceus* and shrews share a laterally shielded nasolacrimal duct (character 16, state 1); and *Solenodon* possess a vomeronasal duct that empties directly into the nasal fossa (character 10, state 1; fig. 34), as does *Dasypus* (Reinbach, 1952a, 1952b) and some specimens of *Chrysochloris* (Broom, 1915b).

When optimized on recently proposed insectivoran phylogenies, these characters are more consistent with one based on osteology and the dentition (Asher, 1999) than one based on mitochondrial rRNA sequences (Stanhope et al., 1998). However, under both hypotheses these soft-tissue characters exhibit homoplasy and potential synapomorphies.

At face value, it may seem unsurprising that two morphological datasets are more consistent with one another than with a molecular dataset. However, there is in fact no a priori reason to expect that anatomical minutiae of cranial vasculature and the anterior nose should correspond more closely with, for example, osteology of the appendicular skeleton than with a sequence dataset, although I do acknowledge that certain aspects of cranial anatomy (e.g., vascular foramina) have obvious correspondences with cranial soft tissues (e.g., arterial supply). In the end, all of these lines of evidence (i.e., osteological, soft tissue, and molecular) are potential indicators of homology, and as such represent the same kind of ''information'' (sensu van Valen, 1982) at different points along a developmental continuum. Each comprises an informative part of a systematic whole.

ACKNOWLEDGMENTS

Most of this study was accomplished during my graduate career in the departments of Anthropology and Anatomical Sciences at the State University of New York at Stony Brook, and in the department of Zoology at Eberhard-Karls Universität, Tübingen. I am grateful to the students, faculty, and staff at both institutions for their guidance and camaraderie. In particular, I thank my committee (Callum Ross, Ross MacPhee, David Krause, Malcolm McKenna, and Marc Allard), Marcelo Sánchez-Villagra, and Wolfgang Maier. For access to histological and photographic equipment at Stony Brook I thank Peter Brink, Beth Peterson, and Ben Walcott. For access to specimens at the American Museum of Natural History, I thank Erik Brothers, Pat Brunauer, Clare Flemming, Darrin Lunde, Ross MacPhee, and Bob Randall. Also at the AMNH, Paula Mikkelson generously allowed me to use her digital photography equipment.

Jaques Cuisin, Christiane Denys, Heinz Künzle, Wolfgang Maier, Maria Rutzmoser, and Peter Vogel provided access to several

important specimens, greatly enhancing the taxonomic sample used here. For hospitality during museum visits in Europe, I thank Heiko Frahm and Gerd Rehkämper (Düsseldorf); Barbara Hallmann, Wolfgang Knabe, Hans-Jurg Kühn, and Irmgard Weiss (Göttingen); and Jaques Cuisin and Christiane Denys (Paris).

I am grateful to John Wible and Marcelo Sánchez-Villagra for criticism which greatly improved the quality of this manuscript, and to Meng Jin and Brenda Jones for facilitating the editorial process.

For financial support I thank the German Academic Exchange Servic, National Science Foundation grant DEB 9800908 (to Callum Ross, Robert Asher, and Ross MacPhee), the Geological Society of America, the Theodore Roosevelt Fund of the American Museum of Natural History, the Doctoral Program in Anthropological Sciences at the State University of New York at Stony Brook, and the Paleontological Research Institute (Ithaca, NY).

REFERENCES

Agur, A. M. R., and M. J. Lee
1991. Grant's atlas of anatomy, 9th ed. Baltimore: Williams and Wilkins.

Ärnbäck-Christie-Lindie, A.
1914. On the cartilago palatina and the organ of Jacobson in some mammals. Morphol. Jahrb. 48: 343–364.

Asher, R. J.
1998. Morphological diversity of anatomical strepsirrhinism and the evolution of the lemuriform toothcomb. Am. J. Phys. Anthropol. 105: 355–367.
1999. A morphological basis for assessing the phylogeny of the ''Tenrecoidea'' (Mammalia, Lipotyphla). Cladistics 15: 231–252.
2000. Phylogenetic history of tenrecs and other insectivoran mammals. Ph.D. diss., State Univ. New York at Stony Brook.

Behrens, H.
1998. Vergleichend anatomische Untersuchungen der Nasenregion von *Potamogale velox*: ein Beitrag zur Funktionsmorphologie der Säugetiere. Doktor in Zahnheilkunde, Georg August Univ., Göttingen.

Bhatnagar, K. P., and J. R. Wible
1994. Observations on the vomeronasal organ of the colugo *Cynocephalus* (Mammalia, Dermoptera). Acta Anat. 151: 43–48.

Born, G.
1883. Die Plattenmodellirmethode. Arch. Mikrosk. Anat. 22: 584–599.

Broom, R.
1896. On the comparative anatomy of the Organ of Jacobson in marsupials. Proc. Linn. Soc. N.S.W. 21: 591–623.
1897. A contribution to the comparative anatomy of the mammalian organ of Jacobson. Trans. R. Soc. Edinburgh 39: 231–255.
1898. On the organ of Jacobson in the hyrax. J. Anat. Phys. 32: 709–713.
1902. On the organ of Jacobson in the elephant shrew. Proc. Zool. Soc. London 1902: 224–228.
1909. On the organ of Jacobson in *Orycteropus.* Proc. Zool. Soc. London 1909: 680–683.
1915a. On the organ of Jacobson and its relations in the ''Insectivora''. –Pt. 1. *Tupaia* and *Gymnura.* Proc. Zool. Soc. London 1915: 157–162.
1915b. On the organ of Jacobson and its relations in the ''Insectivora''. –Part 2. *Talpa, Centetes,* and *Chrysochloris.* Proc. Zool. Soc. London 1915: 347–354.
1916. On the structure of the skull in *Chrysochloris.* Proc. Zool. Soc. London 1916: 449–459.

Bugge, J.
1974. The cephalic arterial system in insectivores, primates, rodents, and lagomorphs, with special reference to the systematic classification. Acta Anat. 87: 1–160.

Butler, P. M.
1988. Phylogeny of the insectivores. *In* M. J. Benton (ed.), The phylogeny and classification of the tetrapods 2:117–141. Oxford: Clarendon Press.

Carroll, R. L.
1988. Vertebrate paleontology and evolution. New York: Freeman.

Cartmill, M., and R. D. E. MacPhee
1980. Tupaiid affinities: the evidence of the carotid arteries and cranial skeleton. *In* P. Luckett (ed.), Comparative biology and evolutionary relationships of tree shrews: 95–132. New York: Plenum.

De Beer, G. R.
1929. The development of the skull of the shrew. Philos. Trans. R. Soc. London B 217: 411–480.
1937 (1985 reprint).The development of the vertebrate skull. Chicago: Univ. Chicago Press.
De Pinna, M. C. C.
1991. Concepts and tests of homology in the cladistic paradigm. Cladistics 7: 367–394.
Dobson, G. E.
1882. A monograph of the insectivora, systematic and anatomical, Pt. 1: including the families Erinaceidae, Centitidae, and Solenodontidae. London: John Van Voort.
Eisenberg, J. F., and E. Gould
1970. The tenrecs: a study in mammalian behavior and evolution. Smithson. Contrib. Zool. 27: 1–137.
Emerson, G. L., C. W. Kilpatrick, B. E. McNiff, J. Ottenwalder, and M. W. Allard
1999. Phylogenetic relationships of the order insectivora based on complete 12s rRNA sequences from mitochondria. Cladistics 15: 221–230.
Farris, J. S.
1982. Outgroups and parsimony. Syst. Zool. 31: 328–334.
1983. The logical basis of phylogenetic analysis. *In* N. I. Platnick and V. A. Funk (eds.), Advances in cladistics 2:7–36. New York: Columbia Univ. Press.
Fischer, E.
1901. Primordialcranium von *Talpa europaea.* Anat. Hefte 17: 467–548.
Fischer, M.
1996. On the position of the Proboscidea in the phylogenetic system of Eutheria: a systematic review. *In* J. Shoshani and P. Tassy (ed.), The Proboscidea: evolution and palaeoecology of elephants and their relatives: 35–38. Oxford: Oxford Univ. Press.
Frahnert, S.
1998. Zur Stellung des Bibers (Castoridea, *Castor*) im System der Nagetiere (Rodentia). Eine craniogenetische Studie zur Ethmoidalregion sciurognather Rodentia. Berlin: Wissenschaft und Teknik.
Gaupp, E.
1908. Zur Entwicklungsgeschichte und vergleichenden Morphologie des Schädels von *Echidna aculeata.* Semon. Zool. Forschungsreisen in Australien 6: 539–788.
Giere, P., C. Freyer, and U. Zeller
1999. Opening of the mammalian vomeronasal organ with repsect to the Glires hypothesis: a cladistic reconstruction of the Therian morphotype. Mitt. Mus. Naturkd. Berl. Zool. Reihe 75: 247–255.
Gill, T.
1884. Insectivora. *In* J. S. Kingsley (ed.), The standard natural history, vol. 5, Mammals: 134–158. Boston: S. E. Cassino.
Göbbel, L.
2000. The external nasal cartilages in Chiroptera: significance for intraordinal relationships. J. Mamm. Evol. 7: 167–201.
Gould, G. C.
1995. Hedgehog phylogeny (Mammalia, Erinaceidae)—the reciprocal illumination of the quick and the dead. Am. Mus. Novitates 3131: 45 pp.
Haeckel, E.
1866. Generelle Morphologie der Organismen, allgemeine Grunzuege der organischen Formen-Wissenschaft, mechanisch begruendet durch die von Charles Darwin reformierte Descendenz-Theorie (2 vols.). Berlin: Georg Reimer.
Hawkins, J. A., C. E. Hughes, and R. W. Scotland
1997. Primary homology assessment, characters and character states. Cladistics 13: 275–283.
Hofer, H.
1977. The anatomical relations of the ductus vomeronasalis and the occurrence of taste buds in the papilla palatina of *Nycticebus coucang* with remarks on strepsirrhinism. Gegenbaurs Morphol. Jahrb. 123: 836–856.
1982a. Anatomy of the oronasal region of some species of Tenrecidae and considerations of tupaiids and lemurids. Gegenbaurs Morphol. Jahrb. 128: 588–613.
1982b. Observation on the anatomy of the proboscis and of the ductus nasopalatinus and ductus vomeronasalis of *Solenodon paradoxus.* Gegenbaurs Morphol. Jahrb 128: 826–859.
Kishino, H., and M. Hasegawa
1989. Evaluation of the maximum likelihood estimate of the evolutionary tree topologies from DNA sequence data, and the branching order in Hominoidea. J. Mol. Evol. 29: 170–179.
Kluge, A. G.
1989. A concern for evidence and a phylogenetic hypothesis of relationships

among *Epicrates* (Bovidae, Serpentes). Syst. Zool. 38: 7–25.

Kuhn, H.-J.
1971. Die Entwicklung und Morphologie des Schädels von *Tachyglossus aculeatus*. Abh. Senken. Naturforsch. Ges. 528: 1–224.

Leche, W.
1902. Zur Entwicklungsgeschichte des Zahnsystems der Säugetiere, zugleich ein Beitrag zur Stammengeschichte dieser Tiergruppe. Teil 1. Zoologica (Stuttg.) 37: 1–103.
1907. Zur Entwicklungsgeschichte des Zahnsystems der Säugetiere, zugleich ein Beitrag zur Stammengeschichte dieser Tiergruppe. Teil 2. Zoologica (Stuttg.) 49: 1–157.

Lee, D. C., and H. N. Bryant
1999. A reconsideration of coding inapplicable characters: assumptions and problems. Cladistics 13: 373–378.

Lindahl, E.
1948. Über die Entwicklung und Morphologie des Chondrocraniums von *Procavia capensis* Pall. Acta Zool. 29: 282–376.

Lindahl, E., and M. Lundberg
1946. On the arteries in the head of *Procavia capensis* Pall and their development. Acta Zool. 27: 101–153.

Liu, F.-G. R., M. M. Miyamoto, N. P. Freire, P. Q. Ong, M. R. Tennant, T. S. Young, and K. F. Gugel
2001. Molecular and morphological supertrees for eutherian (placental) mammals. Science 291: 1786–1789.

MacPhee, R. D. E.
1981. Auditory regions of primates and eutherian insectivores: morphology, ontogeny, and character analysis. Contrib. Primatol. 18: 1–282.
1994. Morphology, adaptations, and relationships of *Plesiorycteropus*, and a diagnosis of a new order of eutherian mammals. Bull. Am. Mus. Nat. Hist. 220: 214 pp.

MacPhee, R. D. E., and M. J. Novacek
1993. Definition and relationships of Lipotyphla. *In* F. S. Szalay, M. J. Novacek, and M. C. McKenna (eds.), Mammal phylogeny, vol. 2: Placentals:13–31. New York: Springer.

Maddison, D. R.
1993. Missing data versus missing characters in phylogenetic analysis. Syst. Biol. 42: 576–581.

Madsen, O., M. Scally, C. J. Douady, D. J. Kao, R. W. DeBry, R. Adkins, H. M. Amrine, M. J. Stanhope, W. W. de Jong, and M. S. Springer
2001. Parallel adaptive radiations in two major clades of placental mammals. Nature 409: 610–614.

Maier, W.
1980. Nasal structures in Old and New World Primates. *In* R. L. Ciochon and A. B. Chiarelli (eds.), Evolutionary biology of the New World Monkeys and continental drift: 219–242. New York: Plenum.
1991. Aspects of ontogenetic development of nasal and facial skeletons in primates. *In* G. Pfeifer (ed.), Craniofacial abnormalities and clefts of the lip, alveolus, and palate: 115–124. Stuttgart: Thieme.
1993. Cranial morphology of the therian common ancestor, as suggested by the adaptations of neonate marupials. *In* F. S. Szalay, M. J. Novacek, and M. C. McKenna (eds.), Mammal phylogeny, vol. 2: Placentals: 165–181. New York: Springer.
1997. The nasopalatine duct and the nasal floor cartilages in catarrhine primates. Z. Morphol. Anthropol. 81: 289–300.

McDowell, S. B.
1958. The Greater Antillean insectivores. Bull. Am. Mus. Nat. Hist. 115: 115–213.

McKenna, M. C., and S. K. Bell
1997. Classification of mammals above the species level. New York: Columbia Univ. Press.

Menzel, K.-H.
1979. Morphologische Untersuchungen an der vorderen Nasenregion von *Solenodon paradoxus* (Insectivora). Doktorgrades der Zahnmedizin, Johann Wolfgang Goethe Univ. Frankfurt am Main.

Mess, A.
1999. The evolutionary differentiation of the rostral nasal skeleton within Glires. Mitt. Mus. Naturkd. Berl. Zool. Reihe 75: 19–35.

Mouchaty, S. K.
1999. Mammalian molecular systematics with emphasis on the insectivore order Lipotyphla. Ph.D. diss., Lund Univ., Sweden.

Mouchaty, S. K., A. Gullberg, A. Janke, and U. Arnason
2000. Phylogenetic position of the tenrecs (Mammalia: Tenrecidae) of Madagascar based on analysis of the complete mitochondrial genome sequence of

Echinops telfairi. Zool. Scr. 29: 307–317.

Murphy, W. J., E. Eizirik, W. E. Johnson, Y. P. Zhang, O. A. Ryder, and S. J. O'Brien
2001. Molecular phylogenetics and the origins of placental mammals. Nature 409: 614–618.

Nixon, K. C., and J. M. Carpenter
1993. On outgroups. Cladistics 9: 413–426.
1996. On simultaneous analysis. Cladistics 12: 221–241.

Novacek, M. J.
1986. The skull of leptictid insectivorans and the higher level classification of eutherian mammals. Bull. Am. Mus. Nat. Hist. 183: 1–111.
1993. Patterns of diversity in the mammalian skull. *In* J. Hanken and B. K. Hall (eds.), The skull: patterns of structural and systematic diversity, 2:438–545. Chicago: Univ. Chicago Press.

Novacek, M. J., G. W. Rougier, J. R. Wible, M. C. McKenna, D. Dashzeveg, and I. Horovitz
1997. Epipubic bones in eutherian mammals from the Late Cretaceous of Mongolia. Nature 398: 483–486.

Nowak, R. M.
1999. Walker's mammals of the world, 6th ed. Baltimore, MD: Johns Hopkins Univ. Press.

Parker, W. K.
1885. On the structure and development of the skull in the mammalia, pt. 3, Insectivora. Philos. Trans. R. Soc. London 176: 121–276.

Platnick, N. I., C. E. Griswold, and J. A. Coddington
1991. On missing entries in cladistic analysis. Cladistics 7: 337–343.

Pleijel, F.
1995. On character coding for phylogeny reconstruction. Cladistics 11: 309–315.

Presley, R.
1979. The primitive course of the internal carotid artery in mammals. Acta Anat. 238: 238–244.

Reinbach, W.
1952a. Zur Entwicklung des Primordialcraniums von *Dasypus novemcinctus*, I. Z. Morphol. Anthropol. 44: 375–444.
1952b. Zur Entwicklung des Primordialcraniums von *Dasypus novemcinctus*, II. Z. Morphol. Anthropol. 45: 1–72.

Rohlf, F. J., and R. R. Sokal
1995. Statistical tables, 3rd ed. New York: Freeman.

Roux, G. H.
1947. The cranial development of certain Ethiopian ''insectivores'' and its bearing on the mutual affinities of the group. Acta Zool. 28: 165–397.

Sánchez-Villagra, M. R.
1998. Patterns of morphological change in the ontogeny and phylogeny of the marsupial skull. Ph.D. diss., Duke Univ., Durham, NC.
2001. Ontogenetic and phylogenetic transformations of the vomeronasal complex and nasal floor elements in marsupial mammals. Zool. J. Linn. Soc. 131: 459–479.

Schneider, R.
1955. Zur Entwicklung des Chondrocraniums der Gattung *Bradypus*. Morphol. Jahrb. 95: 209–301.

Schunke, A.
1996. Zur Ontogenese des Schaedels von *Hemicentetes* und die Systematik der 'Tenrecomorpha'. Diplomarbeit, Univ. Bielefeld, Germany.

Shoshani, J.
1993. Hyracoidea-Tethytheria affinity based on myological data. *In* F. S. Szalay, M. J. Novacek, and M. C. McKenna (eds.), Mammal phylogeny: Vol. 2: Placentals: 236–256. New York: Springer.

Sicher, H.
1913. Die Entwicklungsgeschichte der Kopfarterien von *Talpa europaea*. Morphol. Jahrb. 44: 465–487.

Simmons, N. B.
1993. The importance of methods: archontan phylogeny and cladistic analysis of morphological data. *In* R.D.E. MacPhee (ed.), Primates and their relatives in phylogenetic perspective: 1–61. New York: Plenum.

Simmons, N. B., and J. H. Geisler
1998. Phylogenetic relationships of *Icaronycteris*, *Archaeonycteris*, *Hassianycteris*, and *Palaeochiropteryx* to extant bat lineages, with comments on the evolution of echolocation and foraging strategies in Microchiroptera. Bull. Am. Mus. Nat. Hist. 235: 182 pp.

Simpson, G. G.
1945. The principles of classification and a classification of mammals. Bull. Am. Mus. Nat. Hist. 85: 350 pp.

Stanhope, M. J., V. G. Waddell, O. Madsen, W. W. de Jong, S. B. Hedges, G. C. Cleven, D. Kao, and M. S. Springer
1998. Molecular evidence for multiple origins of the Insectivora and for a new order

of endemic African mammals. Proc. Natl. Acad. Sci. USA 95: 9967–9972.
Stephan, H., G. Baron, and H. D. Frahm
1991. Comparative brain research in mammals, vol. 1: Insectivora. New York: Springer.
Strong, E. E., and D. Lipscomb
1999. Character coding and inapplicable data. Cladistics 13: 363–371.
Sturm, H.
1936. Die Entwicklung des praecerebralen Nasenskeletts beim Schwein und beim Rind. Z. Wiss. Zool. 149: 161–220.
Sweet, G.
1904. Contributions to our knowledge of the anatomy of *Notoryctes typhlops.* Proc. R. Soc. Vic. 17: 76–111.
Swofford, D. L.
2001. Phylogenetic analysis using parsimony (*and other methods), computer program version 4.0b8. Sunderland, MA: Sinauer Associates.
Swofford, D. L., and D. P. Begle
1993. Phylogenetic analysis using parsimony, manual to computer program version 3.1. Washington, DC.: Laboratory of Molecular Systematics, Smithsonian Insitution.
Swofford, D. L., G. J. Olsen, P. J. Waddell, and D. M. Hillis.
1996. Phylogenetic inference; *In* D. M. Hillis, C. Moritz and B. K. Mable (eds.), Molecular systematics: 407–514. Sunderland, MA: Sinauer Associates.
Tandler, J.
1899. Zur vergleichenden Anatomie der Kopfarterien bei den Mammalia. Denkschr. K. Akad. Wiss. Mat-Naturwiss. Klasse 67: 677–784.
Templeton, A. R.
1983. Phylogenetic inference from restriction endonuclease cleavage site maps with particular reference to the humans and apes. Evolution 37: 221–244.
Thewissen, J. G. M.
1985. Cephalic evidence for the affinities of Tubulindentata. Mammalia 49: 257–284.
van Dijk, M. A. M., O. Madsen, F. Catzeflis, M. J. Stanhope, W. W. DeJong, and M. Pagel
2001. Protein sequence signatures support the African clade of mammals. Proc. Nat. Acad. Sci. USA 98: 188–194.
van Valen, L.
1982. Homology and causes. J. Morphol. 173: 305–312.
Weisser, D.
1992. Zur Morphogenese der Nasenregion der Procaviidae (Mammalia; Hyracoidea). Diplomarbeit, Eberhard-Karls Univ., Tübingen.
Wible, J. R.
1984. The ontogeny and phylogeny of the mammalian cranial arterial pattern. Ph.D. Diss., Duke Univ., Durham, NC.
1986. Transformation in the extracranial course of the internal carotid artery in mammalian phylogeny. J. Vertebr. Paleontol. 6: 313–325.
1987. The eutherian stapedial artery: character analysis and implications for superordinal relationships. Zool. J. Linn. Soc. 91: 107–135.
Wible, J. R., and K. P. Bhatnagar
1996. Chiropteran vomeronasal complex and the interfamilial relationships of bats. J. Mamm. Evol. 3: 285–314.
Wible, J. R., and G. W. Rougier
2000. Cranial anatomy of *Kryptobaatar dashzevegi* (Mammalia, Multituberculata), and its bearing on the evolution of mammalian characters. Bull. Am. Mus. Nat. Hist. 247: 124 pp.
Wible, J. R., G. W. Rougier, M. J. Novacek, and M. C. McKenna
2001. Earliest eutherian ear region: a petrosal referred to *Prokennalestes* from the Early Cretaceous of Mongolia. Am. Mus. Novitates 3322: 44 pp.
Woodall, P. F.
1995. The male reproductive system and the phylogeny of elephant shrews (Macroscelidea). Mammal. Rev. 25: 87–93.
Wöhrmann-Repenning, A.
1984. Phylogenetische Aspekte zur Topographie der Jacobsonschen Organe und der Ductus nasopalatini bei Insectivora, Primates, *Tupaia* und *Didelphis.* Anat. Anz. 157: 137–149.
1987. Zur Anatomie des Vomeronasalkomplexes von *Elephantulus rozeti* (Duvernoy, 1830) (Insectivora, Mammalia). Zool. Anz. 218: 1–8.
1991. Functional aspects of the vomeronasal complex in mammals. Zool. Jahrb. Anat. 78: 71–80.

NOTE ADDED IN PROOF

Histological specimens of *Orycteropus, Procavia,* and *Talpa* in the Zoology Department of Eberhard-Karls Universität, Täbingen were made available courtesy of Prof. Wolfgang Maier after this paper was completed. Several characters previously coded as ''missing'' may now be filled in as follows:

Orycteropus: characters 9 and 18, state 1.
Procavia: character 9, state 1; character 16, state 0.
Talpa: characters 1, 6-8, state 1; characters 9, 16, 18, state 0.

Of these additions, *Talpa* is the most notable. It shows an external carotid medial to the thyropharyngeus muscle (character 9, state 0; shared with most tenrecs and *Solenodon*), a bifurcation of the stapedial artery within the braincase (character 7, state 1; shared with *Solenodon* and *Geogale*), an internal carotid artery entering the braincase lateral to the anterior pole of the cochlea (character 6, state 1; shared with chrysochlorids and *Orycteropus*), and the lack of lateral cover for the nasolacrimal duct (character 16, state 0; in contrast to its soricid and erinaceid sister taxa). Inclusion of these new data increases the homoplasy in the trees from both Stanhope et al. (1998) and Asher (1999) discussed herein, but does not change the overall conclusion that the phylogeny derived from set no. 1 of Asher (1999) has a slightly better fit to these soft tissue data than the phylogeny depicted in figure 1 of Stanhope et al. (1998).

Recent issues of the *Novitates* may be purchased from the Museum. Lists of back issues of the *Novitates* and *Bulletin* published during the last five years are available at World Wide World Web site http://nimidi.amnh.org. Or address mail orders to: American Museum of Natural History Library, Central Park West at 79th St., New York, NY 10024. TEL: (212) 769-5545. FAX: (212) 769-5009. E-MAIL: scipubs@amnh.org